5-8-2004

The Physical Phenomena associated with Stator Winding Insulation Condition as Detected by the Ramped Direct High-Voltage Method

Lorelynn Mary Rux

THE PHYSICAL PHENOMENA ASSOCIATED WITH STATOR WINDING INSULATION CONDITION AS DETECTED BY THE RAMPED DIRECT HIGH-VOLTAGE METHOD

By

Lorelynn Mary Rux

A Dissertation
Submitted to the Faculty of
Mississippi State University
in Partial Fulfillment of the Requirements
for the Degree of Doctor of Philosophy
in Electrical Engineering
in the Department of Electrical and Computer Engineering

Mississippi State, Mississippi

May 2004

THE PHYSCIAL PHENOMENA ASSOCIATED WITH STATOR WINDING

INSULATION CONDITION AS DETECTED BY THE

RAMPED DIRECT HIGH-VOLTAGE METHOD

By

Lorelynn M. Rux

Approved:

Stanislaw Grzybowski Professor of Electrical and Computer Engineering (Major Advisor and Director of Dissertation)	Nicholas H. Younan Professor of Electrical and Computer Engineering (Committee Member and Graduate Coordinator)
Noel N. Schultz Associate Professor of Electrical and Computer Engineering (Committee Member)	Herbert Ginn Assistant Professor of Electrical and Computer Engineering (Committee Member)
A. Wayne Bennet Dean of College of Engineering	

Name: Lorelynn Mary Rux

Date of Degree: May 8, 2004

Institution: Mississippi State University

Major Field: Electrical Engineering

MajorAdvisor: Dr. Stanislaw Grzybowski

Title of Study: THE PHYSICAL PHENOMENA ASSOCIATED WITH STATOR WINDING INSULATION CONDITION AS DETECTED BY THE RAMPED DIRECT HIGH-VOLTAGE METHOD

Pages in Study: 168

Candidate for Degree of Doctor of Philosophy in Electrical Engineering

Deregulation of the electric utility industry has increased the need to monitor the state of powerplant equipment, such as critical generators and motors, to improve availability and reduce life cycle costs via condition-based maintenance. To achieve these goals, nondestructive condition assessment and diagnostic tests are necessary to evaluate the quality and condition of a machine's stator winding insulation system. Periodic tests are generally conducted to monitor insulation aging, diagnose problems, or provide some assurance that the winding has a minimum level of electrical strength.

The basic principles of insulation testing are presented herein, and the physical mechanisms that affect the current versus voltage response are described. A stator winding insulation model was developed based on this theoretical foundation for use in understanding and analyzing the macroscopic behavior of complex insulation phenomena.

A comprehensive, controlled laboratory experiment was conducted on a set of stator coils that were deliberately manufactured with and without insulation defects. Specific defects were chosen to represent the types of insulation problems typically encountered during manufacture or as a result of in-service aging, and included lack of resin cure, loosely-applied insulating tapes, internal conductive contamination, reduced density of the groundwall insulation, and thermal cycling damage. Results are presented from a series of electrical tests conducted on the coil specimens to compare the effectiveness of various test methods in detecting the different insulation problems. The tests included insulation resistance, polarization index, ramped direct voltage, dissipation factor, dielectric spectroscopy, partial discharge, and recovery voltage measurements.

Dielectric principles and testing experience obtained during this investigation were applied to a collection of test results obtained by the author from in-service machines during the past ten years. These results and analyses provide a practical illustration of the ability of the ramped direct high-voltage test method to distinguish between normal insulation and that with problems, and to help identify the cause and extent of the deficiencies. While no single diagnostic method is ideally suited to detect all possible stator winding insulation problems, ramped voltage tests are shown to be useful in determining when corrective actions are needed and what the appropriate actions are.

Dedicated to

My husband, Doug

ACKNOWLEDGEMENTS

The author wishes to express her sincere appreciation to her major advisor, Dr. Stanislaw Grzybowski, for his invaluable guidance during this research investigation and preparation of the manuscript.

She also gratefully acknowledges the U.S. Bureau of Reclamation and the U.S. Army Corps of Engineers for their financial assistance during this project. She also thanks Mr. Bert Milano for his support.

The author extends a special debt of gratitude to Mr. William White, the artist and friend who created the graphics for the manuscript.

Finally, she wishes to thank her family and friends for their support and encouragement, and especially her husband for his sacrifice, understanding, and patience.

TABLE OF CONTENTS

LIST OF TABLES

LIST OF FIGURES

CHAPTER I

INTRODUCTION

During operation, large motors and generators (particularly those rated 4160 volts and higher) are continuously subjected to electrical, mechanical, thermal, and environmental stresses. These stresses act and interact in complex ways to degrade the machine's components and reduce its useful life. Deterioration of the stator (armature) winding groundwall insulation is a leading factor for determining the serviceability of large motors and generators.

Insulation life is defined as the period of time during which the insulation system can be used reliably and economically. Good quality stator windings are generally expected to last from 30 to 40 years if they are operated and maintained properly [1,2]. Insulation condition can be affected by various factors, such as moisture absorption, oxidation, thermal decomposition, electrolytic effects of leakage currents, attack by electrical discharges and their chemical by-products, thermomechanical stress, and mechanical wear or abrasion. Unexpected stator winding failure can result in forced outages and costly emergency repairs.

Deregulation of the electric utility industry has increased the need to monitor the state of powerplant equipment, such as critical generators and motors, in order to improve availability and reduce life cycle costs via condition-based maintenance. To achieve

these goals, nondestructive condition assessment and diagnostic tests are necessary to evaluate the quality and condition of the insulation system. In the factory, individual stator winding coils and bars are tested according to requirements of the manufacturer's Quality Assurance program and the customer's specifications. Stator windings are also tested in the field under a variety of circumstances, such as during installation to detect damage or defects; after installation as a condition of acceptance; before returning a machine to service after a system disturbance or extended outage; to verify the efficacy of repairs; and on a routine, periodic basis during the life of the machine.

Periodic tests are generally conducted to monitor aging of the insulation, diagnose problems, or provide some assurance that the stator winding has a minimum level of insulation strength. Conventional techniques include alternating-voltage withstand tests, on-line and off-line partial discharge measurements, dissipation factor measurements, and direct high-voltage withstand and diagnostic tests such as insulation resistance, polarization index, and leakage current measurements.

History of Ramped Direct High-Voltage Testing

Periodic testing of electrical insulation using direct high-voltage is a widely accepted practice in the electric utility industry. The first report revealing the possibility for using measured insulation current versus direct high-voltage to diagnose insulation condition was authored by S. Evershed in 1913 [3]. His studies of the characteristics of insulation resistance laid the foundation for the direct high-voltage testing developments that followed [4]. In 1951, G.L. Hill presented a method of plotting insulation leakage current versus stepped direct-voltage to the Edison Electric Institute, Electrical

Equipment Committee, and subsequently published a paper in the American Institute of Electrical Engineers (AIEE) transactions [5]. Around the same time, A.W.W. Cameron conceived and validated a very similar method for diagnosing the condition of electrical insulation [6]. The benefits of direct high-voltage testing were quickly acknowledged and many companies began using such techniques for insulation maintenance and/or proof testing [7]. In the mid-1950s, F.R. Schleif developed refinements to the conventional stepped direct-voltage method that significantly shortened testing time and improved the accuracy of the current measurements [8-10]. Shortly thereafter, J. S. Johnson and A.W. Zweiner presented modifications to the Schleif method to further improve the ability to properly interpret the test data [11].

The need for standardized direct-voltage testing methods was soon recognized. In 1957, the Insulation Subcommittee of the Rotating Machinery Committee of the AIEE began to prepare a guide for conducting and interpreting direct high-voltage insulation tests. The AIEE No. 95, "Guide for Insulation Testing of Large A-C Rotating Machinery with High Direct Voltage," was published in 1962. The document was revised in 1977 in the form of an Institute of Electrical and Electronics Engineers (IEEE) standard and entitled a Recommended Practice [12].

A variety of direct-voltage testing techniques have been devised to monitor and assess the condition of stator winding insulation systems. These methods range from the simple withstand or proof test to the more refined ramped voltage test in which the direct high-voltage is applied as a linearly increasing ramp function and the current response is recorded for analysis and documentation.

The ramped direct high-voltage method of testing stator windings was first introduced by Bruce McHenry in 1964 and subsequently published in 1967 [13,14]. Using a well-regulated and highly stable electrostatic voltage generator, the insulation system was subjected to a continuously rising direct voltage, and the resulting current was automatically measured and plotted as a function of time and voltage. If desired, a voltage step could first be applied to the insulation under test and held constant for 20 to 30 minutes to obtain the insulation resistance, polarization index, and absorption constants. After the initial "step and dwell" period, the applied voltage would be ramped up at a constant rate of rise to its maximum desired level. By using sophisticated, state-of-the-art instrumentation, the direct high-voltage testing was simplified, test time was reduced, and the accuracy and repeatability of test results greatly improved. Eventually, several North American electric utilities developed their own versions of ramped direct high-voltage test equipment [15-17]. Over the past 25 years, this technique has been used to monitor and evaluate hundreds of large hydroelectric generators and pump motors. In 2002, IEEE Std. 95, "Recommended Practice for Insulation Testing of AC Electric Machinery (2300 V and Above) with High Direct Voltage," was revised to update the document and include ramped direct high-voltage testing experience [18,19].

Study Objectives and Approach

Although the ramped direct high-voltage test is known in North America [20,21], it has not enjoyed widespread use, primarily because the testing equipment has never been commercially available. Only a few electric utilities with the requisite in-house resources have been able to build ramped voltage test instruments and incorporate this

technique into their motor and generator maintenance programs. Consequently, worldwide, only a few persons have expertise in conducting ramped voltage tests and interpreting the results, and only a limited number of generator owners and operators have benefited from this diagnostic tool. And though a large volume of ramped voltage test results has been collected over the years, the information has not been analyzed in depth and investigations involving this method have been very limited. The goal of this research study is to evaluate ramped voltage testing in detail and to rigorously assess its use in diagnosing the condition of stator winding insulation. The approach of this investigation is as follows:

1. Identify the physical phenomena underlying the macroscopic electrical behavior of high-voltage stator winding insulation.

2. Develop a model of the insulation system to aid in characterizing, predicting, and interpreting its electrical behavior and assessing its condition.

3. Describe the ramped voltage test method and analysis of test results.

4. Conduct comparative tests to evaluate the ramped voltage test results against measurements obtained from other insulation testing techniques.

5. Demonstrate typical ramped voltage test response characteristics as well as the types of insulation problems that can be identified using ramped voltage tests.

Major Contributions

The molecular structure of a dielectric material is fundamentally responsible for its physical and electrical properties. Insulation defects, damage, and aging can manifest as anomalies or changes in these properties. Thus, the important molecular phenomena associated with stator winding insulation materials and composite systems [22] are described in detail. The vast majority of large ac electric machines in service today have

windings insulated with mica and asphalt, polyester, or epoxy resins. Therefore, the chemical structure and microscopic characteristics of these materials are emphasized.

The basic principles of high-voltage insulation testing are presented and the physical phenomena that cause variations in the current versus voltage response are described. A stator winding insulation model has been developed based on this theoretical foundation. A comprehensive, controlled laboratory experiment was conducted on stator winding coils that were deliberately manufactured with and without insulation defects. Working in cooperation with a winding manufacturer, a set of twelve custom-made multi-turn stator coils was specified and purchased; two coils with each type of defect. Specific defects were chosen to represent the types of insulation problems typically encountered during manufacture or as a result of in-service aging. Insulation problems include: lack of resin cure, loosely-applied insulating tapes, internal conductive contamination, reduced density of the groundwall insulation, and thermal cycling damage. A series of electrical tests was conducted on the stator coils to compare the effectiveness of various test methods in detecting the different insulation problems. The following tests were performed: insulation resistance, polarization index, ramped direct voltage, dissipation factor, dielectric spectroscopy, partial discharge, and recovery voltage measurements. To the fullest extent possible, tests were performed and measurements made according to IEEE or other applicable testing standards.

And lastly, a number of ramped voltage test results representing the most common types of insulations are provided and interpreted in terms of the insulating system's physical and molecular properties. Test data obtained from in-service machines

are included to illustrate and catalog the types of stator winding problems that have been detected and diagnosed using ramped voltage tests.

CHAPTER II

GENERATOR AND MOTOR STATOR WINDINGS

The stator windings of large synchronous machines are typically comprised of three individual phases that are wye-connected at the neutral end. Each phase may consist of a single circuit of series-connected coils or of two or more parallel circuits, as illustrated in Figure 2.1. The neutral point is generally connected to ground to minimize voltage stress across the stator groundwall insulation in the event of a phase-to-ground insulation failure. A high-resistance neutral grounding scheme is often used to limit the magnitude of fault current.

Stator windings may be manufactured as either multi-turn coils or half-coils, also known as bars or Roebel bars. (Figure 2.2) The required turns-per-coil is a function of

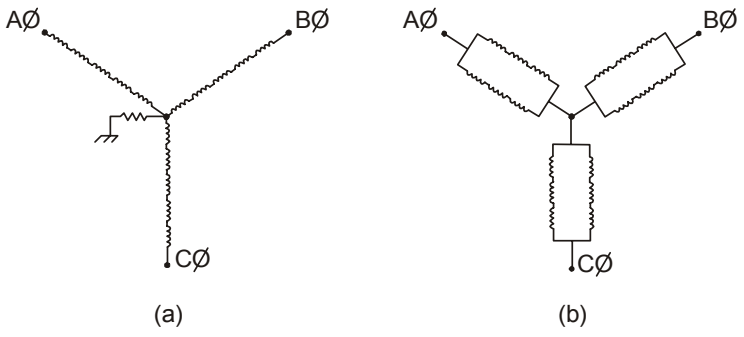

Figure 2.1 Schematic representations of two configurations of three-phase wye-connected stator windings comprised of (a) one parallel circuit per phase, and (b) two parallel circuits per phase. In (a), a fault current-limiting resistor is connected from the neutral point to ground.

the machine's voltage rating and number of series-connected coils per phase. The number of coils per phase is determined by the number of rotor poles and slots in the stator core.

Figure 2.2 (a) A multi-turn diamond stator coil, and (b) a coil comprised of two bars, or half-coils.

Stator coils are typically embedded in the core slots in two layers. (Figure 2.3) Coil-supporting materials include bottom, side, and depth packing; center filler; stator slot wedges, and an under-wedge spring or compression system. The purpose of the slot materials is to ensure the coils are held tight in the core to prevent winding movement and vibration during machine operation. The resistance of the slot materials must be low enough to allow good electrical contact between the slot portion of the coil surface and the grounded core yet high enough to prevent shorting of the stator core laminations. After the coils are inserted and wedged into the stator core, the inter-coil series connections are made, typically by brazing the coil leads together. These connections are then electrically insulated and braced to prevent end winding vibration during normal operation and distortion during short-circuit conditions.

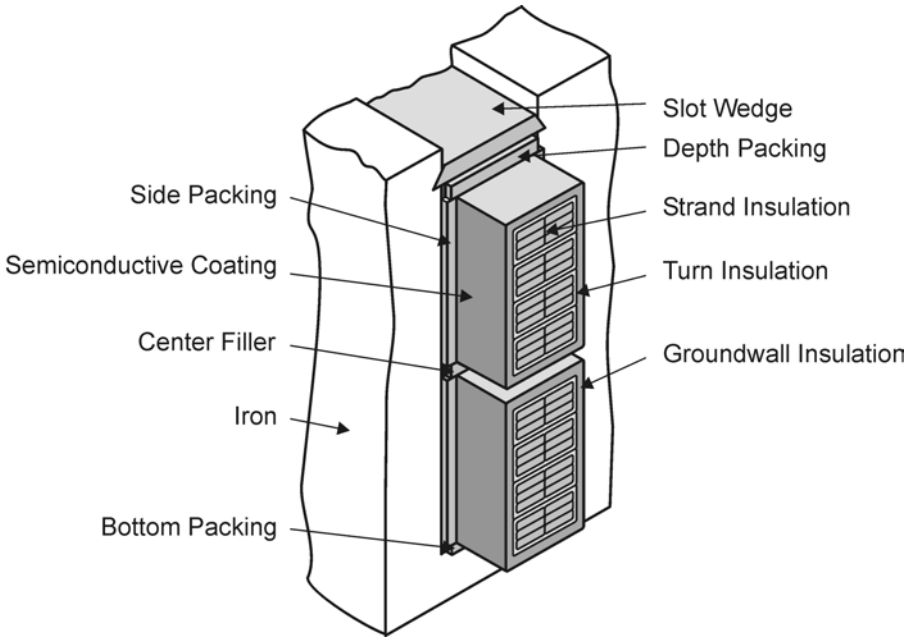

Figure 2.3 Cross section of a 4-turn stator winding installed in the stator core slot in two layers. Shows components of the insulation system, slot packing materials, and wedges.

Stator winding conductors of large cross-section are subdivided into strands for both mechanical and electrical reasons. Stranding makes the conductor more flexible and easier to manufacture. Also, when strands are insulated from one another eddy currents within the conductor are reduced, thereby lowering the associated I^2R heating losses. Strand insulation must be reliable and capable of withstanding high operating temperatures (up to 155°C for Class F equipment). Strand insulation is typically comprised of glass film, glass fiber, or glass and fused polyester fibers (Daglas™). Synthetic resin is often used to bond the fiber insulation to the copper wire. Although the potential between adjacent strands is typically only a few volts, a short circuit between them could result in significant losses and heating in the copper conductor. Arcing and

overheating due to strand shorts can eventually compromise the integrity of the inter-turn and groundwall insulation systems.

In multi-turn coils, each conductor turn (*i.e.*, bundle of strands) must be carefully insulated to prevent short circuits between adjacent turns. Failure of the inter-turn insulation can rapidly cause machine failure because high currents will circulate between the shorted turns, resulting in very high temperature at the site of the short circuit. The high temperature may melt the copper strands and damage the groundwall insulation, leading to groundwall insulation puncture and a fault to the stator core or, even worse, between adjacent phases. Although the normal operating voltage between turns is generally less than 100 volts, much higher steep-fronted voltage surges are possible during switching operations. Thus, at a minimum, the inter-turn insulation must be designed to withstand the full line-to-line operating voltage. For machines rated 4160 volts and higher, each turn is usually insulated with mica tape which provides excellent dielectric strength as well as long-term resistance to partial discharges. The mica tape used today is typically comprised of mica paper, although in the past mica splittings supported by thin fabric were often used.

The stator winding groundwall, or main, insulation is applied over the copper conductor and turn insulation (if present) to prevent breakdown between the energized conductor and the grounded stator core. The groundwall insulation must, therefore, have sufficient dielectric strength to withstand normal line-to-ground operating voltage, as well as moderate transient overvoltages. Groundwall insulation may be applied using either resin-rich B-stage tape or vacuum pressure impregnation (VPI) techniques. In

resin-rich systems, an ample amount of synthetic resin is incorporated into the mica tape, which is then wound around the conductor while the resin is still pliable. The wound component is then heated under pressure to cure the resin and form a solid, consolidated insulation system of proper dimensions. During the VPI process, a lightly doped mica tape is wound around the conducting components, which are then put into a vacuum-pressure tank. The tank is first evacuated to remove air from the insulation, and then filled with low viscosity impregnating resin under pressure. When the interstices of the groundwall are filled with resin, the coil is removed from the tank and heated under pressure to completely cure the resin and mold the slot portion of the coil. Regardless of the manufacturing method used, an appropriate stator winding design, high quality materials, and careful control of the production process are essential to ensure good results.

Insulating Materials

The groundwall insulation of rotating machine stator windings is usually comprised of mica with organic reinforcing, bonding, and impregnating materials. Machines in service today were typically manufactured using asphalt, polyester, or epoxy resins. The exact proportion of the constituent dielectric materials will vary according to the particular insulation system design but a typical composite insulation would roughly consist of 55 percent mica, 30 percent resin binder, and 15 percent reinforcing material.

The chemical elements and atomic structure of an insulating material have a profound influence on the deterioration mechanism likely to occur during operation as well as on the dielectric response observed during electrical testing. Electrical and

physical properties such as dielectric constant, electric strength, resistivity, hardness, melting point, etc. may be correlated to a compound's molecular structure. To fully understand and predict an insulation's electrical behavior and aging characteristics, one must have knowledge of the chemical elements involved, the atomic-molecular arrangement, and the nature of the chemical bonds.

Mica

Mica's unique combination of physical, thermal, and electrical properties has made it an important component of high-voltage insulation systems. The ability to be split into very thin, incompressible sheets while maintaining flexibility, toughness, and high tensile strength in the other two axes is a consequence of mica's layered atomic structure. The two classes of mica most commonly used in electrical applications are muscovite and phlogopite. Their chemical formulas are $KAl_2(Si_3Al)O_{10}(OH,F)_2$ and $KMg_3(Si_3Al)O_{10}(OH,F)_2$, respectively [23,24].

Mica minerals are comprised of layers of silicates separated by alternating layers of metal oxides and metal ions. Structurally, mica can be thought of as a repeating three-layer system, as illustrated in Figure 2.4. The two outer-layers are comprised of silicate tetrahedra where one fourth of the silicon atoms are replaced by aluminum atoms. Each silicon or aluminum atom is surrounded by four oxygen atoms. The inner-layer consists of octahedrally coordinated aluminum atoms (or magnesium atoms, in the case of phlogopite mica). The aluminum atom is surrounded by a repeating pattern of oxygen atoms and hydroxide (OH) groups. Positive potassium ions are located between the triple tetrahedra-octahedra-tetrahedra layers, and share ionic bonds with oxygen atoms in the

octahedral layers. Because the cohesive attraction between the potassium and oxygen is weak, the ionic bonds are easily broken and mica exhibits an easily cleaved morphology giving flexible sheets that can be very thin.

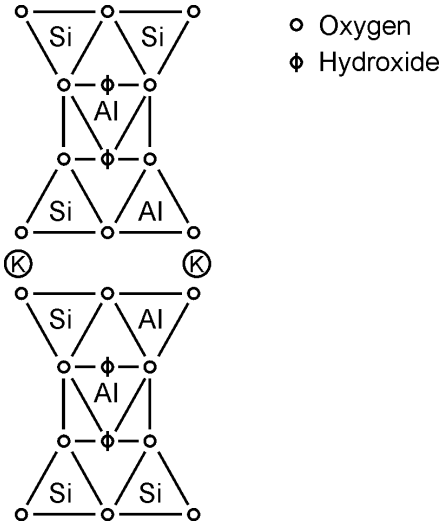

Figure 2.4 Cross-section of muscovite mica showing the silicate-metal oxide-silicate layers where one of every four silicon atoms is replaced by an aluminum atom. Each three-layer structure is separated by a layer of potassium ions.

The molecular structure of mica also helps in understanding its electrical properties. The separation of positive potassium ions with respect to negative oxide ions gives rise to permanent dipoles, even in the absence of an electric field. Because of its polar nature, mica exhibits a relatively high dielectric constant. Furthermore, micas exhibit high dielectric strength and low conductivity due to the infinite two-dimensional structure of tetrahedra-octahedra-tetrahedra layers with few defects where conductive paths might develop.

High interatomic bond strengths within the alumino-silicate layers enable mica to be chemically stable and virtually inert to the action of water, solvents, oils, alkalies, and acids (except hydrofluoric in the case of muscovite mica, and concentrated sulphuric acid in the case of phlogopite acid). One of the most valuable characteristics of mica is its resistance to erosion by prolonged electrical discharge, which is much greater than that of any other flexible material. Another important attribute for high-voltage, high-power applications is thermal stability. Mica minerals are fireproof, noninflammable, and completely unaffected by temperatures of 600 to 700°C or higher, depending on the specific type of mica [25]. When mica is heated above its thermal decomposition temperature, the OH groups in the structure decompose with the production of steam, and the mica becomes brittle and powdery. Mica is slightly hygroscopic because of its crystalline layer structure. To achieve optimum dielectric properties, mica must be carefully selected and properly dried.

Mica deposits occur in almost all areas of the earth's surface, although the majority of the world's supply of electrical mica is obtained from India. In its natural form, mica is difficult to apply to components in a continuous manner. Mica cleaves very easily and must be supported in some way to stop it from delaminating. One method of application is to build up mica flakes or splittings onto a fabric or glass backing, usually with a binder. The mica tape can then be wound onto the surface of a conductor to form an insulating layer. Another method of application involves the manufacture of mica paper in which mica flake material is exfoliated into very tiny plate-like particles and formed into sheets by settling from suspension in a machine similar to a

normal paper-making machine. The cohesive force between the platelets is sufficient to give mica paper the strength to permit gentle handling, but its tear strength is too low for most purposes until it has been treated with a binding resin. The use of a binder limits the useable temperature of the mica tape to the maximum that the resin will stand.

Asphalt

From the 1920s to early 1960s, asphalt-based compounds were used extensively as bonding and impregnating agents in the groundwall insulation of high-voltage stator windings of small- and medium-sized rotating machines [26]. Many generators and motors from this era are still in service today, particularly those that have operated with moderate levels of thermal and electrical stresses.

Although the terms "asphalt" and "bitumen" are frequently used interchangeably, strictly speaking, bitumen refers to any of various mixtures of high-molecular-weight hydrocarbon compounds and their non-metallic derivatives [27]. Bitumens may be obtained from naturally occurring petroleum deposits or as a by-product of petroleum distillation. Asphalt is one type of bitumen, and is normally obtained from crude oil using the pyrogenic process of fractional distillation. As the crude oil is gradually heated, the lowest-boiling fractions (natural gas, gasoline, and kerosene) distill off first, followed by progressively higher boiling-temperature constituents (heating oils and lubricating oils). Asphalt is a residue of this distillation process. Additional processing and/or purification may be necessary before the asphalt can be used for electrical purposes.

The asphaltic bitumens used in electrical insulation are black to dark brown solids or semisolids. They are thermoplastic, cement-like, and gradually liquefy when heated.

The flow characteristics of a particular asphaltic substance are dependent on the temperature, pressure, and chemical compositions involved. In cases where higher flow points, higher viscosities, or a more rubbery type of compound is desired, high temperature or high pressure processing methods are used to remove the volatile constituents.

Asphalts are comprised of mixtures of hydrocarbons and typically contain small amounts of sulfur, nitrogen, and oxygen as well [28]. These so-called "heteroatoms" attach to carbon atoms in different configurations and in the form of different compounds. The molecules of hydrocarbons are held together by covalent bonds. The number of covalent bonds that are possible for a particular atom is determined by the number of its valence electrons. A hydrogen atom needs one electron to complete its outermost electronic shell, whereas a carbon atom needs four. A single covalent bond is created when two adjacent atoms share one pair of electrons, as in the bond between carbon and hydrogen atoms (C─H). A double or triple bond is formed when two atoms share two or three pairs of electrons, respectively, such as C═O and C≡C. Atoms are able to rotate around a single bond whereas double and triple bonds are quite rigid.

Hydrocarbons that contain double and triple covalent bonds are termed chemically "unsaturated." When atoms in a molecule are not bonded to the maximum number of other atoms, the addition of atoms or groups of atoms is possible without first removing atoms or groups that are already bonded to the hydrocarbon chain. The physical and dielectric properties of hydrocarbons are inherently related to the molecular weight and bond structure of the material. Although the chemical composition of asphalt

is complex and varies widely, it is principally comprised of long, straight-chain molecules with a high degree of unsaturation. Unsaturated molecules are highly reactive, enabling asphalt to combine with a wide variety of functional groups.

When two atoms of different electronegativity (*i.e.*, tendency to accept valence electrons) are covalently bonded together, there is an unequal sharing of electrons, with the atom of higher electronegativity assuming a greater share of the electron density. The resulting asymmetry of the electric charge centers gives rise to bond dipoles. The double covalent bond between carbon and oxygen atoms, for example, leads to a very significant permanent dipole in which the oxygen is negative and the carbon positive. (Figure 2.5) This imbalance of electrochemical forces within the compound strongly influences the material's physical characteristics and electrical performance. Many of the compounds in asphalt are polar in nature [29,30]. As a result, asphalts generally exhibit relatively high dielectric loss and moderate dielectric strength.

Figure 2.5 Permanent dipole formed by double covalent bond between carbon and oxygen atoms due to their different electronegativities.

Asphalts display a strongly negative coefficient of dielectric strength with increasing temperature, restricting their use to Class B (130°C) applications. When heated at high temperature, the oil constituents present in the asphalt are removed by volatilization or are destroyed by chemical oxidation or molecular cracking. The overall

result is a change in the viscosity and flow point of the asphalt together with a reduction in its bonding strength. There is also an increase in its brittleness and friableness at room temperatures and below, and a greater tendency to form cracks and fissures on solidification. At very high temperatures, the asphalt may carbonize, leading to the formation of permanent, continuous internal carbon tracks and an increase in dielectric losses. In asphalt-based insulation systems, groundwall failure at or near the ends of the stator core is commonly observed due to compound migration and tape separation induced by differential thermal expansion and thermal cycling. This mode of stator winding deterioration is commonly referred to as "girth cracking." Although asphalts have good resistance to the transmission of moisture, moisture can ingress through cracks and fissures. Asphaltic bitumens are characterized by a high degree of solubility in common insulating oils and askarels.

Polyester

Early electric machines were insulated using naturally occurring materials (*e.g.*, air, mica, asphalt) or those which were easily derived from natural sources (mineral oil, rosin, oleovarnishes, and cellulose). The steadily increasing demand for higher operating temperatures and voltage gradients, however, compelled the development of insulating materials of greater thermal, mechanical, and electrical stability. In the 1940s and 1950s, advances in polymer chemistry made possible the commercial use of synthetic insulating compounds, such as polyester and epoxy resins [31].

The term "polymer" is used to describe a very long chain that is made up of many smaller, repeating molecular units. The starting units from which the polymer is formed

are called "monomers," and the synthesis that joins the monomers together is called "polymerization." Most synthetic polymers are derived from hydrocarbons in which the molecules are held together by covalent bonds. Polymers are generally subdivided into two broad classifications: thermoplastic and thermosetting. Solid materials that soften and melt reversibly are classed as thermoplastics. In contrast, thermosetting materials undergo a chemical reaction upon heating and become a solid that does not soften upon subsequent reheating. Polyester resins may be either thermoplastic or thermosetting, depending on their molecular structure.

Thermoplastic polymers are comprised of long-chain linear molecules without linkages interconnecting individual strands. The chains may possess branches but the branches do not connect to other molecules. Thermoplastic polyesters, such as Mylar and Dacron, are flexible and elastic. The use of thermoplastic polyesters in high temperature applications (*e.g.*, continuous operation above 150°C) may be limited by their thermoplasticity.

Thermosetting polyesters possess linear chain groups that are cross-linked at various positions by either short chains or single bonds between atoms, forming a three-dimensional or spatial polymer. The cross-links create very strong intermolecular bonds that will not break down when exposed to temperatures at which thermoplastics soften or melt. Thermosetting resins are hard and strong, although some types may exhibit excessive brittleness.

Polyester resins are produced by the condensation or stepwise reaction of a dibasic organic acid and a di- or tri-hydric alcohol to form the species polymer and a low-

molecular-weight by-product. The alcohol and acid molecules must contain at least two functional groups for the reactions to produce a long-chain polymer. The first stage condensation reaction between glycerol and phthalic acid forms glyceryl monophthalate (a half-ester). The condensation reaction of half-esters to form a linear polyester resin and water as the by-product is illustrated in Figure 2.6 [32]. The remaining –OH groups may then react similarly with terminal –COOH groups of other chains or –OH groups to form –O– linkages, resulting in a structure of chains of the type shown in Figure 2.6. To control or prevent the cross-linking reactions, additives may be introduced to use up some of the reactive groups in non-polymerising reactions.

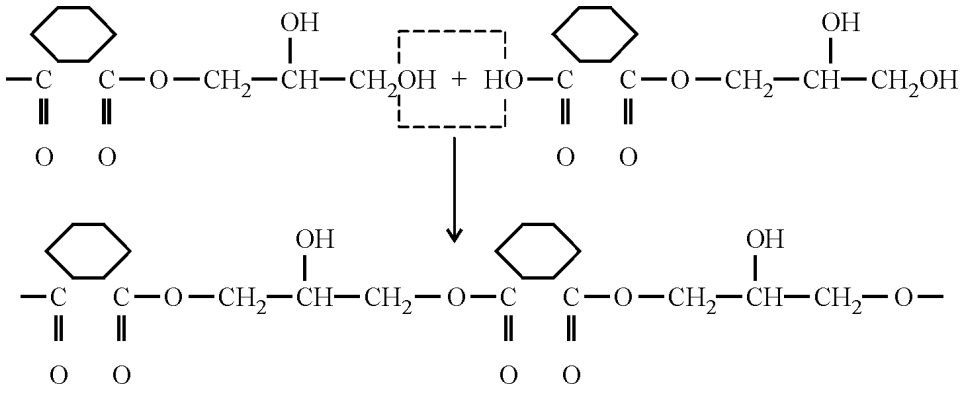

Figure 2.6 Formation of a liner polyester chain by the condensation reaction of half-esters.

In many applications, the base polyester composition is blended with a reactive monomer such as styrene. The presence of the unsaturated bonds yields a high degree of cross-linking which produces an infusible and insoluble material. The resulting three-dimensional polyester resin is illustrated in Figure 2.7 [32]. The cross-linking between polyester and the polymerizing compound may be initiated by a catalyst and/or elevated

heat. This is an addition reaction giving off no volatile products. However, polymerization of this type is accompanied by approximately 6 to 8 percent of volume shrinkage. Polyesters to be used as varnish resins are frequently modified by adding drying oils or other compounds to improve the hardness, adhesion, and electrical tracking properties of the cured resin. These resins are called alkyds or glyptals.

Condensation polymerization of thermoplastic polyesters introduces C═O polar groups at regular intervals in the polymer chain. When an electric field is applied to the insulating material, the permanent dipoles will tend to align in the direction of the field, causing an increase in the dielectric constant. The polar groups also attract and absorb water. This, in turn, leads to a measurable increase in dc conductivity.

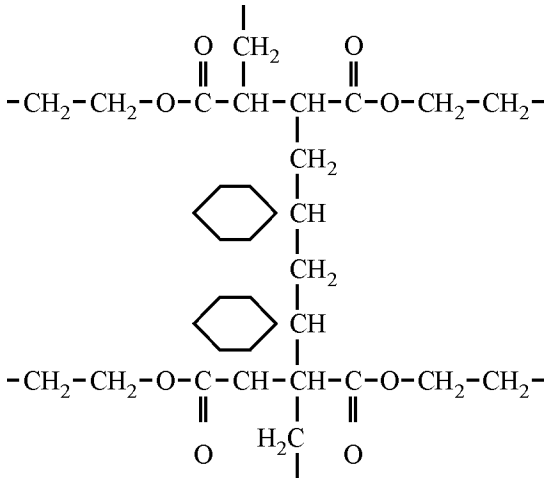

Figure 2.7 Polyester molecule cross-linked with styrene.

Symmetry of charge around every atom is not essential for a molecule to be non-polar. As a whole, a molecule may be electrically neutral even though the centers of gravity of the positive and negative charged particles do not coincide. Any rigid symmetrical molecule is essentially non-polar, since opposed internal dipoles in tend to

cancel one another. Highly cross-linked compounds are generally non-polar. In general, non-polar materials tend to have better electrical characteristics and the polar ones tend to have better mechanical characteristics. Because polyester compounds are often polar in nature, they have dielectric properties which are somewhat poorer than those exhibited by epoxies. Generally speaking, polyester resins are relatively inexpensive and characterized by good electrical properties and good resistance to heat and mechanical impact.

Epoxy

Epoxy coatings and impregnants have been widely used since the late 1940s. Epoxy resins are valued for their high strength, good adhesion to most materials including metals, and resistance to moisture, solvents, and other chemicals. The main obstacle to their wider use is their relatively high cost. Epoxies take their name from the epoxide functional group (three-membered oxygen-containing ring) which forms part of the epicholorhydrin molecule, one of the two reactants used to make the resin. The other component most commonly used is diphenyl propane, often called bisphenol A. The polycondensation reaction of epicholorhydrin and bisphenol A results in a linear structure of the type shown in Figure 2.8 [33].

To be made into a useful end product, epoxy must be cured by the action of hardeners. Many different curing agents are used to bring about cross-linking of thermosetting epoxy resins. They may be either room temperature curing or oven curing. The curing releases no water or other by-products (including volatiles) and results in a hard, strong, and heat-resistant resin with very good adhesion properties and low

shrinkage characteristics. Two-part epoxy systems are generally preferred for dielectric applications. Epoxies are non-polar polymers exhibiting a low dielectric constant and low loss characteristics.

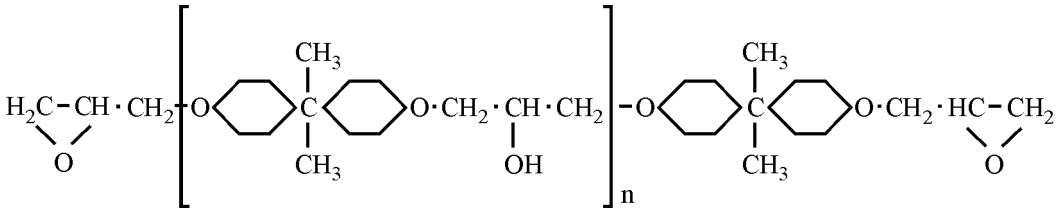

Figure 2.8 Molecular structure of basic epoxy resin prepolymer.

CHAPTER III

DIELECTRIC PHENOMENA

Defects, deterioration, and adverse conditions can affect the electrical properties of dielectric materials and insulation systems. Since variations in electrical properties can be measured, quantified, and trended, they are often used to diagnose insulation condition. When performing off-line high-voltage tests of stator winding groundwall insulation, a voltage source is connected to the conductor of the winding, usually one phase at a time with the neutral-end wye connection broken and the other two phases isolated and grounded. A voltage is applied and the total current to the grounded stator core is measured. (Figure 3.1) The resulting current is comprised of geometrical capacitance charging, dielectric polarization, surface and volume conduction, and ionization current components. Evaluation of these components has proven useful in determining the quality and condition of the insulation system.

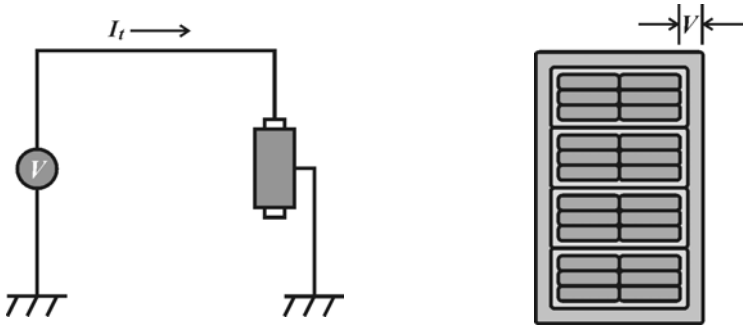

Figure 3.1 Diagram of a test voltage V applied to a stator winding, and the resulting current I_t flowing through the insulation to ground.

Geometrical Capacitance

A simple capacitor may be constructed by arranging two metallic plates in parallel, separated by a small distance. If the plates are placed in vacuum and charged to opposite surface charges $\pm Q$, a potential difference V_0 will be developed across the capacitor. The vacuum, or geometrical, capacitance [34-36] of this system is defined as

$$C_0 = Q/V_0 \tag{3.1}$$

The charge on the capacitor gives rise to an electric field E_0 between the electrodes. This field represents the force acting to displace a unit of positive charge toward the negatively charged plate, and conversely. The intensity, or strength, of the electric field in vacuum is given by

$$E_0 = V_0/d \tag{3.2}$$

Since the electric field is defined by the force on a positive charge, it follows that the direction of E_0 will always be away from the positive electrode and toward the negative electrode. If the surface area A of the electrodes is relatively large compared to the distance d between them, E_0 will be practically homogeneous and directed perpendicular to the surface of the plates [37], as illustrated in Figure 3.2.

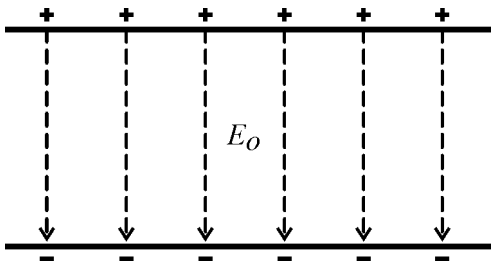

Figure 3.2 The electric field E_0 between two charged parallel plates in vacuum.

The geometrical capacitance of a stator winding is a function of the conductor-to-core geometry (*i.e.*, size, shape, and spacing). In the general case, the geometrical capacitance may be somewhat complicated to calculate, but broadly speaking, it varies inversely with the distance between electrodes and directly with their surface area. Thus, the stator windings of physically large generators and motors exhibit a relatively higher value of geometrical capacitance as compared to smaller machines. Since C_0 represents stator winding geometry and does not take into account the insulation between the electrodes, geometrical capacitance is not generally considered when evaluating the condition of the stator winding groundwall insulation.

Dielectric Polarization

If the space between the electrodes of the vacuum capacitor is filled with a dielectric material while keeping the charge on the plates unchanged, the presence of the dielectric will cause the voltage across the capacitor to drop from V_0 to a smaller value V. The capacitance of the system is thereby increased from C_0 to a greater value C given by

$$C = Q/V \tag{3.3}$$

The increase in capacitance due to the dielectric material is typically described by the dielectric constant or relative permittivity, ε_r, of the material, where

$$\varepsilon_r = C/C_0 \tag{3.4}$$

By definition, the relative permittivity of vacuum (free space) is equal to 1. For all practical insulating materials, ε_r is greater than unity, its actual value being strongly dependent on the molecular structure of the dielectric, particularly on polarity within the molecules.

Insertion of the dielectric material between the electrodes of the capacitor causes the intensity of the electric field to decrease to

$$E = E_0 / \varepsilon_r \tag{3.5}$$

Since the reduction in field strength observed upon insertion of the dielectric could also be achieved by reducing the density of the electric charge on the electrodes, in effect, the dielectric material tends to neutralize the charges at the electrode surface, thereby reducing their contribution to the external electrical field. This phenomenon is known as dielectric polarization. As illustrated in Figure 3.3, dielectric polarization may be visualized as the action of dipole chains that are induced by the applied field, binding countercharges with their free ends on the electrode surfaces. This reaction is possible because the dielectric material consists of positive and negative elementary charges. Although these charges cannot move freely through the insulating medium (as in a conductor), they can be displaced under the influence of an electric field. The negative

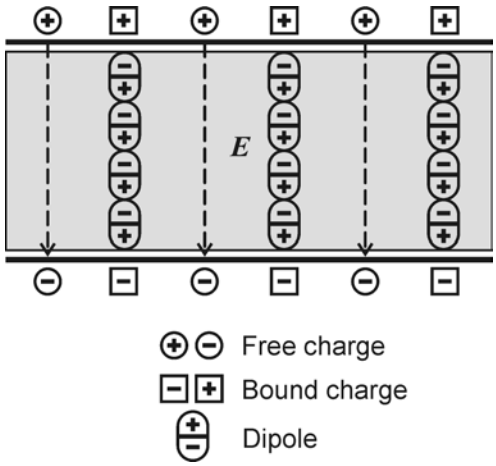

Figure 3.3 Schematic representation of dielectric polarization showing how induced dipole chains tend to neutralize charges on the electrode surfaces.

charges will be shifted toward the positive electrode and, conversely, the positive charges will be shifted toward the negative electrode; an electric dipole moment (product of the charge magnitude and separation distance) results. The neutralized charges are sometimes referred to as "bound" charges, whereas the remaining charges on the capacitor plates are called "free" charges.

The average electric dipole moment per unit volume determines the extent to which the surface charges are neutralized at the electrodes by the polarized dielectric, thereby reducing their contribution to the external electric field. For static electric fields, the density of bound charge on the dielectric surface is constant and is denoted as the polarization P of the dielectric, where

$$P = q(1 - 1/\varepsilon_r) = q(\varepsilon_r - 1)/\varepsilon_r \tag{3.6}$$

and q represents the total or "true" charge density.

The dielectric polarization effects described by P are caused by four distinct molecular polarization mechanisms: electronic, atomic, dipole, and space charge polarization. Because these microscopic polarization phenomena influence the current versus voltage response of dielectric materials, changes in their characteristics may be observed during diagnostic testing and used to assess the condition of an insulation system.

Electronic Polarization

An electric dipole may be induced in an atom or molecule that is normally electrically symmetric [38]. As shown in Figure 3.4, physical matter consists of atomic nuclei surrounded by electron clouds. An external electric field causes the electron cloud

to shift or become slightly displaced with respect to the positively charged nucleus, and a dipole moment is created. This result is termed electronic polarization and it occurs in all materials without exception.

At frequencies below the ultraviolet range (*i.e.*, less than approximately 8×10^{14} Hz), there is no appreciable time lag between the applied alternating field and the electron oscillations. Thus, in the range of frequencies typically used in electric power systems, electronic polarization represents a completely elastic process with zero power loss. The effect of temperature on electronic polarization is very small, although it may not be completely negligible. With an increase in temperature, thermal expansion generally reduces the density of dielectric materials, thereby lowering the number of atoms or molecules per unit volume. As a result, electronic polarization (and, thereby, the dielectric constant) falls slightly as density decreases. Thus, the temperature coefficient of electronic polarization is negative.

Atomic Polarization

The application of an external field will also cause displacement of atoms and ions with respect to each other. When different types of atoms are held together by interatomic bonds, they normally will not share their electrons symmetrically; the electron clouds will be displaced toward the atoms with greater electronegativity so that adjacent atoms may acquire charges of opposite polarity. An external field acting on these charges will create a force that tends to change the equilibrium position of the atoms themselves. Displacement of charged atoms or groups of atoms results in atomic

polarization, as illustrated in Figure 3.5. Atomic polarization occurs in both polar and non-polar dielectric materials.

Due to their much larger mass, atomic nuclei have natural frequencies of vibration in the infrared region of the spectrum (between 3×10^{11} and 4×10^{14} Hz), considerably lower than those of the electronic vibrations. In the range of working frequencies, however, dielectrics generally exhibit negligible power loss from atomic polarization. Atomic polarization often introduces a slightly positive temperature coefficient because increased thermal vibrations tend to induce dissociation of the positive and negative charges within the structure of the dielectric material. The magnitude of this effect is typically one tenth that of electronic polarization [39].

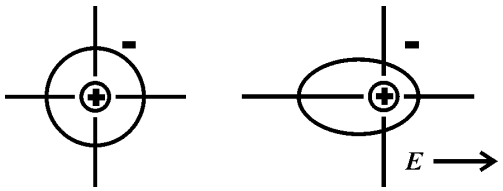

Figure 3.4 Electronic polarization is caused by an external field *E* acting on an atom or molecule that is normally electrically symmetric.

Figure 3.5 Atomic polarization results from the relative displacement of electrically charged ions on response to an electric field *E*.

Dipole Polarization

Permanent dipole moments exist in some molecules by virtue of an asymmetrical arrangement of positively and negatively charged regions. Such molecules are termed polar molecules. In the absence of an external field, the polar molecules will be pointing in all directions and continually jump from one orientation to another due to thermal

agitation. At any given instant, the dipoles will be oriented at random and no net dipole moment will be exhibited. With the application of an external field, however, the permanent dipole moments experience a torque that tends to orient them in the direction of the field since the forces resisting the displacement are much weaker than the primary binding forces within atoms or between neighboring atoms. Consequently, a dipole, or orientation, polarization may arise, as illustrated in Figure 3.6.

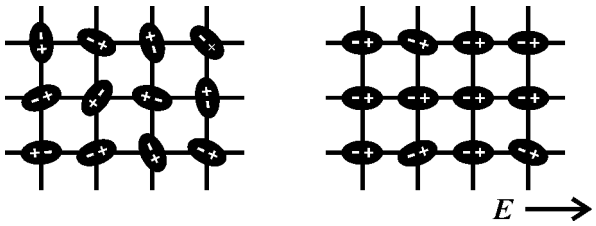

Figure 3.6 Permanent electric dipoles tend to align with the applied electric field, producing dipole polarization.

In the case of dipole polarization, the moving component of the structure (*i.e.*, the permanent dipole) is much larger than an individual electron or atom. Consequently, dipole polarization is sluggish as compared to electronic and atomic polarizations. Moreover, the forces opposing the displacement are not elastic but behave like a viscous medium in which the dipoles rotate. Dipole polarization results in energy being absorbed, allowing the dipoles to jump from one equilibrium position to another, or dissipated as heat due to friction between the shifting dipoles and adjacent atoms or molecules.

Thermal agitation tends to cause random movement of neighboring atoms or molecules as well as disorder in the distribution of orientations among dipolar groups. At

higher temperatures, thermal agitation within the local environment increases and dipole polarization is hindered and counteracted.

Space Charge Polarization

Electronic, atomic, and dipole polarization mechanisms are due to charges that are locally bound in atoms, molecules, or the structures of solids and liquids. In addition to bound charges, charge carriers exist that can migrate for some distance through the dielectric. When such carriers accumulate within the material or at interfaces a space charge, or interfacial, polarization occurs resulting in considerable molecular interaction. The individual molecules are not only subjected to the influence of the external field but also to the internal field created by the trapped charges. Calculation of the internal field distortion is relatively complex, as it requires information about the geometrical arrangement and polarizability of the atoms and molecules. Therefore, it is generally expedient to simply recognize, qualitatively, that the internal field opposes the external field and an apparent increase in dielectric constant results.

Space charge polarization is illustrated in Figure 3.7. In composite insulations or those using filler materials, space charge polarization may contribute significantly to the value of the dielectric constant. The concentration of ionic species increases with temperature, as does their mobility due to greater available kinetic energy. As a result, interfacial polarization typically increases with temperature.

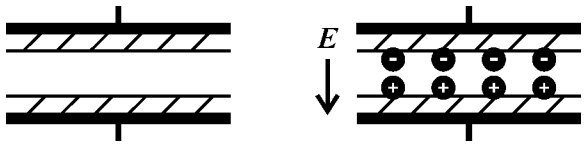

Figure 3.7 Interfacial polarization caused by charge buildup at heterogeneous interfaces due to the influence of the electric field.

Each type of dielectric polarization is characterized by a relaxation time τ, which represents the time taken for the polarization to respond to the applied electric field. Electronic polarization establishes in a time $\tau_e \approx 10^{-16}$ seconds. The relatively heavier atoms are a little slower to respond, and the relaxation time of the atomic polarization τ_a is on the order of 10^{-12} to 10^{-13} seconds. Dipole and space charge polarizations take longer due to dipole inertia and charge carrier transport time. In solid materials there is often a broad distribution of dipole orientation relaxation times. The relaxation time of the dipole orientation τ_d depends markedly on the molecular structure and state of the material and on the temperature, but it generally lies in the region of 10^{-3} to 10^{-10} seconds. The relaxation time of space charge polarization depends on the conductivity and arrangement of the constituent dielectric components, but is usually slow and on the order of 1 to 10^{-3} seconds.

Complex Permittivity

To account for the losses accompanying dielectric polarization, it is customary to introduce complex permittivity, ε^*, where

$$\varepsilon^* = \varepsilon' - j\varepsilon'' \tag{3.7}$$

The real part of permittivity, ε', is simply the relative permittivity ε_r and relates to the charge displacement component of the polarization current. The imaginary part of permittivity, ε'', is called the loss factor or loss index because it represents the dissipative effects of dielectric polarization. The smaller the value of ε'', the more the dielectric material approaches the condition of a perfect insulator. The loss index ε'' represents the resultant loss under alternating-field conditions and should not be confused with the dc conductivity of the dielectric. The loss tangent is defined as

$$\tan \delta = \varepsilon''/\varepsilon' \tag{3.9}$$

When an alternating electric field of frequency f is applied to the dielectric material, each type of polarization can only make its full contribution to the total polarization as long as the period of oscillation of the field $t = 1/f$ is much greater than the relaxation time τ, so that the polarization is able to establish itself completely before the field is reversed. When f is on the order of $1/\tau$, the polarization is only partially established before the field reversal, and hence there is a decrease in the contribution to the permittivity. When f is much greater than $1/\tau$, the particular polarization mechanism becomes inoperative, since it cannot respond to the rapid oscillations of the field and it ceases to contribute to ε'. The variation of ε' with frequency, the so-called dispersion curve, is shown in Figure 3.8.

Under static field conditions and at very low frequencies, electronic, atomic, dipole, and space charge polarization mechanisms contribute to ε'. As the frequency of the applied electric field increases, the time needed for a dipole to reorient or a trapped charge to disperse may exceed the time period of the alternating frequency.

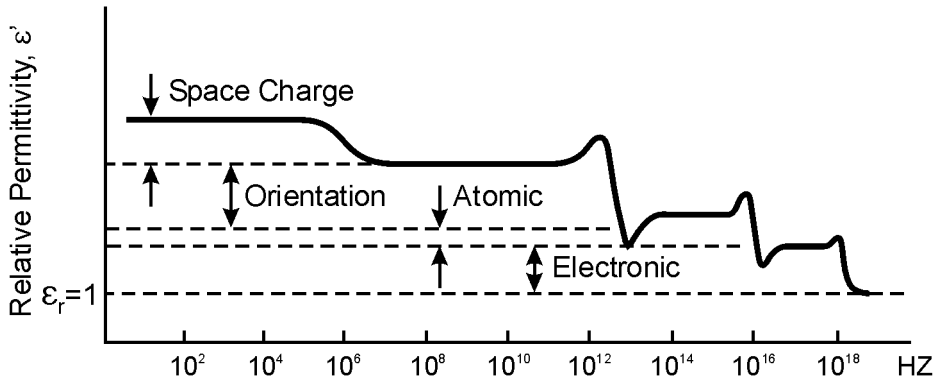

Figure 3.8 Dispersion curve showing variations of relative permittivity with the frequency of an alternating electric field. Electronic, atomic, orientation, and space charge polarization contributions to ε' are indicated.

The loss index ε'' also varies with frequency as shown in Figure 3.9. While the dispersion curve is generally characterized by a region of constant value followed by a slow fall of ε' to a lower value as the frequency increases, the corresponding variation of ε'' is a broad peak. This peak is due to a resonance effect in the dielectric loss mechanism around that particular frequency.

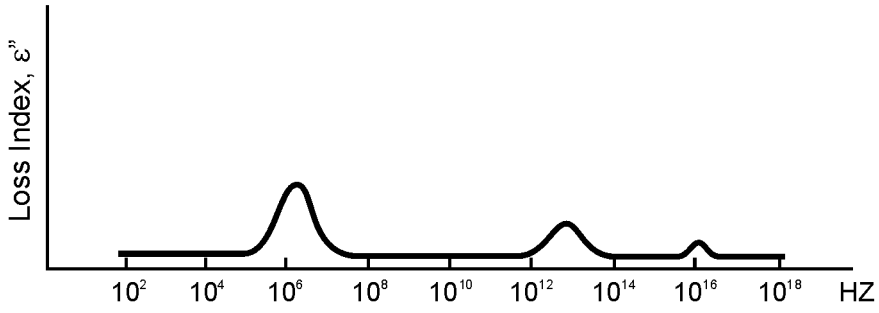

Figure 3.9 Variation of loss index with frequency.

Conduction

The conduction current observed during insulation testing is caused by the continuous, irreversible movement of charge carriers that occurs when a voltage is applied across an insulation having finite electrical resistivity. These charges pass through the volume (bulk) of the insulation and over its surfaces. The relative values of volume and surface conduction depend on temperature, humidity, contaminants, and voltage stress, as well as on the quality and condition of the insulation being tested.

Electrical conduction through dielectrics is predominately undertaken by ions. Both cations and anions possess an electrical charge and are capable of migration or diffusion when under the influence of an applied electric field. An electric current results from the net movement of these charged ions. The presence of ionic impurities such as absorbed moisture or residual catalyst, voids in the bulk of the insulating material, and trapped space charge may result in ionic flow of current under the application of high electric stress. Electronic conduction is much less likely because of the strong binding forces between the outer electrons and the atomic nuclei of the insulator atoms. However, in situations where the insulation has been contaminated by dirt, oil, moisture, etc., electronic conduction may be more likely to occur.

Because the electrical conductivity of dielectric materials is very low and the surface creepage paths of practical insulators are designed to be sufficiently long, the conduction current of high-quality insulation will normally be small and nearly linear with respect to applied voltage. As the insulation starts to age and weaken, however, or its surface becomes contaminated, conductivity may rise, thereby producing a measurable

increase in conduction current during high-voltage tests. A sharp, sustained increase in conduction current with test voltage may indicate a serious problem with the insulation system, such as a fault or crack in the groundwall. As the applied stress approaches the level of insulation breakdown, conduction current increases exponentially as evidenced by a steep positive increase in the slope of the current response.

Partial Discharges

Partial discharges are localized ionizations which occur in gas cavities (voids) within a solid insulation or in gaseous spaces adjacent to conductors. When the stress gradient in the gas exceeds a critical value, a sudden transient electrical discharge occurs. Since the discharge only partially bridges the insulation between conductors, it is referred to as a partial discharge. A full discharge would be a complete fault between the line and ground terminals. [40]

A minimum of approximately 300 volts must be present across a void or small gap in order to initiate the ion-generation process (depending on gas density and gap spacing) [41]. Under conditions of sufficiently high electric stress, an "initiating" electron, which is present in the gas due to external radiations such as cosmic rays, x-rays, nuclear radiations, thermal ionization, or other naturally occurring processes, becomes accelerated by the field and collides with a gas atom or molecule in its path. Additional electrons are freed by the energy acquired from the incident electron, and the impacted atom or molecule becomes ionized. The resulting mobile ions and electrons continue to gain kinetic energy in the electric field, leading to more molecular collisions and eventually resulting in an avalanche of electrons that forms a passage of current

through the gas. As the electrons rapidly migrate toward the positive electrode, the positive ions drift more slowly toward the negative electrode [42,43]. The distribution of charges tends to cancel the electric field within the gaseous space, and the current ceases to flow. The duration of the electron avalanche is on the order of nanoseconds. The displacement of the heavier positive ions can take milliseconds or more. [44]

Partial discharges can occur under direct and alternating voltage stresses, as well as under impulse conditions [45]. During normal operation or when performing off-line tests involving an applied alternating voltage, partial discharges generally occur near the peaks of the voltage waveform. Although the local discharge current cannot be directly measured by an external measuring circuit, the voltage drop due to the partial discharge causes a rapid, detectable charge transfer to the terminals of the test object. This "apparent charge" can be measured and used to evaluate the quality and condition of the insulation system [46-49]. Most PD measuring instruments are designed to detect the rapid migration of negative charge (*i.e.*, electrons). The flow of positive ions tends to be too slow to be detected. Given the stochastic nature of partial discharges owing to the random availability of an initiating electron, a single partial discharge is not generally adequate to determine PD initiation. In practical applications, the magnitude of the current induced on the external conductor must be sufficiently large to be detected and the charge transfer must occur with sufficient repetition (*e.g.*, 10 or more pulses per second) to signal the onset of partial discharge activity.

There are several possible sites of partial discharges in high-voltage electrical machines, such as between the surface of the slot portion of the generator stator winding

and the grounded core, at either boundary of the voltage stress grading treatment in the end turn area, in the winding overhang region where large potential differences exist between adjacent coils separated by small spaces, and internal to the ground insulation at the site of defects or other discontinuities. Consequently, partial discharges may indicate the presence of voids or delaminations caused by overheating or load cycling, or other defects such imperfect impregnation, incomplete curing, inadequate bonding, gas-evolution during manufacture, shrinkage, wrinkling, inclusions of foreign particles or contaminants, and projections or sharp points [50,51]. Partial discharges are not only a symptom of a defective insulation system, the ionized gas resulting from discharges contains chemically reactive electrons, ions, excited molecules, and free radicals which can decompose and further degrade the surrounding solid insulation. While the damage caused by a single partial discharge event is minute, the cumulative effect of many discharges can eventually lead to insulation failure [52,53].

Insulation Model Using Lumped Parameters

The macroscopic behavior of geometrical capacitance charging, dielectric polarization, conduction and partial discharges may be modeled using lumped electric circuit parameters. Such models are useful for studying and predicting electrical insulation characteristics as well as recognizing abnormalities and changes that may indicate deterioration or adverse conditions [54]. It should be noted that appropriate parameter values must be selected for the given conditions of temperature, humidity, and voltage frequency and magnitude.

When an external voltage is applied to a capacitive specimen such as a stator winding, the geometrical capacitance draws current from the voltage supply and stores charge to establish the electric field between the electrodes. The magnitude of the geometrical charging current is equal to the rate-of-change of voltage times the geometrical capacitance. That is,

$$I_0 = C_0 \, dV/dt \tag{3.8}$$

In alternating fields, I_0 leads V by a temporal phase angle of 90°. Thus, the geometrical capacitance may be modeled as an ideal (loss-free) capacitor C_0, representing a stored reversible energy.

Each dielectric polarization mechanism may be represented by resistive and capacitive elements chosen to indicate the magnitude of the polarization and loss effects as well as the relaxation time of the polarization process. At power frequencies and below, electronic and atomic polarization phenomena are practically instantaneous and loss-free. Therefore, the losses which could be described by R_e and R_a are negligible for these processes and the mechanisms are simply represented by C_e and C_a.

Dipole and space charge polarizations may be represented by several combinations of R and C to reflect the range of relaxation times resulting from a diversity of polar species and charge carriers. However, for the purposes of this investigation, it is sufficient to represent each polarization effect using a single combination of resistance and capacitance. Thus, dipole polarization is modeled using a series combination of R_d and C_d. Similarly, space charge (interfacial) polarization is modeled using R_i and C_i.

The conduction current of high-quality insulation is typically small and practically proportional to applied voltage. Accordingly, a single resistor R_L is used to represent the sum of surface and volume conduction (leakage) current effects.

The effects of surface and internal discharges may be represented by a series arrangement of a capacitor C_{pd} and resistor R_{pd}. Partial discharges produce heat, light, and sound. This consumption of energy increases the dielectric losses and is represented by R_{pd}. Partial discharges in air-filled voids effectively short-circuit the air space and an apparent increase in winding capacitance results [42,43]. The incremental increase in capacitance is represented by C_{pd}. In the case of severely defective insulation, representative values of resistance and capacitance vary depending on the level of stress and resulting ionizations. When the electrical stress exceeds the partial discharge inception voltage, the losses and capacitance increase accordingly.

The detailed lumped parameter circuit representation of a typical stator winding insulation is shown in Figure 3.10., taking into account the various dielectric phenomena which occur during high voltage testing.

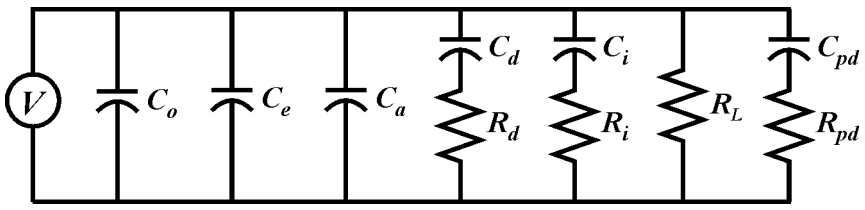

Figure 3.10 Lumped parameter representation of stator winding groundwall insulation showing contributions due to the effects of geometric capacitance charging (C_0); electronic (C_e), atomic (C_a), dipole (R_d and C_d), and interfacial (R_i and C_i) polarizations; surface and volume conduction (R_L); and internal and external partial discharges (C_{pd} and R_{pd}).

The insulation model may be simplified by combining the four individual mechanisms of polarization and corresponding energy loss into an equivalent capacitor C_P in series with a resistor R_P, as shown in Figure 3.11.

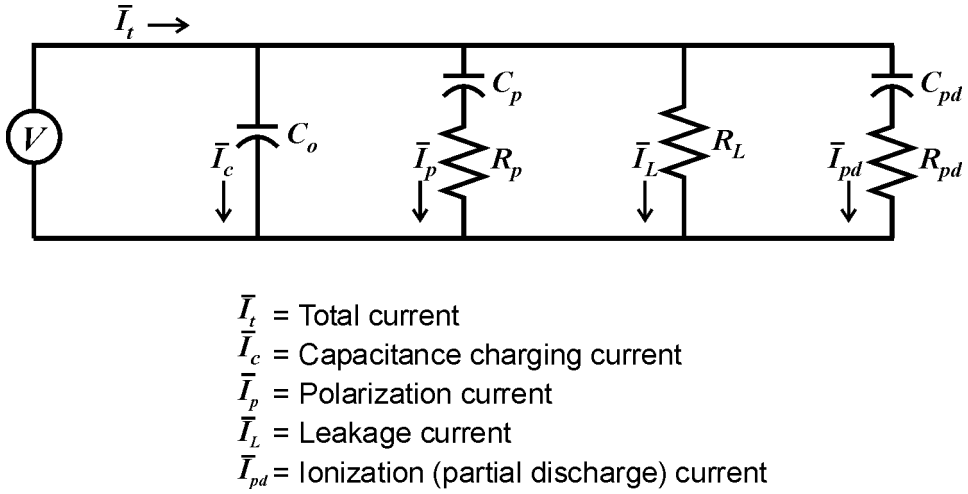

Figure 3.11 Simplified lumped parameter model of stator winding insulation in which the dielectric polarization mechanisms have been combined.

The geometric capacitance charging, polarization, conduction, and partial discharge components represented in Figure 3.11, as well as the total current observed when performing insulation tests, are indicated on the phasor diagram in Figure 3.12. During alternating-voltage tests, the geometric capacitance charging current I_0 leads the voltage by an angle of 90°. The imaginary part of the displacement current I_P' due to the combined effects of electronic, atomic, dipole, and space charge polarization also leads the voltage by 90°. The real part of polarization I_P'' represents energy absorption, dipole friction, and space charge losses, and is in phase with the applied voltage. The conduction current I_L due to the movement of free electrons and ions is also in phase with the voltage. The ionization current resulting from partial discharges is comprised of a

real component I_{pd}" representing losses and an imaginary component I_{pd}' representing the observed increase in capacitance. The resulting total current I_t leads the applied voltage by an angle θ which is somewhat less than 90°.

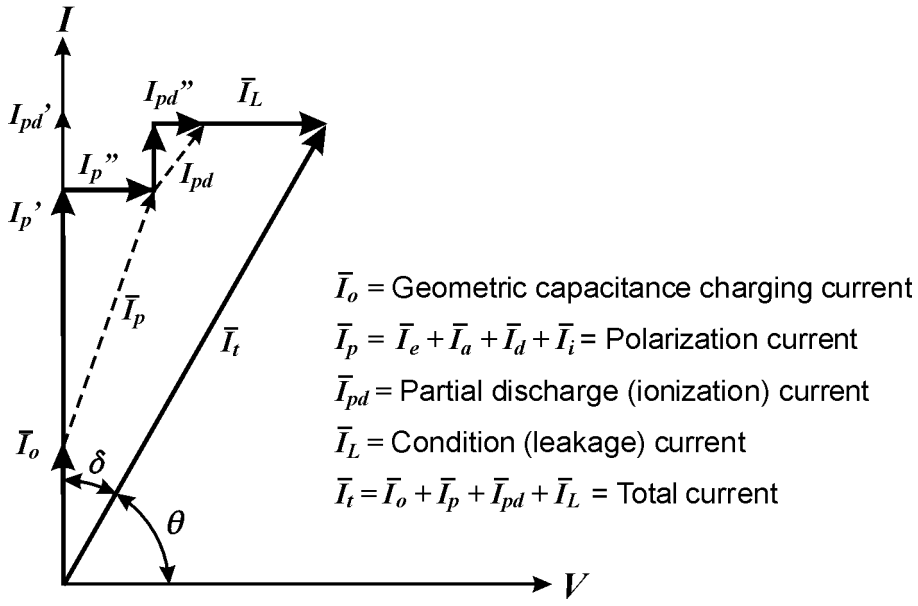

Figure 3.12 Phasor diagram showing individual current components and the resulting measured current.

The difference angle δ shown in Figure 3.12 is termed the loss angle because it represents the sum of all irreversible insulation losses. The dissipation factor, or tan δ, is routinely measured and has proven to be a useful indicator of insulation quality and condition. Winding manufacturers strive to design and build stator coils with low dielectric loss. If the coil insulation is well consolidated, properly cured, and has low void content, the dissipation factor should be quite low.

A further simplification of the insulation model is a parallel or series arrangement of a single equivalent resistor and capacitor. The parallel representation is illustrated in Figure 3.13, where R and C account for all charging, polarization, conduction, ionization,

and loss effects and are chosen so that δ is unchanged from that shown in Figure 3.12. Although this simple model is most often used to describe the relative losses observed during dissipation factor measurements, the detailed representation in Figure 3.10 is more useful for understanding and analyzing complex insulation phenomena.

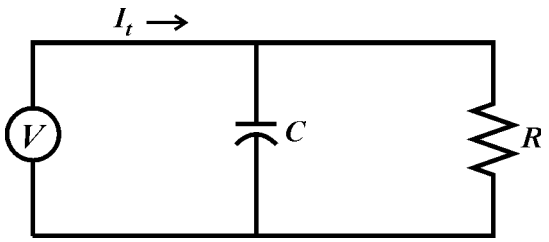

Figure 3.13 Simple representation of stator winding insulation where all dielectric effects are combined into a single *C* and *R* parallel arrangement.

Current Response to a Ramped Direct High-Voltage

Operational and environmental stresses may produce physical changes and severe deterioration of the insulation. Chemical degradation may cause the formation of water, ionizable acidic materials, and gases, resulting in moisture migration and concentration, and a decrease in dielectric strength. Temperature variations and thermal cycling may lead to the formation of gas pockets and voids due to unequalized expansion and contraction. Mechanical embrittlement, cracking, and shrinking may be caused by aging and oxidation effects due to the presence of air. Changes within the insulation may upset the voltage distribution, leading to stress concentrations which promote further ionization, culminating in partial discharges and accelerated degradation of the organic materials. Over time, these aging factors may act to deteriorate the stator winding insulation—possibly leading to unexpected, catastrophic failure and forced outages.

The current versus voltage (*I-V*) response observed during ramped direct high-voltage tests has been used to evaluate insulation condition, and to determine when and what corrective actions are needed. To conduct the test, an automatic high-voltage power supply is used to linearly increase the applied direct voltage from zero up to some maximum value at a constant ramp rate, typically 1 to 2 kilovolts per minute. The current is measured and plotted, and used to evaluate the condition of the insulation by noting deviations from the normal shape of the test curve. Any departure from a smooth curve could be an indication of insulation problems. Because the maximum test voltage is above the normal operating stress, the test also serves as a proof test.

The ramped voltage technique is generally considered to be a type of direct-voltage test [20]. However, because the magnitude of the voltage is continuously increased throughout the test period, the capacitance charging and dielectric polarization effects are more akin to those observed during low-frequency alternating-voltage tests. Thus, it may actually be more appropriate to consider the ramped voltage test as a type of alternating-voltage (albeit, not sinusoidal) test. As illustrated in Figure 3.14, ramped voltage tests typically involve only the increasingly negative portion of the voltage waveform.

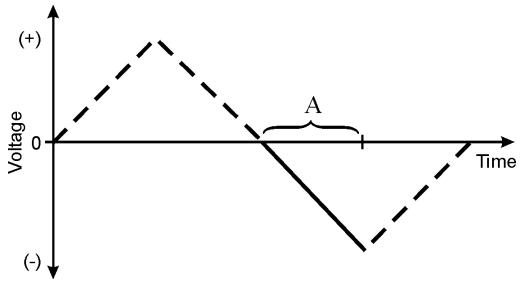

Figure 3.14 Alternating (zigzag) voltage profile, where "A" represents the increasingly negative portion of the waveform used for ramped voltage tests.

A typical 20-minute ramped voltage test is roughly equivalent to a frequency of 0.2×10^{-3} Hz. The very low frequency test voltage produces capacitance charging current that is on the same order of magnitude as the polarization and conduction currents. Thus, only moderately sensitive current measuring instrumentation is required to detect relative changes in charging, polarization, conduction, and ionization current components.

The response to an applied ramped direct voltage is shown in Figure 3.15. The observed current I_t is comprised of the sum of the geometric capacitance charging, dielectric polarization, surface and volume leakage, and partial discharge current components. In the ideal case, geometrical capacitance charging would be constant throughout the test since the rate-of-change of the applied voltage dV/dt is constant. In practice, however, the geometric capacitance charging lags the applied voltage somewhat due to the surge-limiting resistor in series with the test leads, which increases the time constant and hinders the charge build-up on the specimen electrodes. The resulting delay is evidenced by the slightly rounded portion at the beginning of the I_0 trace.

The dielectric polarization component I_P exhibits an even greater time lag between the applied voltage and the resulting displacement current, primarily due to the relatively slow dipole orientation mechanism. The steepness of the trace varies according to the polarizability of the dielectric materials comprising the insulation system. A highly polar substance such as asphalt exhibits a much steeper slope than does epoxy, which is a relatively nonpolar material. Under the influence of an applied electric field, asphalt will incur a greater number of dipoles per unit volume than will epoxy. The effect is that

more charges will be neutralized on the specimen electrodes and a corresponding increase in polarization current I_P is required to maintain the applied potential.

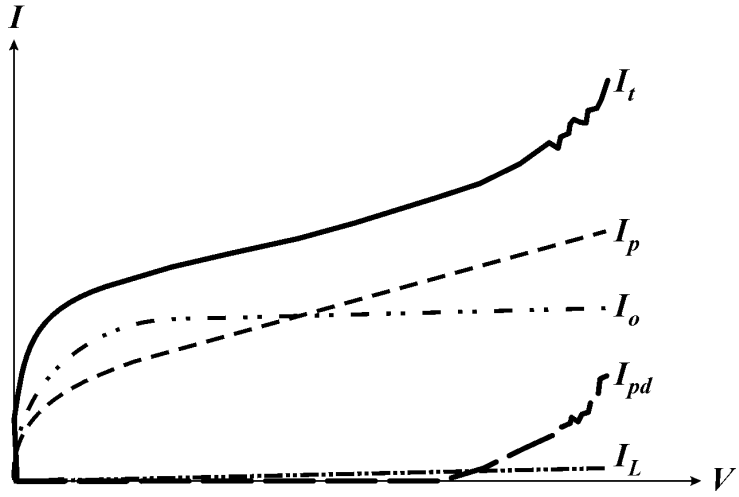

Figure 3.15 Response of stator winding insulation to an applied ramped high direct voltage. The total current I_t is the sum of the geometric capacitance charging (I_0), dielectric polarization (I_P), leakage (I_L), and ionization (I_{pd}) current components.

Leakage current over the surface and through the bulk of the insulation is very small and practically linear in the case of high quality insulation in good condition. However, if the insulation surface is exposed to conductive contamination or if internal defects exist which reduce the insulation's volume resistivity, the leakage current I_L may become pronounced and increase nonlinearly with respect to applied voltage.

Ionizations at the insulation surface or within internal gas spaces may be evidenced by a partial discharge current I_{pd}. Ionizations are generally not present until the electric stress is sufficiently high to exceed the discharge inception voltage. Once the inception voltage is reached and discharges begin to occur, current pulses can be measured at the specimen electrodes. Given the intentionally slow response time of the

current measuring instrumentation, individual discharges are not accurately measured and displayed. Rather, ionizations attributed to numerous sites of discharges throughout the insulation are generally observed as an irregular, nonlinear current increase. Internal ionizations also cause an increase in observed capacitance which may be manifest as a sustained increase in measured current.

During ramped direct voltage tests, the total current I_t is measured and plotted against the applied voltage; the metering instrumentation cannot process the signal to separate the total current into individual current components. Consequently, to properly interpret deviations and abnormal characteristics in the current response, one must have an understanding of dielectric behavior during high voltage testing and experience in diagnosing insulation defects.

CHAPTER IV

COMPARISON OF THE RAMPED DIRECT HIGH-VOLTAGE METHOD AND OTHER DIAGNOSTIC TECHNIQUES

To compare the capabilities and limitations of the ramped direct-voltage test versus other diagnostic methods, an extensive, controlled laboratory experiment was conducted on stator winding coils that were manufactured with and without deliberate groundwall insulation defects. Specific defects were chosen to represent the types of insulation problems typically encountered during manufacture or as a result of aging. Working in cooperation with a winding manufacturer, a set of twelve custom-made multi-turn stator coils was specified and purchased, two coils with each type of defect. Coil designations and their corresponding defects are given in Table 4.1.

The experimental stator winding coils are insulated with Class F insulation and rated 13.8 kV. The conductor of the stator coil specimens is comprised of copper strands insulated with fused Dacron glass fibers. Eight strands were bundled into a conductor turn and then wrapped with B-stage resin rich mica paper with a glass fiber backing. The conductor was looped five times and then spread into the desired size and shape. The five-turn coil was pressed and heated to consolidate the conductor turns and inter-turn insulation. The groundwall insulation was applied next using the same B-stage epoxy mica paper tape used to build the turn insulation. A semi-conducting tape was applied over the slot section of the groundwall, and the coil was partially cured using a

short cycle of heat and pressure. The voltage stress grading treatment was applied next, and the coil was then put into an oven for the final post-bake cure.

The insulation defects incorporated into the coils during manufacture include internal conductive contamination, loose application of groundwall tapes, a reduced number of tape layers, inadequate final cure, and extreme thermal cycling.

Table 4.1

Stator Winding Coil Designations and Defects

Coil Designation	Description of Defect
237 and 253 - Standard production	Normal process and cure, without insulation defects – The "control coils" were randomly selected from standard production.
302 and 304 – No final cure	After taping and pressing, but before final cure – Coils were taken from standard production before post-bake. The turn insulation was pressed and heated. The groundwall insulation was not completely cured; it was cold pressed and heated at 160ºC for 10 minutes.
297 and 314 – Reduced tape layers	Normal process and cure, but with a reduction in the number of tape layers – In an effort to introduce voids and/or long shaped gaps into the groundwall, the number of tape layers was reduced for the same final leg width (*i.e.*, press-to-stop) dimensions. The mica tape is weighed before being applied. Thus, a reduction in tape quantity of 12.5 % provides a lower density groundwall with the right overall coil dimensions.
300 and 301 – Conductive contamination	Normal process and cure, but with internal conductive contamination – A 1-foot long section of conductive armor tape (10,000 ohms per square) was applied in the middle of the straight section of the coils.
296 and 305 – Loose tapes	Normal process and cure, but with loose or wrinkled insulating tapes – The normal tension of the automatic taping machine is around 16 lbs. Tape tension was lowered to 10 lbs, a reduction of 37 percent.
265 and 273 – Overheated	Normal process and cure, but overheated – The coils were subjected to extreme thermal cycling after post-bake. The coils were heated from 40 to 200ºC for ten cycles to create severe thermal stress and differential expansion at the copper-to-insulation interface.

It should be noted that the factory processes used to manufacture the defective coils could only be varied to pre-determined limits established by the automatic production machines and the specific insulating materials used. It was also necessary to ensure that the artificial defects would not be so severe as to preclude the groundwall insulation from withstanding the planned series of high-voltage tests. Consequently, the insulation defects fabricated for this investigation are not gross defects and would not necessarily prevent the stator coils from being put into service. Nevertheless, the artificial defects do permit a reasonable comparison between standard production coils and those that are abnormal.

The evaluation performed on the experimental coils included insulation resistance, polarization index, recovery voltage, dissipation factor, dielectric spectroscopy, partial discharge, and ramped direct high-voltage tests. A description of the techniques, results, and analyses follow. Test data are in Appendices B through F.

Insulation Resistance Measurements

Insulation resistance is defined as the quotient of an applied direct voltage over the resulting current ($R = V/I$). Measurements are made by applying a negative-polarity voltage step across the specimen electrodes, measuring the resulting current, and then calculating R. Capacitance charging and dielectric polarization effects cause the measured current to start out high and then decay exponentially with time. To maintain consistency, insulation resistance is determined at a specific time, typically one minute after the test voltage is applied. Insulation resistance measurements combine both surface and volume resistances, and are mainly used to detect moisture absorption,

conductive contamination, degree of cure, and cracks or fissures. Because dielectric polarization effects may persist beyond one minute, it should be recognized that the measured current may not accurately reflect only surface and volume conduction.

The applied voltage must be restricted to a value appropriate for both the voltage rating of the insulation system and the basic insulation condition. If the test voltage is too high, it may overstress the insulation and cause failure. Insulation resistance measurements of large generator and motor stator windings are generally obtained using voltages ranging from 500 to 10,000 volts. Insulation resistance may decrease slightly with an increase in applied voltage. However, for insulation in good condition, roughly the same insulation resistance will be obtained for any test voltage up to the withstand capability of the insulation. Guidelines for performing insulation resistance measurements are given in IEEE Std. 43-2000, "Recommended Practice for Testing Insulation Resistance of Rotating Machinery." [55] This document recommends a direct test voltage of 5,000 to 10,000 volts for insulation systems rated 13.8 kV. The stator coils manufactured for this investigation were tested at 5,000 volts dc conductor-to-ground.

Insulation resistance values are affected by the dielectric materials that comprise the insulation system as well as the manufacturing processes used to apply those materials. In general, insulation resistance varies directly with insulation thickness and inversely with conductor surface area. It is usually desirable to have the insulation resistance as high as possible; abnormally low values may indicate a problem with the quality or condition of the insulation system. Comparison of individual phases and

trending over time are generally the best means of evaluating insulation resistance measurements.

Increasing the temperature of a dielectric material provides additional thermal energy that frees charge carriers, thereby increasing the material's conductivity. As a result, changes in specimen temperature can significantly affect the insulation resistance measurements. To minimize the effects of temperature variations and permit more meaningful comparisons of insulation resistance values obtained at different temperatures, insulation resistance measurements may be normalized to a standard temperature. IEEE Std. 43-2000 recommends a common base temperature of 40°C. The temperature correction is made as follows

$$R_C = K_T R_T \tag{4.1}$$

where R_C is the insulation resistance (in megohms) corrected to 40°C, K_T is the insulation resistance temperature coefficient at temperature T°C, and R_T is the measured insulation resistance (in megoms) at temperature T°C.

The general rule-of-thumb is that insulation resistance is roughly halved for each 10°C rise in specimen temperature. Therefore, the value of K_T may be approximated by

$$K_T = (0.5)^{(40-T)/10} \tag{4.2}$$

It should be noted that the standard correction coefficient is based on tests performed in the 1950s on asphaltic insulation and this correction factor may not be appropriate for some polymer insulations. More recent experiments have indicated a temperature increase of 5 to 20°C may be required to effect a 50-percent reduction in resistance of modern polyester and epoxy insulations. It is generally recommended that

insulation resistance measurements be obtained at several temperatures on new stator windings while the insulation system is clean and in good condition in order to determine the most accurate temperature correction coefficient.

IEEE Std. 43-2000 considers the minimum acceptable corrected insulation resistance (in megohms) to be equal to the kilovolt rating of the insulation system plus one, that is

$$R_{\min} = V_{LL} + 1 \tag{4.3}$$

Thus, a minimum resistance of 14.8 megohms is required for the 13.8-kV coils manufactured for this investigation. Experience has shown that sound, high-quality insulation will typically exhibit hundreds to thousands of megohms of insulation resistance.

Insulation resistance measurements were obtained using an AVO Megger S1-5005®. Values were recorded every 15 seconds. To avoid temperature variations, all measurements were made on the same day under constant temperature conditions. Atmospheric humidity and surface contamination can also influence insulation resistance measurements and may affect the accuracy of the insulation condition assessment. Thus, the stator coils were stored and tested indoors in a clean and dry environment. On the day the coils were tested, the ambient temperature was 22°C and the relative humidity was approximately 38 percent.

To conduct the test, an individual coil was placed on a laboratory bench and a pair of rectangular aluminum electrodes was carefully clamped around each coil leg. The length and width of the electrodes were adjusted to match the dimensions of slot section

of the coil leg. The electrodes were connected together and then to ground to simulate the grounded stator core. The test voltage was applied to the coil conductor, and the current between the conductor and grounded electrodes was measured.

The maximum resistance that could be measured by the test instrument was 5 TΩ (5×10^{12} ohms). In most cases, the 5-TΩ limit was exceeded after 4 to 6 minutes of energization. To determine the 10-minute insulation resistance value needed to calculate the polarization index, a regression analysis of the raw data was performed by fitting a natural logarithmic curve to the insulation resistance data points using the least squares method of curve fitting (Appendix A). The measured 1-minute and extrapolated 10-minute insulation resistances are given in Table 4.2.

The tabulated insulation resistance values were not normalized for this investigation. Since the standard correction factor is less than unity (K_T is 0.29 at 22°C), normalizing the measurements would compress the readings and reduce the differences observed between the individual coils. Because all coils were tested under the same ambient conditions, relative comparisons are best made without attempting to correct to a standard temperature.

The insulation resistance measurements versus time for each of the stator coils are shown in Figures B.1 through B.12 in Appendix B. The best-fit logarithmic function and the R^2 value (square of the correlation coefficient) are included on the plot. A regression analysis is most reliable when the R^2 value is at or near 1. The R^2 value for all coils was 0.96 or higher except for coil 302, which had an R^2 value of approximately 0.85.

Table 4.2

Uncorrected Insulation Resistance (R) and Polarization Index Values

Coil	Defect	R @ 1 minute (TΩ)*	R @ 10 minutes (TΩ)**	Polarization Index (R_{10}/R_1)
237	Standard production	0.88	5.78	6.57
253	Standard production	0.94	6.73	7.12
302	No final cure	0.53	3.70	7.04
304	No final cure	0.53	3.38	6.43
297	Reduced layers	0.72	6.24	8.73
314	Reduced layers	0.80	5.97	7.51
300	Contamination	0.99	6.30	6.40
301	Contamination	0.86	5.98	6.99
296	Loose tapes	1.00	6.58	6.62
305	Loose tapes	0.92	6.42	7.01
265	Overheated	1.07	7.13	6.66
273	Overheated	1.00	7.13	7.13

* Measured insulation resistance
** Resistance value extrapolated from regression curve

The lowest 1-minute insulation resistance values were exhibited by coils that did not receive the final oven curing (0.53 TΩ each). This result reflects the larger number of residual ionic impurities that exist in incompletely cured epoxy resins. Under the influence of the applied field, the impurities conduct and thereby reduce the insulation resistance.

The highest 1-minute insulation resistance measurements were obtained from coils subjected to extreme thermal cycling after manufacture (1.00 and 1.07 TΩ). Thermally aged epoxy-based insulation generally exhibits higher resistance as a result of

chemical reactions that take place when the resin is heated. At high temperature, solvents and other volatile compounds evaporate, reducing the density of conductive, ionic species in the insulation. Thermal exposure also promotes further polymerization and cross-linking, again reducing the number of ionic compounds and, thereby, the conductivity of the insulating resin.

The standard production coils and those with internal contamination exhibited similar 1-minute insulation resistance values (0.88 and 0.94 TΩ versus 0.86 and 0.99 TΩ). This result suggests that the 1-foot section of conductive armor tape intended to "contaminate" the insulation has little effect on insulation resistance when measurements are made perpendicular to the conductor and coil surfaces. The internal conductive layer merely acts as an intermediate electrode but does not affect the field distribution or the bulk resistivity of the groundwall insulation. Under conditions of higher electrical stress, however, increased conduction due to internal contamination may become more pronounced.

Coils with loose tapes exhibited nominally higher 1-minute insulation resistance values than the standard production coils (0.92 and 1.00 TΩ). This result may be due to interfacial polarization at the heterogeneous phase structures within the insulation. Under the influence of an applied direct voltage, mobile charge carriers diffuse across the solid insulation up to gaseous spaces where they become stationary. Because some charges are trapped and prevented from reaching the opposite electrode, an apparent increase in insulation resistance occurs. As charges pile up, the surface charge density increases, as does the repulsive force between charge carriers. Eventually, the surface area becomes

"saturated" and no more charges may accumulate. At that time, the measured insulation resistance returns to a normal value. The quantity of charges that can accumulate at the gas-to-solid insulation interface increases with the size of the surface area between loose tape layers. The results of this test indicate only minor gas spaces exist in the bulk of the insulation as compared to the normal coils.

The coils with reduced tape layers were manufactured using the normal process, although the number of laps applied to build the groundwall insulation was reduced approximately 12.5 percent (by weight). The average 1-minute insulation resistance of these coils is 16.5 percent less than that of the standard production coils (0.72 and 0.80 TΩ). Because there is less solid material comprising the groundwall insulation, the density of the insulation is reduced and the volume resistance between the electrodes is decreased. Reducing the density of the insulation also results in a decrease in the number of polar molecules per unit volume of insulation. Consequently, the dipoles encounter less opposition from adjacent molecules as they attempt to orient in the direction of the applied field. As more dipoles become aligned, they tend to neutralize charge on the electrodes. To maintain the applied voltage, additional charges must be supplied to the electrodes, causing an apparent decrease in measured insulation resistance.

Although differences between the 1-minute insulation resistance values were observed for the various coil specimens, all values are in the thousands of megohms range and every coil would be considered fit for service according to the IEEE testing standard. This result reinforces the view that changes over time and differences between similar machines are most useful when evaluating insulation resistance measurements.

Unless a measurement is significantly outside of the expected range and additional information is available to assist with a diagnosis, it is generally difficult make more than go/no-go conclusions based on insulation resistance values.

Polarization Index

A polarization index test is similar to the insulation resistance test except that readings are taken at two time intervals, normally one and ten minutes after application of the voltage step. The quotient of these two readings (R_{10}/R_1) is termed the polarization index and gives an indication of insulation dryness, contamination, cure, and physical integrity. When a voltage step is applied to a stator winding, the insulation resistance first increases rapidly and then gradually approaches a fairly constant value. The resistance of a clean, dry winding in good condition may continue to increase for several hours after energization, whereas the resistance of a very dirty or wet winding may approach its maximum relatively quickly. Because the insulation resistance response is affected by the relative magnitudes of the polarization and conduction current components, the slope of the insulation resistance curve, or polarization index, is used as an indicator of insulation condition. Since the polarization index is the ratio of two measurements made under identical conditions, it is less sensitive to temperature variations than are insulation resistance values.

IEEE Std. 43-200 recommends a polarization index greater than or equal to 2 for Class F insulation. As shown in Table 4.2, the polarization indices for the experimental coils ranged from 6.40 to 8.73, significantly exceeding the minimum value recommended by IEEE. The highest polarization index values were exhibited by coils having a reduced

number of tape layers (7.51 and 8.73). As noted previously, the 1-minute insulation resistance values were lower than those of the standard production coils due to the reduced density of the groundwall insulation. However, the 10-minute insulation resistance values were similar to those of the normal coils. Since dc conduction remains relatively constant for the duration of the test, the increase in insulation resistance indicates a slight decrease in polarization current at 10 minutes. This suggests that dipole orientation is established more quickly, presumably because the internal forces opposing dipole movement are lessened when insulation density is reduced. As a result, the orientation process is more complete and the polarization current has been reduced at the 10-minute reading.

The lowest polarization index values were obtained from the stator coils with internal contamination (6.40 and 6.99), as expected for insulation with excess conduction. The polarization index values of the uncured coils were slightly lower than those of the standard production coils (6.43 and 7.04 versus 6.57 and 7.12), reflecting a decrease in resistivity at 1 and 10 minutes due to the availability of additional free charge carriers in incompletely cured resin. There were no significant differences between polarization indices for the normal coils and those that were overheated (6.66 and 7.13) and loosely-taped (6.62 and 7.01).

In general, polarization index is a somewhat ambiguous indicator of insulation defects and deterioration. Normal variations in conductivity and dielectric polarization characteristics exist for different insulating materials, affecting the insulation response and making it difficult to diagnose condition based solely on polarization index values.

As was noted for insulation resistance, trending polarization index values over time or comparing measurements against those obtained from similar machines are the most effective ways to use the polarization index results.

Recovery Voltage

Recovery or return voltage measurements (RVM) have been used to evaluate the polarization and discharge characteristics of an insulation system since these processes are strongly influenced by the quality and condition of the dielectric materials. To conduct the test, a step voltage is applied to one electrode of a completely discharged specimen while the other electrode is grounded. The specimen is charged for a short time then the voltage is removed and the specimen is briefly short-circuited. The recovery voltage is immediately measured across the electrodes under open circuit conditions using a high-impedance voltmeter. The recovery voltage response is plotted versus time. The main parameters of interest are the maximum value of recovery voltage, time to peak value, and initial slope of the recovery voltage.

The use of RVM to assess insulation condition first began in Hungary in the mid-1970s. Recovery voltage measurements on transformers and cables having oil-paper insulation have been used to evaluate moisture content and the extent of insulation aging [56,57]. Experience using RVM on rotating machine insulation is very limited and no guidelines or standards exist for this application. Therefore, the technique used during this investigation was based on procedures established for testing power transformers. The RVM equipment and measurement technique developed for testing machine insulation were provided by Kinectrics, Inc. of Toronto, Canada [58].

To test stator coil insulation, a 1000-volt step is applied to the conductor while electrodes over the slot section are grounded. After charging the geometric capacitance and polarizing the dielectric for 60 seconds, the voltage is removed and the coil is short-circuited for 15 seconds to discharge the geometric capacitance. While the short circuit is applied, the dielectric begins to depolarize. Thus, the duration of the short-circuit period is intentionally kept short to minimize the amount of dielectric depolarization. After the geometric capacitance has been discharged, the short circuit switch is opened. The excited dipoles and trapped space charge cause a return voltage to appear across the insulation. The recovery voltage is measured between the conductor and slot electrodes using a high-impedance voltmeter. The return voltage reaches a peak and then gradually decreases to zero due to conduction losses in the internal and external resistive components. Readings are taken every second for a minimum of 1000 seconds.

The recovery voltage curves for the stator winding coils are plotted in Figure 4.1. The maximum value of recovery voltage V_M, time to peak value t_M, and initial slope of the recovery voltage curve S_0 for each coil are listed in Table 4.3. The initial slope of the recovery voltage was calculated during the first 10 seconds of the depolarization cycle.

Thermal aging of oil-paper insulation promotes chemical reactions that increase the density of polar species, yielding the potential for a higher stored polarization charge and a corresponding increase in peak recovery voltage and shorter time to peak. Deterioration of polymer insulation, however, may either increase or decrease the polarizability of the insulation system. Ionic impurities, oxidation, and chemical changes leading to the formation of voids tend to increase the stored polarization charge.

Conversely, loss of volatiles resulting from thermal exposure reduces the density of ionic species so that the field-induced polarization is expected to decrease, thereby decreasing the peak recovery voltage. Conductive contamination and moisture absorption increase conduction and polarization losses, reducing the maximum value of recovery voltage and increasing the time to peak.

Given the many different deterioration mechanisms to which machine insulation may be subjected, it is more difficult to interpret variations in RVM parameters for polymer insulation than it is for apparatus insulated with oil-paper systems. To assist in evaluating the RMV measurements, correlation coefficients were calculated to measure the association between insulation resistance, polarization index, and RVM parameters. These results are presented in Table 4.4.

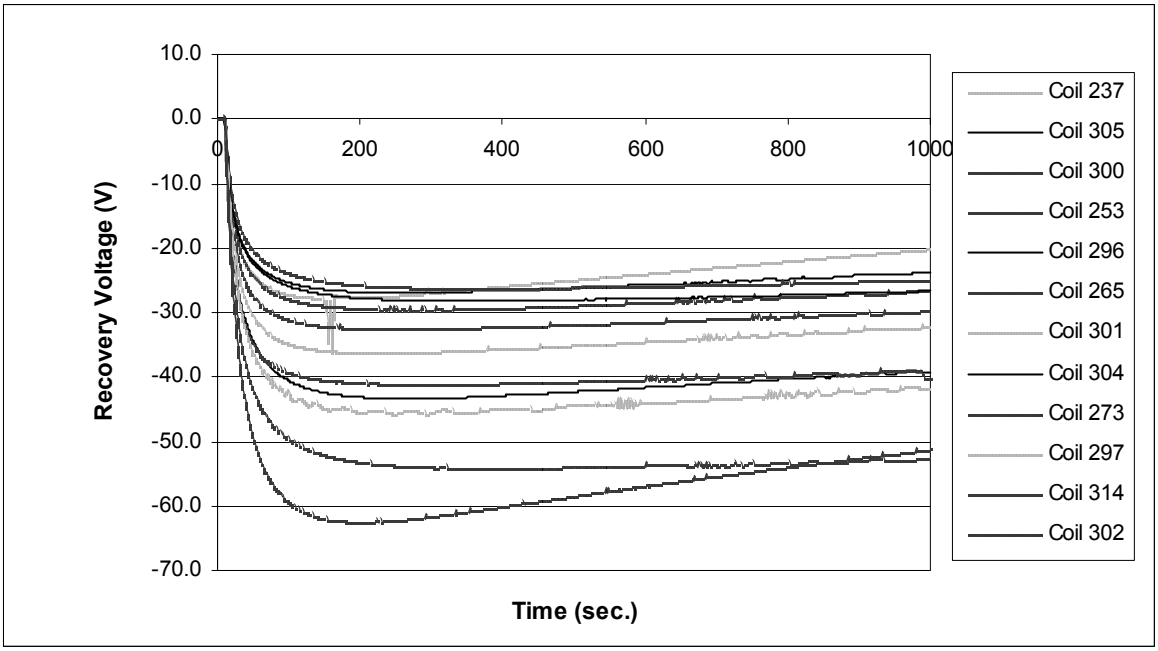

Figure 4.1 Recovery voltage versus time for stator coils manufactured with deliberate defects.

Table 4.3

Key Parameters from Recovery Voltage Measurements

Coil	Defect	Peak Recovery Voltage, V_M (volts)	Time to Peak Value, t_M (sec.)	Initial Slope, S_0 (volts/sec.)
237	Standard production	31.4	154	1.28
253	Standard production	29.6	236	1.33
302	No final cure	54.2	352	2.05
304	No final cure	43.4	243	1.74
297	Reduced layers	45.7	243	1.88
314	Reduced layers	62.5	188	2.25
300	Contamination	26.2	279	1.12
301	Contamination	36.3	224	1.60
296	Loose tapes	28.2	281	1.15
305	Loose tapes	27.0	233	1.30
265	Overheated	32.6	263	1.46
273	Overheated	41.2	280	1.72

Table 4.4

Correlation Coefficients for Insulation Resistance, Polarization Index, and Recovery Voltage Measurements

Correlation Coefficient	V_M	t_M	S_0
R @ 1 Minute	–0.65	–0.16	-
R @ 10 Minutes	–0.47	–0.21	-
Polarization Index	0.53	–0.29	–0.55

Correlation coefficients always have a value between –1 and +1. Positive correlations indicate that an increase in the first variable is associated with an increase in the second variable. Negative correlations indicate that as the first variable increases the second variable decreases. The magnitude of the correlation coefficient indicates how tightly the data points cluster about a straight line. A correlation coefficient equal to –1, for example, means that all data points fall on a perfectly straight line having a negative slope. A correlation coefficient of 0 indicates that the two variables are not associated.

In principle, low values of insulation resistance are expected to correlate with low values of peak recovery voltage and long times to peak. High values of polarization index are expected to correlate to high values of peak recovery voltage, shorter times to peak value, and greater initial slope. The correlation coefficients for the 1-minute and 10-minute insulation resistance versus peak recovery voltage are –0.65 and –0.47, respectively. This indicates a somewhat negative association exists between insulation resistance and peak magnitude of recovery voltage—a result that is contrary to the expected positive correlation. The correlation coefficients for the time to peak voltage versus the 1- and 10-minute insulation resistance measurements are –0.16 and –0.21, respectively. A negative correlation between these variables is expected. The correlation coefficient for the polarization index and peak recovery voltage is 0.53, indicating a fairly positive association, as expected. The correlation between the polarization index and initial slope is –0.55, a result that is opposite to the expected relationship.

Given the RVM data obtained during this investigation, it is not clear what conclusions can be drawn about the condition of the stator coil insulation. Some

investigators working with transformers have used the RVM technique to obtain the polarization spectra by varying the charge and discharge times to determine the conditions under which the recovery voltage reaches its maximum value [59,60]. It was not possible to obtain the polarization spectra during this investigation, although this approach may provide data that offers a more meaningful correlation between insulation resistance, polarization index, peak recovery voltage, time to peak, and initial slope. The practicality of using this type of procedure in the field is questionable, however, since it can take several hours of testing to determine the key RVM parameters of one specimen as the charge/discharge cycle is varied and repeated many times.

Dissipation Factor

The dissipation factor tan $\delta = \varepsilon'' / \varepsilon'$ represents the total loss per unit volume of insulation and is the net result of several phenomena occurring in the insulation structure. A relative increase in losses due to dielectric polarization and/or conduction will produce an increase in dissipation factor. Partial discharges at electrode edges, in voids, or within faults in the dielectric also result in higher dissipation factor measurements as the critical stress gradient is exceeded. Evaluation of tan δ measurements and Δ tan δ (tip-up) calculated at two different voltages provide a well-established means for assessing insulation quality and condition [62,63].

Testing of individual stator coils is typically conducted in the factory as a condition of acceptance, although the test may also be used as a maintenance test on complete windings to evaluate changes in insulation condition over time. Factory measurements usually involve guarding out the coil end windings so that only the slot

section of the insulation is tested. This is generally preferred since only the slot area of the winding is subjected to the full phase-to-ground voltage during operation and, therefore, the insulation in the slot section is most critical. Also, the rectangular geometry of the slot portion of the coil allows the groundwall insulation to be pressed and compacted during manufacture. The curved end windings, on the other hand, cannot be processed in this way so there is always less uniformity and compaction in the end turns. As a result, high dielectric losses in unguarded end windings may mask the relatively lower losses in the slot area. It is impractical to guard the end windings of several hundreds of coils installed in a machine, so it is difficult to directly compare factory and field dissipation factor values. Comparisons among similar machines and trending of measurements over time provide the best means of assessing insulation condition.

Dissipation factor measurements of the experimental coils were made in conjunction with the dielectric spectroscopy measurements (described later), under the same conditions of varying voltage (0.5 to 10 kV) and frequency (0.01 to 100 Hz). The stress grading treatment on the coil end windings was guarded out during the measurements. Because dissipation factor measurements are normally made at power frequency, tan δ versus voltage values measured at 60 Hz are given in Table C.1 in Appendix C. The data have been plotted and are shown in Figures C.1 through C.5. The value of Δ tan δ was calculated for each coil specimen by substracting tan δ measured at 2 kV (0.25 V_{LN}) from tan δ at 8 kV (1.0 V_{LN}). Results are summarized in Table 4.5. Acceptable limits for Δ tan δ of new equipment vary somewhat among purchasers;

however, a maximum allowed tip-up of 1 percent is typical. As shown in Table 4.5, all coil specimens met this requirement.

Table 4.5

Dissipation Factor (tan δ) and Tip-Up (Δ tan δ) measured at 60 Hz

Coil	Defect	tan δ @ 2 kV	tan δ @ 8 kV	Δ tan δ (%)
237	Standard production	0.006	0.008	0.2
253	Standard production	0.006	0.007	0.1
302	No final cure	0.008	0.010	0.2
304	No final cure	0.007	0.008	0.1
297	Reduced layers	0.006	0.008	0.2
314	Reduced layers	0.007	0.008	0.1
300	Contamination	0.005	0.011	0.6
301	Contamination	0.006	0.015	0.9
296	Loose tapes	0.006	0.009	0.3
305	Loose tapes	0.007	0.007	0.0
265	Overheated	0.006	0.009	0.3
273	Overheated	0.005	0.008	0.3

The standard production and overheated coils are compared in Figure C.1. As shown, tan δ of the thermally aged insulation is practically linear and identical to tan δ of the standard production coils for an applied voltage between 0.5 and 6 kV. This result indicates normal, proportional increases in electronic, atomic, and dipole polarization and corresponding losses with increasing applied stress. Above 6 kV, a nonlinear increase in losses is exhibited by both pairs of coils, although the increase is more pronounced in the case of the overheated coils. This difference may be attributed to chemical and/or physical changes in the insulation structure of the overheated coils as a result of thermal

deterioration. Overheating destroys chemical bonds, creates ionic impurities, promotes oxidation, and leads to the formation of voids. These changes tend to increase dipole and interfacial polarization and partial discharges, leading to increased losses as evidenced by higher values of tan δ and Δ tan δ.

The coils with no final cure are compared to the standard production coils in Figure C.2. The uncured coils exhibit dissipation factor measurements which are approximately 20 percent higher over the entire range of test voltage, indicating a higher level of losses due to increased conduction and electronic, atomic, and dipole polarization effects. The uncured coils also display a subtle characteristic of increasing tan δ from 0.5 to 4 kV and then decreasing tan δ between 4 and 6 kV. Above 6 kV the loss tangent again increases with applied voltage. None of the other experimental coils exhibited this behavior. The underlying physical cause of this response is unknown; however, it may be associated with dipole polarization involving particular ionic species present as a result of incomplete curing. Further investigation is warranted to understand this unique characteristic and to assess its ability to distinguish uncured insulation from other defects.

Figure C.3 compares the coils with internal conductive contamination versus the standard production coils. All four coils exhibit similar values of tan δ when tested below 4 kV. This result closely correlates with the insulation resistance and polarization index measurements described earlier where negligible differences were observed between the contaminated and normal coils when tested at 5 kV dc. As the applied stress exceeds 4 kV ac (which is equal to 5.66 kV peak), however, the contaminated coils exhibit a marked increase in tan δ as compared to the standard production coils. This

response suggests that the carbon contamination within the insulation significantly increases conduction-related losses when the voltage exceeds a critical value. As shown in Table 4.5, the tip-up value of both contaminated coils was 0.9, many times higher than that of all other specimens and approaching the standard 1 percent $\Delta \tan \delta$ limit.

Figure C.4 presents the dissipation factor measurements of coils having a reduced number of insulating tape layers. Comparison of these coils to the standard production coils are expected to yield minimal differences in $\tan \delta$ and $\Delta \tan \delta$ over the range of applied voltage since the loss tangent measures the ratio of losses to displacement, and should be independent of specimen size, insulation thickness and, presumably, insulation density. As seen in Figure C.4, three of the coils exhibit the expected response of gradually increasing $\tan \delta$ with increasing voltage. A notable discrepancy is observed with coil 314 (reduced layers), however, which exhibits a significantly elevated dissipation factor value at 0.5 kV with tan δ continuing to decrease until the applied voltage exceeds 6 kV. Coil 314 also exhibited the largest value of peak recovery voltage V_M of all coil specimens during the recovery voltage measurements. The divergent behavior of coil 314 may reflect lower density insulation, although it is not evident why the losses would first be high and then decrease with increasing voltage. Further testing is required to confirm these results and to conclusively assess the anomalous response exhibited by coil 314.

Figure C.5 compares the coils with loose tapes against the standard production coils. Between 2 and 6 kV, the dissipation factor of coils 296 and 305 (loose tapes) averages approximately 14 percent higher than the dissipation factor of the normal coils.

This difference may reflect the presence of interfacial polarization in internal voids between loose tape layers. Above 6 kV, the dissipation factor values of the coils with loose tapes track those of the standard production coils, and the value of $\Delta \tan \delta$ for both sets of coils are similar. Contrary to what might be expected for insulation having internal air spaces, no clear evidence of increased losses due to partial discharges is indicated.

Dielectric Spectroscopy

The complex permittivity $\varepsilon^* = \varepsilon' - j\varepsilon''$ of many dielectric materials varies significantly with frequency, reflecting differences in the displacement and loss phenomena corresponding to the dielectric polarization mechanisms. Plots of ε' and ε'' versus frequency can be obtained using dielectric spectroscopy measurements, and the ε' and ε'' spectra may be analyzed to assess changes or abnormalities in the insulation system.

In principle, dielectric spectroscopy may be used to detect dipole orientation effects and, thereby, an increase in polar molecules due to aging, moisture absorption, contamination, and incomplete curing. Changes in permittivity in the frequency domain may also reflect space charge polarization or partial discharges that can occur in composite insulations having internal voids or delaminations. The plot of ε'' versus frequency may be used to evaluate increased losses due to charge carrier movement, polarization effects, and partial discharges.

The dielectric spectroscopy method of measuring permittivity and dissipation factor versus frequency was developed in Europe and has typically been applied to

transformers and extruded polymeric or oil-paper cables. Very little information exists in the literature on the use of this technique to diagnose rotating machine insulation.

The dielectric spectroscopy tests conducted during this research investigation were performed using a WaBTech IDA, a commercial instrument capable of making ε' and ε'' measurements in the frequency range of 0.0001 to 1000 Hz. The WaBTech uses an active bridge design whereby a reference signal is generated in phase quadrature with the current measured on the test object. The dielectric loss is related to the phase difference between the reference signal and applied voltage. The test voltage was obtained using a Trek 20/20 amplifier. Both the bridge and power supply were under computer control and the entire measurement sequence was automated.

Displacement and loss measurements were obtained on the stator coils across four decades of frequency, from 0.01 to 100 Hz. The applied voltage was varied from 0.5 to 10 kV rms. At the higher voltages (8 and 10 kV) the data set does not span the entire frequency range due to limitations in the power supply output. The stress grading coating on the coil end windings was guarded out during these tests.

Analysis of the dielectric spectroscopy data indicates that measurements made at the lowest frequencies provide the greatest distinction between the standard production and defective coils. Displacement and loss measurements versus voltage obtained at 0.01 Hz are given in Table D.1 in Appendix D. Figures D.1 through D.10 graphically present the ε' and ε'' versus voltage characteristics.

Figure D.1 shows that the magnitude and rate of increase of displacement ε' is consistently higher in the overheated coils as compared to the normal coils. The

dielectric loss factor ε'' is also higher in the overheated coils, as illustrated in Figure D.2. Thermal aging of organic insulation promotes irreversible chemical reactions, such as decomposition and oxidation. These changes may create internal voids and/or increase the density of polar molecules, resulting in partial discharges and increased dipole polarization along with their corresponding losses, particularly with increased voltage. Thermal aging also tends to decrease conduction losses. As evidenced by these test results, the ε' and ε'' characteristics of the overheated coils correlate well with their predicted response.

Uncured insulation has a higher density of polar molecules and charge carriers due to incomplete cross-linking and the presence of residual catalysts and volatiles. The increased number of polar species results in a much larger value of ε', as shown in Figure D.3. Increased dipole polarization and conduction also contribute to significantly greater dielectric losses. As shown in Figure D.4, not only are the losses in the uncured insulation greater, they exhibit a unique characteristic. As the stress across the insulation is increased from 0.5 to 6 kV the losses decrease, whereas above 6 kV the losses increase with voltage. The initial decrease and eventual increase in ε'' is most pronounced at very low frequencies and appears to be a distinctive trait of incompletely cured insulation. All other coil specimens displayed a steady increase in ε'' over the entire range of applied voltage.

The underlying physical cause of this unusual response is unknown. However, since the displacement component consistently increases with voltage, the drop in dielectric losses does not appear to be related to polarization effects. Additional tests are

necessary to further investigate this interesting phenomenon. (For instance, the effect of test duration could be explored.) While the 60-Hz tan δ measurements have been traditionally used to provide a practical method of screening for incompletely cured insulation in the factory and, perhaps, in the field, this investigation suggests that very low frequency measurements are much more sensitive and discerning.

The displacement and loss curves of the contaminated coils, shown in Figures D.5 and D.6, respectively, are consistently higher than those of the normal coils, indicating increased polarization and losses over the entire range of applied voltage. A sharp rise in the slope of the displacement curve of the contaminated coils is evident at 6 kV. A similar increase above 4 kV appears in the loss curve of the contaminated coils. The knees in the displacement and loss curves are likely due to conduction processes and/or discharges in the carbon-contaminated region of the groundwall insulation. These phenomena appear to be triggered when the electric stress exceeds a critical value. Elevated values of dielectric polarization, partial discharges, and losses were not evident during the insulation resistance measurements, presumably because the applied voltage (4 kV dc) was below the initiation voltage.

By reducing the number of tape layers while maintaining the total thickness of the groundwall, the density of the insulation is lowered. Although this type of defect may not significantly influence tan δ which is a relative measure of loss to displacement, it is expected that the individual components of permittivity will reflect differences in polarization and losses when insulation density is varied. Measurements suggest that a reduction in insulation density may allow dipole polarization to take place more easily

because the dipoles have more space and encounter less opposition, allowing them to become oriented with the applied field more quickly and completely. This finding is supported by the recovery voltage measurements in which coils 314 and 297 (reduced layers) exhibited the first and third highest values of peak recovery voltage V_M and slope S_0, respectively. Dipoles excited during the brief charging period are responsible for the magnitude of V_M. Hence, the more complete the polarization process, the greater the stored charge and the higher the value of V_M. The polarization indices of coils 297 and 314 were also the highest of all coils, another indication of the degree of dipole polarization. The displacement ε' versus voltage curves are shown in Figure D.7, where the standard production coils are compared to those with reduced layers. Both coils with reduced insulation layers, and coil 297 in particular, exhibit increased displacement. This is another indication that the polar molecules encounter less interference when attempting to align with the alternating field. As illustrated in Figure D.8, dielectric losses are also higher in the coils with reduced insulation density. Since inelastic dipole displacement has losses associated with it, the losses exhibited by the coils with reduced insulation layers are higher. As expected, the losses of coil 297 are the highest.

Loosening the tension on the automatic taping machine was intended to introduce wrinkles and voids between overlapping tape layers where space charges could accumulate and partial discharges could occur. As shown in Figure D.9 this appears to have been successful, as evidenced by significantly higher values of ε' in the case of the coils with loose tapes. Along with an increase in dipole and possibly interfacial

polarization, Figure D.10 shows the accompanying dielectric losses are also greater in the coils with loose or wrinkled tapes.

Partial Discharges

Partial discharges in stator windings are manifest by positive and negative current pulses of a few nanoseconds in duration. A single partial discharge is equivalent to the injection of a rapidly rising voltage and current pulse at the point in the stator winding where it occurs. Two traveling waves will be set up moving in opposite directions, one to the line terminal and the other to the neutral terminal. The discharge pulse will propagate through the winding as in a transmission line with a series inductance and capacitance to ground dependent on the winding configuration. As the wave propagates toward the winding terminals it becomes attenuated and the wavefront becomes longer.

Since the early 1940s, considerable partial discharge data have been obtained on electrical equipment such as transformers, capacitors, cables, and rotating machines in an effort to quantify the level of discharge activity and determine its source. [64] The early test techniques measured radio interference voltage (RIV), and peak values were typically recorded from an analog meter in milivolts. Later, oscilloscopes and bridge circuits were used to evaluate partial discharges in terms of pico-coulombs. Another type of analog detection system utilized a high frequency ferrite-cored coil to detect localized partial discharge currents. More recently, advances in digital electronics have made microprocessor-based measuring and analysis techniques possible. Much progress has been made in the development of partial discharge instrumentation in terms of bandwidth selection, calibration, and pulse discrimination. These advances have especially

enhanced the use of partial discharge measuring equipment in electrically noisy environments, such as power generating plants.

IEEE Std. 1434-2000, "Trial-Use Guide to the Measurement of Partial Discharges in Rotating Machinery," describes typical systems for conducting off-line partial discharge (PD) measurements on individual form-wound coils [65]. The PD measurements described herein were obtained using a standard method and involved energizing an individual coil specimen to 8 kV rms conductor-to-ground with an external alternating voltage power supply. Discharges were measured using a differential coupler system with two 80-pF epoxy-mica capacitive couplers (acting as high-pass filters) terminated in 50 ohms at the detector. This configuration makes it possible to discriminate between PD from the test specimen versus external electrical noise by using the propagation characteristics of PD pulses. An Iris Engineering PDA-IV Analyzer was used as the detection system. This instrument is equipped with a phase-resolving pulse height analyzer which can determine the number and magnitude of pulses (measured in mV) as well as the phase position relative to the applied alternating voltage at which each PD event occurs. The bandwidth of the detection system is 0.1 to 350 MHz.

Partial discharges are usually much higher immediately after voltage application and gradually reduce to a lower value with time. Therefore, a 5-minute pre-energization or conditioning time is generally recommended to ensure conditions have stabilized and the PD measurements will be repeatable and representative of in-service conditions. During this research investigation, the supply voltage was held for between 10 to 15 minutes prior to making the measurements to ensure a steady-state condition was

reached. The stress control coating on the end windings was fully functional. The ambient temperature was approximately 22°C and the relative humidity was approximately 18 percent.

The two parameters generally used to gauge the severity of partial discharge activity in stator windings are the maximum pulse magnitude and the pulse repetition rate. The peak positive and negative discharge magnitudes are designated QM+ and QM–, respectively, and are evaluated with respect to the pulse count rate. A minimum of 10 discharges per cycle must be detected in order for the QM value to be recorded for a given range of pulse magnitudes. In general, a deteriorated winding will exhibit increased partial discharge activity, evidenced by higher discharge magnitudes and more discharges per second.

To standardize interpretation of partial discharge measurements and aid in trending PD activity over time, the normalized quantity number, or NQN, was developed to represent the average condition of the stator winding insulation [52]. The NQN+ and NQN– values are proportional to the area under the relevant pulse height analysis line (pulse count rate versus peak magnitude curve) and are related to the total charge transfer due to positive and negative partial discharges, respectively. The ratio of NQN+ to NQN– is useful in determining whether the deterioration is at the stator coil surface, within the bulk of the insulation, or at the copper conductor-groundwall insulation interface.

Partial discharge measurements were recorded using three different scales: 2 to 32 mV, 5 to 85 mV, and 20 to 320 mV. No discharges were detected above 320 mV.

The scale showing the highest values of NQN and QM for each specimen was selected from the test data and the graphical results are presented in Figures E.1 through E.12 in Appendix E. Table 4.6 summarizes the peak positive and negative discharge magnitudes (QM+ and QM–), total positive and negative discharge activity (NQN+ and NQN–), and the ratio of the positive and negative charge energy (NQN+/NQN–).

Table 4.6

Partial Discharge Summary Variables

Coil	Defect	QM+ (mV)	QM– (mV)	NQN+	NQN–	NQN + / NQN –
237	Standard production	0	0	12	21	0.6
253	Standard production	0	0	n/a	2	n/a
302	No final cure	0	0	n/a	2	n/a
304	No final cure	0	0	24	23	1.0
297	Reduced layers	0	0	4	9	0.4
314	Reduced layers	81	126	144	228	0.6
300	Contamination	0	0	7	13	0.5
301	Contamination	0	0	19	10	1.9
296	Loose tapes	0	0	9	15	0.7
305	Loose tapes	35	36	18	22	0.8
265	Overheated	51	87	72	148	0.5
273	Overheated	36	28	37	20	1.8

Acceptable levels of PD activity vary with the type of stator winding insulation system as well as the detection technique used to make the measurements. PD detectors having different characteristics (e.g., detection impedances, filters, and amplifiers) give rise to different reported values of partial discharges. Furthermore, because PD pulses

become attenuated and distorted as they travel, the distance from the discharge site to the detector may also affect the PD measurement. There are presently no standards governing the requirements of PD measuring systems. Thus, experience and judgment must be used when classifying PD levels as being normal versus unusually high. According to guidance provided by the manufacturer of the PD instrument used in this investigation, for a complete epoxy-mica winding installed in a machine, an NQN above 250 indicates significant partial discharge activity is occurring. If the positive PD activity is at least two times higher than the negative activity, the discharges are primarily occurring on the surface of the insulation, either between the coil and the slot or in the endwinding area outside of the slot. If the negative discharges are significantly higher than the positive discharges, then the deterioration is most likely to be at or near the copper conductor surface. Discharges within the bulk of the insulation result in approximately equal positive and negative partial discharge activity. Tests of individual coils are usually performed in the factory by coil manufacturers, therefore, results are generally considered proprietary and not published. Thus, for the purposes of this investigation, comparison between coil specimens is the best means of evaluating differences in test results.

As shown in Table 4.6, all stator coils exhibited NQN values below the entire-winding threshold of 250. The standard production coils (237 and 253), the coils with no final cure (302 and 304), and the contaminated coils (300 and 301) all exhibited negligible values of positive and negative partial discharges. One of the coils with reduced tape layers (297) also showed only minimal signs of PD. The second coil with

reduced layers (314), however, exhibited considerably more PD than all of the other specimens. The peak positive and negative pulses were 81 and 126, and the positive and negative discharge activity was 144 and 228, respectively. In other tests conducted during this investigation, Coil 314 also exhibited the largest value of peak recovery voltage V_M and a significantly elevated dissipation factor. The partial discharge measurements further support the conclusion that the reduction in the number of tape layers was more successful in compromising the groundwall insulation of Coil 314 than of Coil 297. Coil 314 also exhibited a somewhat negative pulse predominance, suggesting that discharges were mainly occurring near the copper conductor.

One of the coils with loose tapes (296) exhibited negligible PD. The other coil (305) displayed just slightly higher values, although not enough to be considered significant. The two thermally deteriorated coils (265 and 273) displayed somewhat elevated values of peak and total discharge activity as compared to the other specimens (with the exception of Coil 314). Coil 265 exhibited slightly negative pulse predominance, whereas coil 273 exhibited slightly positive pulse predominance. These results suggest that cyclic overheating may damage the surface treatment as well as the bond between the copper and groundwall insulation.

Ramped Voltage Tests

When performing a ramped voltage test, an automatic high-voltage power supply is used to linearly increase the direct voltage output from zero up to some maximum value at a constant ramp rate, typically 1 to 2 kilovolts per minute. The current response versus applied voltage is measured and plotted, and the test results are used to evaluate

the condition of the insulation by noting deviations from the normal shape of the curve. The application of a ramped voltage, rather than discrete voltage steps, effectively linearizes the normal geometric capacitance charging, electronic, atomic, and orientation polarization, and conduction components of insulation current so that unusual deviations in the response are more easily seen.

The polarity of the direct high-voltage may be either positive or negative. Historically, however, negative polarity tests have been thought to be more searching due to the effect of electroendosmosis. This phenomenon occurs when moisture migrates through a solid material under the influence of an applied electric field. The net movement of water molecules is generally toward the negatively-charged electrode. Thus, moisture on the surface of the insulation tends to be driven into cracks and fissures during negative-voltage tests, making such defects more likely to be detected.

The ramped voltage test equipment used during this investigation was designed and constructed in the Hydroelectric Research Laboratory of the U.S. Bureau of Reclamation in Denver, Colorado [15]. In accordance with IEEE Std. 95-1977, "Recommended Practice for Insulation Testing of Large A-C Rotating Machinery with High Direct Voltage," tests were performed on individual coils to 25 kV conductor-to-ground using a ramp rate of 1 kV per minute. The ambient temperature was 21°C and the relative humidity was 27 percent.

The current versus voltage plots are shown in Figures F.1 through F.12 in Appendix F. The key features of the test curves are the magnitude of measured current, the increase in the current with respect to voltage, and the appearance of nonlinearities or

other unusual characteristics. To facilitate comparison among the coil specimens, the magnitude of measured current at 5 kV, the initial slope of the current response, and the voltage at which the trace first becomes nonlinear have been determined from the test curves and are summarized in Table 4.7. Because the physical dimensions of the coils and thickness of the insulation were held to close tolerances, the geometric capacitance will not vary significantly between specimens. Thus, differences among coils are mainly attributed to variations within the groundwall insulation.

As evidenced in the figures, all curves exhibit a step increase in current as the voltage is first applied, the result of geometric capacitance charging and electronic, atomic, and dipole polarization in reaction to the electric field. The sharpness of the rise reflects the relatively short time lag between the changing field and the corresponding dielectric response. The slope of the traces ($\Delta I/\Delta V$) is also fairly flat, particularly during the lower voltage portion of the test. A steep initial rise and relatively flat trace are characteristic of epoxy-mica insulation in which the dielectric materials exhibit low dipole polarization and minimal conduction. Asphaltic and polyester-based insulations tend to exhibit steeper *I-V* curves, mainly due to the increased polarizability of these binder materials. Insulations comprised of sheet mica or large mica flakes also display greater polarizability as compared to those manufactured with mica paper.

The "initial" slope of the curve has been defined as the change in current between 5 and 10 kV divided by the corresponding increase in voltage. This portion of the test curve was selected to represent the slope because the trace is beyond the initial step response and is generally absent of any voltage-related anomalies. Therefore, variation

among coil specimens is principally due to differences in polarization, particularly dipole and space charge polarization. As shown in Table 4.7, the values of slope ranged from 0.370 to 1.235 $\times 10^{-3}$ μA/kV, with the majority of the coils exhibiting a slope of 0.556 $\times 10^{-3}$ μA/kV. The coils with no final cure exhibited the greatest slope, nearly double that of the average slope. This result is indicative of insulation having incomplete polymerization and cross-linking, and a corresponding greater density of polar species. The lowest slope, 0.370 $\times 10^{-3}$ μA/kV, was exhibited by a coil with loose tapes (305); however, the small difference as compared most of the other coils does not appear to be significant.

Table 4.7

Key Features of the Ramped Voltage Test Curves

Coil	Defect	Initial Slope* ($\times 10^{-3}$ A/kV)	I @ 5 kV (μA)	Nonlinear @ (kV)
237	Standard production	0.556	0.117	17.1
253	Standard production	0.556	0.119	16.3
302	No final cure	0.926	0.131	12.9
304	No final cure	1.235	0.127	15.1
297	Reduced layers	0.556	0.118	9.6
314	Reduced layers	0.556	0.119	13.3
300	Contamination	0.556	0.118	8.0
301	Contamination	0.926	0.119	7.0
296	Loose tapes	0.556	0.119	11.6
305	Loose tapes	0.370	0.116	10.5
265	Overheated	0.556	0.111	11.6
273	Overheated	0.741	0.113	13.3

* $\Delta I/\Delta V$ calculated between 5 and 10 kV

The slope from the ramped voltage test response was compared to the 0.01-Hz displacement and loss curves obtained during the dielectric spectroscopy measurements (Figs. D.1 through D.10). Since an applied voltage of 3.5 to 7.0 kV rms has a peak value of 5 to 10 kV, this region of the dielectric spectroscopy curves was evaluated. It might be expected that specimens showing the greatest increase in loss and/or displacement over the specified voltage range might also exhibit the greatest slope in the ramp test curves due to increased dipole polarization, losses, and conduction. Similarly, coils exhibiting the smallest change in loss or displacement might also display the smallest slope in the *I-V* response of the ramped voltage test. Although one coil with loose tapes (305) did exhibit both the least change in loss versus voltage and the lowest slope, no other correlations were evident. For example, the incompletely cured coils, which showed a significantly greater slope than the other coils, did not display the highest increase in loss or displacement during the dielectric spectroscopy measurements.

The magnitude of current measured at 5 kV was read from the ramped voltage test curves to analyze variations in polarization, loss and conduction phenomena at a specific value of applied voltage. (No evidence of ionizations were observed on any of the test results at this voltage level.) Eight of the twelve specimens exhibited current in the range of 0.116 to 0.119 μA. The lowest values of current, 0.111 and 0.113 μA, were obtained from the overheated coils (265 and 273). This result correlates with the insulation resistance measurements where the thermally aged coils exhibited the highest 1- and 10-minute resistance values when energized at 5 kV dc. This result is expected since exposure to high temperature causes solvents and other volatile compounds in the

insulation to evaporate, reducing the density of conductive, ionic species. Thermal cycling also increases polymerization and cross-linking, again reducing the number of ionic compounds and, thus, the conductivity of the insulating resin. As evidenced in Figs. F.3 and F.4, the low current effect persists over the entire range of test voltage, and results in the current traces of the overheated coils having a negative offset as compared to the traces of all other specimens. The highest current measurements, 0.131 and 0.127 μA, were obtained from the coils with no final cure (302 and 304). This can be observed in Figs. F.5 and F.6, where the curves are shifted upward, reflecting the greater number of residual polar molecules and conductive impurities that exist in incompletely cured epoxy resins. This result also correlates with the insulation resistance measurements where the lowest values of 1- and 10-minute insulation resistance were exhibited by the incompletely cured coils. Analogous results were observed during the dielectric spectroscopy measurements, where the magnitude of the displacement and loss values exhibited by the uncured coils were the highest of all specimens.

Although a gradual, steady increase in current with voltage is expected due to slight increases in dipole polarization, losses and conduction as the electric stress is raised, a sudden or nonlinear increase may indicate abnormal dipole or space charge polarization effects, volume or surface conduction, and/or ionization losses. Such indications are known to signal the presence of defects or other insulation problems. Thus, the voltage at which the *I-V* response becomes nonlinear is an important feature of the ramped voltage test curve. The curves of the standard production coils (253 and237), shown in Figures F.1 and F.2, are the smoothest of all traces and appear linear until the

applied voltage exceeds 16.3 and 17.1 kV. Above that point, the curves exhibit a minor increase in slope and an irregular, spiking behavior. These changes likely indicate the onset of partial discharges or increased conduction, and may be either surface or volume effects. It is not unusual for stator coils to exhibit minor nonlinearities at high stress levels. Since the coils manufactured for this investigation are rated 13.8 kV rms phase-to-phase, only those installed at the line end of the winding would be energized to the full 8 kV conductor-to-neutral during operation, which is equivalent to approximately 11.3 kV peak. This voltage is well below the point at which the current response becomes nonlinear. Therefore, in their present state, the standard production coils would not experience damaging ionization, polarization, or leakage current effects. In the case of a complete, in-service winding, changes in the trace over time would be used to monitor insulation condition and rate of deterioration.

The *I-V* traces of all other coils exhibited nonlinearities at a lower voltage than those of the standard production coils. The two specimens with internal conductive contamination (300 and 301), shown in Figures F.7 and F.8, begin to exhibit pronounced spiking behavior and an increase in slope around 7 and 8 kV, the lowest voltage of all coils. This erratic behavior is likely caused by abnormal conduction that begins to occur as the applied stress exceeds a critical value. Partial discharge measurements performed at 8 kV did not reveal any abnormal ionizations. During the dissipation factor measurements (Figs. C.1 through C.5), however, the coils with internal contamination exhibited typical values of tan δ at 2 kV and the highest values at 8 kV, making the tip-up (Δ tan δ) the greatest of all specimens. The tan δ measurements began to increase sharply

around 5 kV rms or 7 kV peak, which is approximately the same voltage at which the erratic behavior is first exhibited in the ramped voltage test curves. During the dielectric spectroscopy tests, the displacement and loss values were fairly flat until the applied voltage exceeded 5 to 6 kV. No indications of problems with the contaminated coils were detected during the insulation resistance measurements, which were performed at 5 kV dc per the accepted testing standard. Because insulation resistance measurements are generally performed using a test voltage that is well below the normal peak operating stress, partial discharges, nonlinear conduction, or other abnormal effects that could be present during use often go undetected by this test method.

The *I-V* responses obtained from the coils with loose tapes (296 and 305) and reduced layers (297 and 314), shown in Figures F.9 through F.12, displayed only subtle variations compared to the responses of the normal coils; the voltage at which the traces become nonlinear is lower and the overall increase in slope above this point is greater, most likely due to increased dipole and space charge polarization. The most pronounced variations are exhibited by a coil having reduced layers (297). Of the two coils with reduced layers, this one exhibited the highest increase in displacement and loss values between 6 and 10 kV during the dielectric spectroscopy measurements, as well as the highest increase in dissipation factor measurements in the same range. The partial discharge test performed on coil 297, however, did not indicate elevated discharge levels.

Summary of Comparative Test Results

A series of comparative diagnostic tests was made on standard production coils as well as on coils with reduced groundwall insulation density, loosely applied tape layers,

no final post-bake cure, internal conductive contamination, and extreme thermal degradation. Tests included insulation resistance, polarization index, recovery voltage, dissipation factor, dielectric spectroscopy, partial discharge, and ramped direct high-voltage tests. The results of the investigation provide a means of comparing the ramped voltage test against other available diagnostic techniques—both conventional and novel.

Insulation resistance and polarization index tests were confirmed to be best suited for identifying gross defects that affect the conduction properties of the insulation, such as incomplete cure and thermal deterioration. Minor variations among the other specimens were observed, although all resistance and polarization index values were well within limits established by testing standards.

The recovery voltage and partial discharge measurements did not reveal clear differences between the specimens that would lead to consistent identification of insulation problems. Although on-line partial discharge measurements of complete windings are widely used and have proven to be successful in monitoring problems with in-service machines, trending of discharge levels over time is generally required to determine if damaging discharges are occurring and if the winding is at risk of failure. It is worth noting that the particular test equipment used to perform the partial discharge measurements for this investigation was designed to optimize PD measurements on full stator windings rather than on individual coils. More definitive partial discharge results may have been obtained if a laboratory- type test instrument had been available for making the PD measurements.

Intriguing results were obtained from the dielectric spectroscopy tests, where the dissipation factor and the displacement and loss components of permittivity measurements were made. Results clearly showed that measurements at the very low frequency end of the spectrum are better at detecting variations among the coil specimens because they allow more time for the sluggish orientation polarization, space charge, and conduction processes to be more fully realized. The dielectric spectroscopy technique has not been used in the field on complete machines, but the possibilities appear promising and more research is warranted. One issue that may present a problem relates to guarding out the voltage stress grading treatment on the end windings. Although guarding is feasible in the laboratory, it is not practical on a complete stator winding comprised of 300 to 400 coils, each coil having four graded end arms. This difficulty may impact the quality of the data that can be obtained using this technique.

Ramped direct high-voltage test results were examined and, as expected, the standard production coils exhibited the most linear current response over the full range of applied voltage. Also, the magnitude of current was found to correlate with the 1- and 10-minute insulation resistance values, particularly in the case of the overheated and incompletely cured coils. The ramp test results of the contaminated coils also correlated with the dielectric spectroscopy and dissipation factor measurements which indicated an abrupt increase in losses as the stress level exceeded a critical value. The ramped voltage test results did not show significant differences between the coils with loose tapes and reduced insulation density. In fact, none of the diagnostics tests indicated clear and consistent differences between these specimens, suggesting that the variations within the

insulation achieved during manufacture may not be very severe. With operation and the concurrent thermal cycling, however, these defects would likely become more distinct and begin to exhibit greater differences, particularly with respect to dipole and space charge polarization and partial discharge levels. Although these types of deficiencies may not produce immediate failures, they do lead to accelerated aging and a reduced service life.

CHAPTER V

RAMPED DIRECT HIGH-VOLTAGE TEST RESULTS FROM IN-SERVICE MACHINES

Field experience with ramped direct high-voltage tests has shown that this method can be used to detect cracks and fissures, moisture absorption, tape separations, conductive contamination, lack of resin cure, and internal delaminations. The following practical examples illustrate how ramped voltage test results have been used to assess whether an insulation system is in good condition or if a serious groundwall defect threatens to cause the machine to fail while in service. These results are taken from actual machines, and the analyses and conclusion were confirmed using physical inspection, corroborating electrical tests, insulation dissections, and/or other means [68,69]. The ramp rate for all the examples given here is 1 kV per minute.

Asphalt-Mica Insulation

Different insulation systems and manufacturing processes are known to be susceptible to specific types of defects and modes of deterioration. Asphaltic insulations exhibit girth cracking at or near the ends of the stator core due to compound migration and tape separations caused by differential thermal expansion and thermal cycling. Asphalt-based systems are also vulnerable to moisture absorption through cracks and fissures which result from heat-induced volatilization, chemical oxidation, and molecular

cracking of the asphalt. (Electric space heaters are often installed in the stator air housings to keep the winding a few degrees above the dew point to prevent moisture from condensing on winding surfaces during machine outages.) Asphaltic windings sometimes appear to be "self-healing" because of the thermoplastic nature of the binder. During operation, I^2R losses in the copper conductor heat the asphalt to the point where it softens and gradually liquefies, flowing into and temporarily sealing cracks or fissures.

Figure 5.1 represents a ramped voltage test result obtained from an asphalt-mica insulation in very good condition. As expected, the *I-V* response is linear over the full range of applied voltage. The geometric capacitance charging current is constant and proportional to the rate-of-change of the applied voltage. The polarization current is linear, although relatively large compared to the capacitance charging current as indicated by the steep slope of the *I-V* curve. In this machine, the dipole polarization component accounts for a large percentage of the total measured current because the groundwall insulation is comprised of large mica splittings and an asphalt binder—two highly polar materials. And as further evidenced by the linear response, the leakage current is negligible up to the maximum test voltage, and no signs of partial discharges or space charge polarization are apparent. This characteristic curve is typical of sound, high-quality asphalt-mica stator winding insulation.

Figure 5.2 provides an example of an aged and deteriorated asphalt-mica insulation system. The *I-V* response exhibits a gradual, nonlinear increase in current with respect to voltage. This indicates that generalized thermal degradation of the groundwall insulation has taken place—a typical mode of deterioration for asphaltic insulation

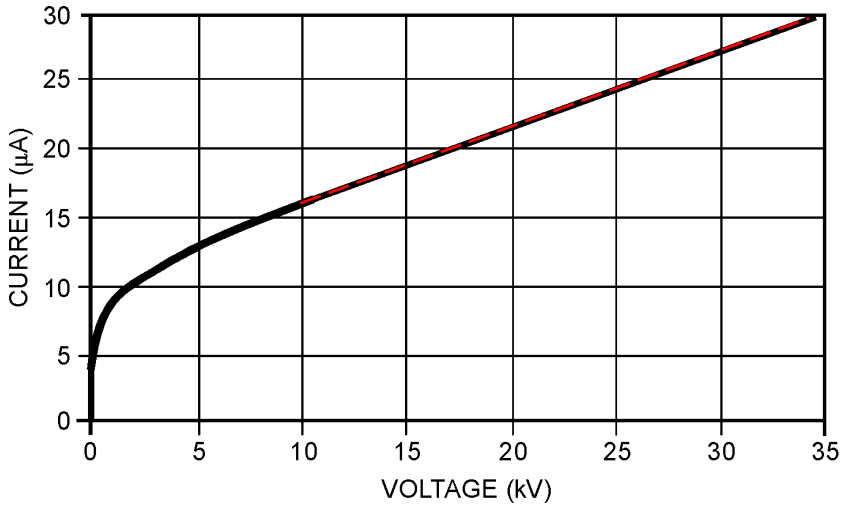

Figure 5.1 Typical ramped voltage test result for asphalt-mica winding insulation in very good condition. The polarization current is relatively large compared to the capacitance charging current due to the polarizability of the mica splittings and asphalt binder. The leakage current is negligible up to the maximum test voltage.

systems. Severe thermal deterioration destroys the bonds between tape layers, particularly in the endwindings immediately adjacent to the stator core boundary, and results in the formation of voids. Thermal damage may also create permanent carbonized paths within the groundwall. These defects become sites where abnormal space charge polarization, ionizations, and leakage current can occur. As is typical for badly deteriorated insulation, the slope of the current response continues to rise in a nonlinear manner as the test voltage is increased. Insulation breakdown is predicted to occur as the current asymptotically approaches the vertical. To prevent unintentional failure, testing should be halted well before this point is reached.

The data displayed in Figs. 5.1 and 5.2 were obtained from two generators located at the same powerplant. The identical units were manufactured and put into operation in the early 1950s. Unit 1, represented in Figure 5.2, historically had been operated in a first

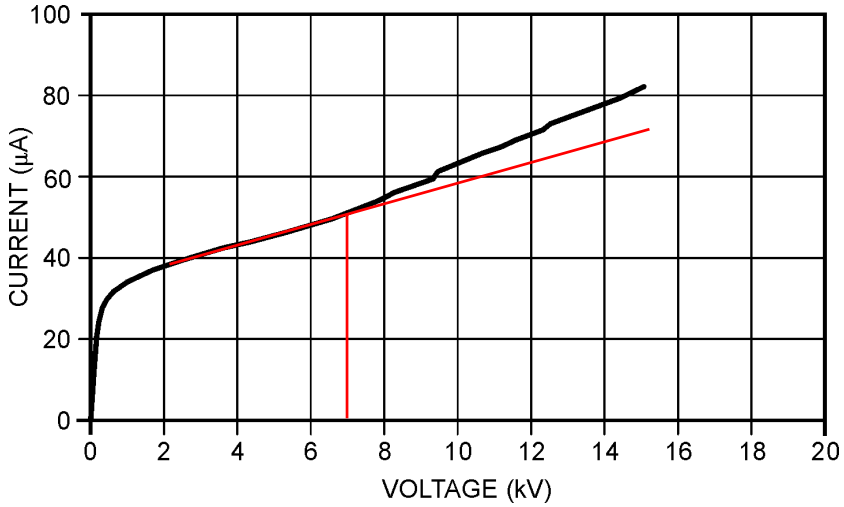

Figure 5.2 Example of a ramped voltage test result of an aged and deteriorated asphalt-mica insulation. The nonlinear *I-V* response is due to thermal deterioration of the groundwall insulation and a resulting increase in polarization, conduction, and ionization.

on/last off mode and, therefore, experienced significantly more use and thermal cycling (and deterioration) over its 40-year lifetime. Unit 2 had been operated much less and its stator winding was in better overall condition. Based on the ramped voltage test results, new operating priorities were placed on the generators to maximize their useful lives. To the extent possible, Unit 1 was based loaded and Unit 2 was used to provide peaking power. The ramped voltage tests were also helpful in determining that a rewind of Unit 1 should be considered in the near future, and that if economic factors made it feasible to rewind both units then Unit 1 should be rewound before Unit 2.

The curve in Figure 5.3 was obtained from an asphalt-mica insulation in which a localized fissure had absorbed moisture while out of service during a very rainy and humid period. Space heaters were available in the stator air housing but had not been used during the eight-week outage. A ramped voltage test was performed prior to

returning the machine to service. All three phases of the stator winding were tested simultaneously. As the voltage was raised, the leakage current increased nearly asymptotically due to a conductive path between the winding conductor and grounded stator core. To avoid insulation breakdown and permanent damage to the insulation, the test was stopped prior to reaching the normal maximum test voltage. Heaters were then used in the stator air housing for a few days in an attempt to dry out the insulation. Subsequent tests indicated only marginal improvements in the *I-V* response, and the maximum test voltage achieved was only 65 percent of the usual limit. The machine was, nevertheless, returned to service. It failed within the first few minutes of operation. The failed stator coil was located and electrically bypassed from the affected parallel circuit. A ramp test was performed on the repaired winding to the full test voltage to assure the weak insulation had been completely eliminated. The *I-V* response appeared normal. The unit was returned to service (at a somewhat reduced load limit) and operated without incident. The three 50-year-old generators at the plant were already planned to be rewound within the next five to ten years. In the meantime, this experience reinforced the need to consistently use heaters during maintenance outages to keep the winding temperature above the dew point to prevent moisture from being absorbed by the aged and weakened insulation. It also made clear that once moisture has been absorbed, the use of low-wattage space heaters is not sufficient to adequately dry the insulation.

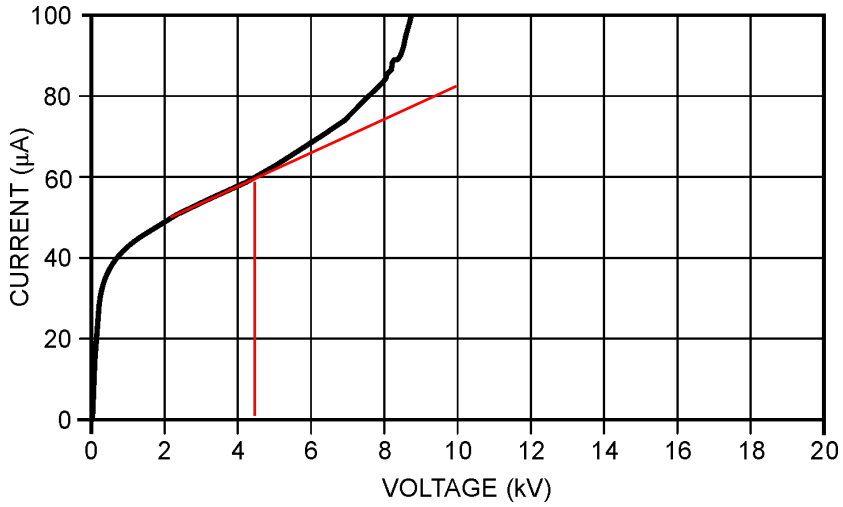

Figure 5.3 A ramped voltage test result for an asphalt-mica insulation with a fissure in the groundwall insulation. The exponential increase in leakage current is due to moisture absorption during an extended maintenance outage. The absorbed moisture created a conductive path between the winding conductor and the grounded stator core, and eventually lead to insulation failure.

Polyester-Mica Insulation

Polyester windings are particularly sensitive to chemical reaction with moisture, which can cause both electrical and physical degradation. Depending on the specific chemical formulation involved, polyester windings are also susceptible to shrinkage and, therefore, mechanical wear due to vibration in the stator slot. Movement of the winding during operation may damage the semi-conductive slot coating, leading to intense slot discharges and ozone production. Once initiated, this type of deterioration is very difficult to repair.

The data shown in Figure 5.4 was obtained from a polyester-mica stator winding in very good condition. Although the magnitude of dipole polarization is not as great as that for asphalt-based insulation, it still causes a rather steep slope in the current trace, reflecting the relatively high polarizability of the mica splittings and polyester resin. The

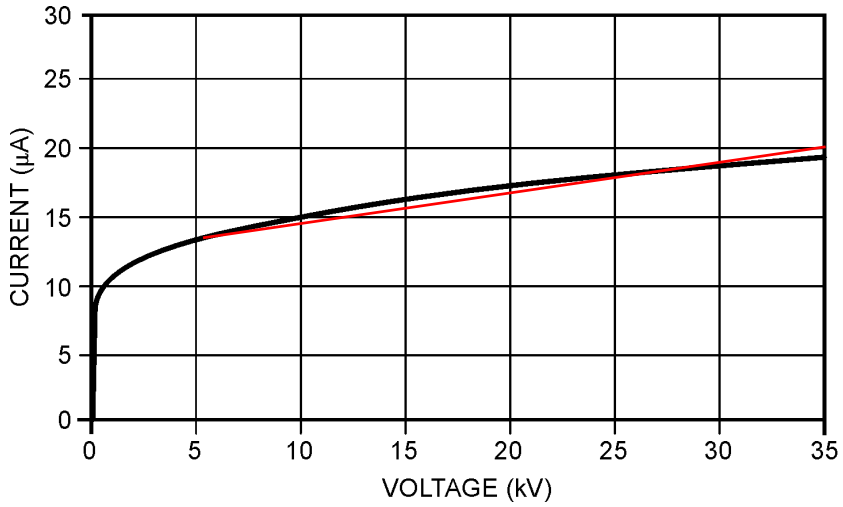

Figure 5.4 Typical ramped voltage test result for a polyester-mica winding in good condition. The polarization current, although lower than that of asphalt, is relatively large compared to the charging current. As expected for good insulation, the leakage current is negligible up to the maximum test voltage.

current trace is somewhat rounded at the beginning and throughout the test due to the time lag between the increasing electrical stress and the resulting dipole orientation. As expected for insulation in good condition, the *I-V* response shows no evidence of abnormal space charge polarization, partial discharges, or conduction current.

The curve of Figure 5.5 was obtained from a stator winding that was exposed to a water leak from overhead piping [70] while the machine was idle. For an undetermined number of days, water from the ceiling above dripped onto the deck covers of the stator air housing and was able to pool and continually trickle through a bolt hole onto a small number of stator coils directly below. This problem was unknown to plant personnel. When an attempt was made to start the unit, the stator winding ground fault relay tripped the generator off line. A ramped voltage test was conducted to evaluate the integrity of the winding before further attempts were made to restart the generator. As shown in the

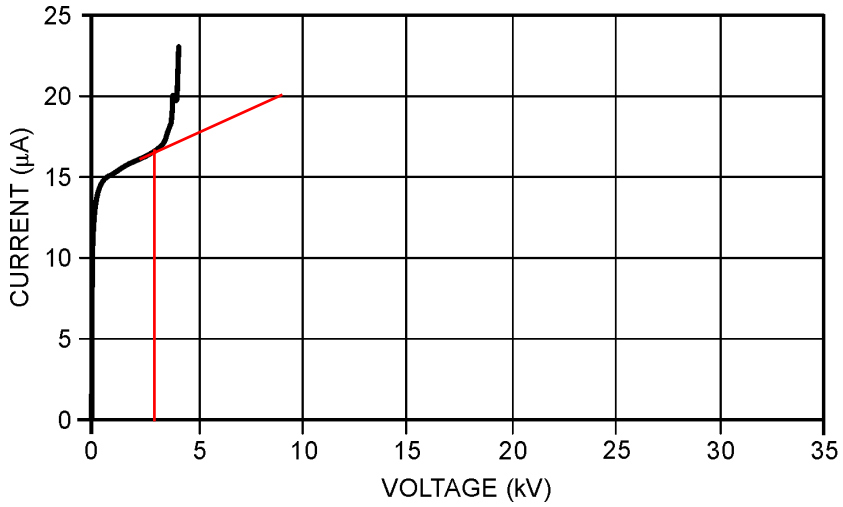

Figure 5.5 Example of a ramped voltage test result for a polyester-mica insulation where water had leaked from overhead piping onto the stator winding, creating a conductive path through the groundwall insulation.

figure, the *I-V* response appeared normal initially but as the test voltage exceeded a few kilovolts, the curve began to exhibit a nearly exponential increase in conduction current. Subsequent investigation into the failure revealed that a single coil near the line end of the phase suffered a ground fault about one-third of the way down from the top of the stator core, the result of damage to the insulation caused by exposure to water.

Figure 5.6 represents a new polyester-mica winding with delaminated groundwall insulation. This particular insulation system is comprised of Mylar-backed mica mat tape, which is bonded with polyester resin and over wrapped with B-stage, epoxy-coated armor tape. A ramped voltage test was performed on the newly installed stator winding as a condition of acceptance, before the machine was put into service. As shown in the figure, the measured current appears normal as the applied voltage is increased from zero to a few kilovolts. But as the voltage exceeds approximately 3.2 kV, the slope of the trace sharply increases and the current becomes nonlinear and somewhat erratic.

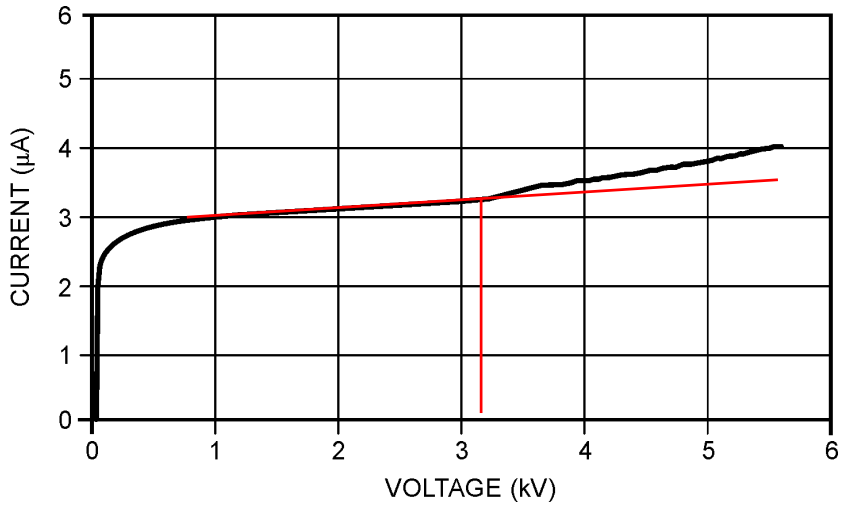

Figure 5.6 Example of a ramped voltage test result for a polyester-mica winding with improperly processed and delaminated insulation. The nonlinear *I-V* response is due to dipole polarization and conduction in the uncured resin, and space charge polarization and ionizations between layers of solid insulation and gas space.

Investigation into the abnormal results revealed that during the final cure at the factory, insufficient temperature and pressure were applied to the coils to properly fuse and consolidate the insulation layers. As a result, the insulation suffered widespread delaminations. The nonlinear increase in slope and irregularities in the current response are indicative of space charge polarization and internal ionizations. Under the influence of the applied stress, mobile charge carriers pass through the more-conducting solid insulation to the interface with the less-conducting gas spaces, where they become stationary and build up a surface charge. A significant reverse field develops from this interfacial polarization and increased polarization current and losses result. The incompletely cured B-stage resin also possesses a greater density of conductive and polar species, leading to increased dipole polarization and leakage current.

Hard, thermosetting insulation systems have proven to be vulnerable to mechanical wear and cracks. Therefore, it is especially important that care be used when shipping and handling coils with this type of insulation. The stator coil wedging system also must be properly designed and installed to hold the coils tight in the stator slots during operation to prevent vibration or mechanical shock. The curve of Figure 5.7 was obtained from a polyester-mica winding with a crack in the groundwall insulation of a coil, believed to have been caused by unusually rough handling during installation of the winding. (Many of the coils in this machine had to be removed and reinstalled several times before the winding passed the final ac high-potential withstand test.) The location of the crack was near the middle of the slot, allowing it to remain relatively clean and dry. As a result, the machine operated for 16 years before failing during a routine test. As shown, insulation breakdown through a clean, dry crack is frequently indicated by a sharp rise in conduction current due to capacitive discharge at the failure location.

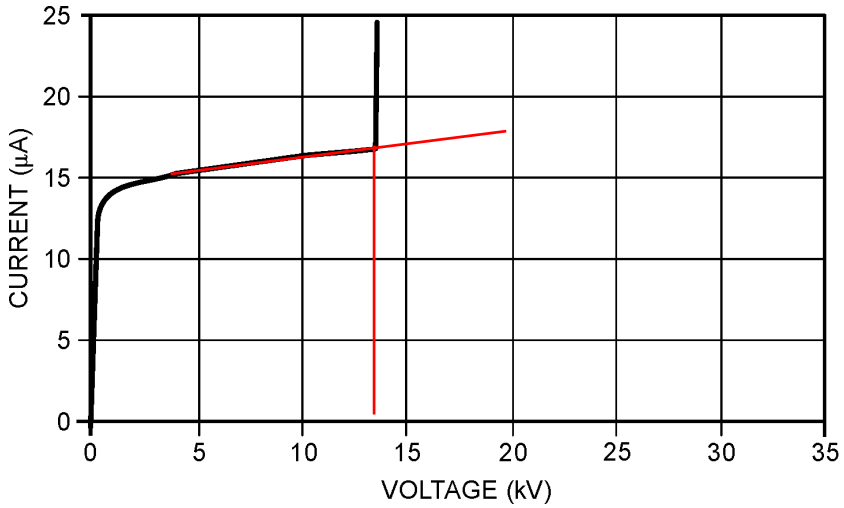

Figure 5.7 Example of a ramped voltage test result for a polyester-mica winding with a clean, dry crack in the groundwall insulation. Note the winding failed suddenly, giving no warning of impending failure.

Epoxy-Mica Insulation

Problems with insulation systems may arise due to improper resin viscosity, insufficient resin to fill all the crevices, resin shrinkage during curing, and inadequate bonding strength of the resin to the conductor or between the insulation layers. Any of these difficulties may cause voids to be present in the finished groundwall insulation. If the operating voltage is high enough to ionize gases in the internal spaces, the discharges will lead to a decomposition of the organic resin component. The net result is a slow decline in insulation condition and electrical strength, eventually leading to failure.

The curve in Figure 5.8 is typical of high-quality epoxy-mica insulation when tested with a ramped direct voltage. The geometric capacitance charging current is proportional to the ramping rate of the applied voltage and produces a positive offset in the *I-V* curve. The polarization current is linear and increases with voltage. As indicated by the relative flatness of the *I-V* response, dipole polarization is relatively small compared to capacitance charging, affirming the non-polar structure of epoxy molecules and the fact that dipole polarization does not contribute significantly to the measured current. In the case of a winding in good condition, the capacitance charging and the polarization current constitute the majority of the total measured current, whereas the surface and volume conduction components are very low, typically negligible, up to the maximum test voltage. Also, no indications of partial discharges or space charge polarization are apparent. In general, the smooth, practically linear curve is characteristic of stator winding groundwall insulation that is in good condition.

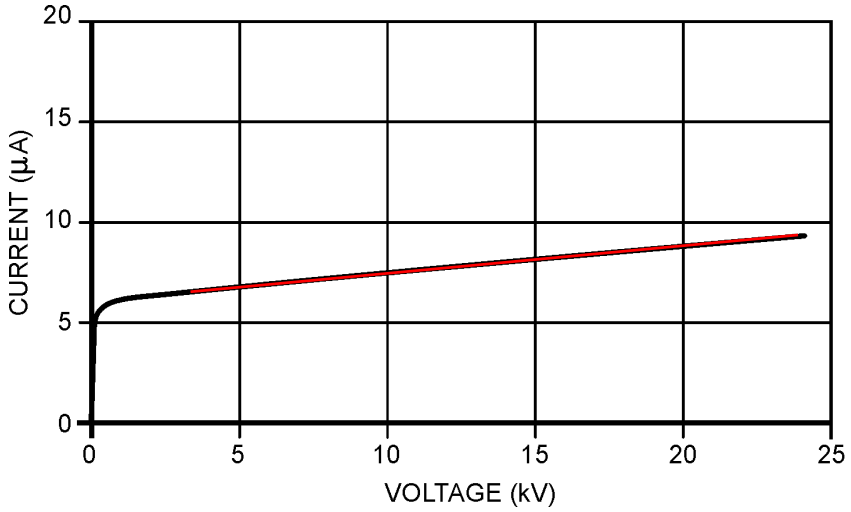

Figure 5.8 Typical ramped voltage test result for a new epoxy-mica insulation. The relatively flat *I-V* response indicates that the dipole polarization current component is relatively small compared to the geometric capacitance charging. As evidenced by the smooth and linear trace, the leakage current is negligible and no signs of space charge polarization or partial discharges are observed.

Field-insulated connections and repairs to the groundwall insulation must be properly cured before the winding is placed service. In some cases, a long curing time or the use of external heaters is required. The shelf life of epoxy (and polyester) resins is limited and the materials require cool storage conditions to prolong their useful life. Special mixing procedures are also necessary to achieve good results. Improperly cured resins, varnishes, and other coatings may result in increased conduction during high voltage tests. Under conditions of high electrical stress, increased conduction can lead to insulation breakdown across the surface or through the groundwall.

Figure 5.9 provides an example of a newly installed winding having uncured epoxy-impregnated insulation on the winding lead connections and incompletely cured insulating surface paint. The *I-V* response initially appears normal but as the voltage is

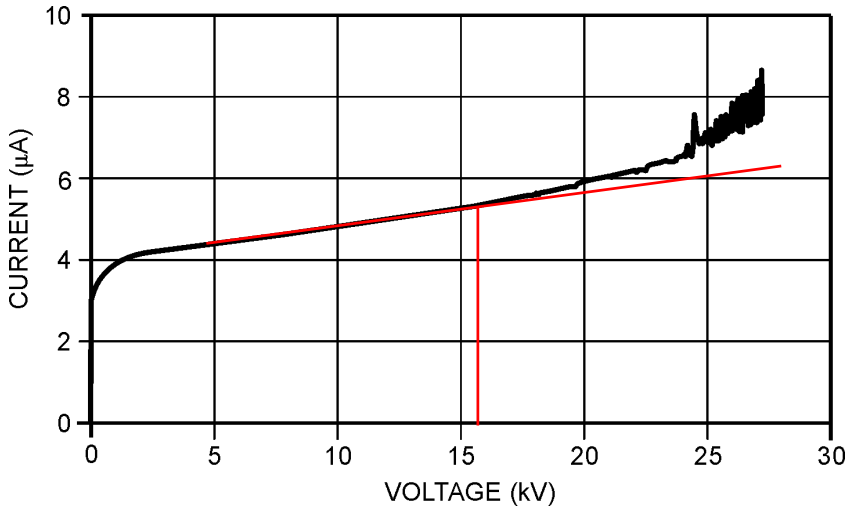

Figure 5.9 Example of an epoxy-mica insulation with incompletely cured epoxy-impregnated neutral lead connections and insulating surface paint. The leakage current exhibits a significant nonlinear increase and an erratic, spiking behavior.

increased, the current begins to exhibit a significant upturn and an erratic, spiking behavior. This characteristic is indicative of abnormal conduction, in this case, across the winding surfaces. This test was performed prior to the final ac withstand test and demonstrated the need for additional time and heat to complete the resin curing process. Heaters and fans were applied for several days to accelerate the curing process. A retest of the winding indicated significant improvement in the ramped voltage test results (not shown). A subsequent 1-minute ac withstand test was performed successfully at $2V_{LL}$ +1. In this situation, the ramped voltage test enabled the problem to be found and rectified, rather than having an insulation failure during the acceptance test that would have required a repair to correct.

The curve in Figure 5.10 was obtained from an epoxy-mica stator winding with incompletely cured repairs to the groundwall insulation. Minor damage to a small area

on the surface of the stator winding had been patched and, after what was thought to be sufficient curing time, a ramped voltage test was performed to verify the success of the repair. Rather than exhibiting a normal *I-V* response, however, a step-like increase in current occurs near the end of the test, caused by a sudden, localized increase in conduction through the partially cured resin as the electrical stress exceeds a certain value. After an additional day of curing time, the test was repeated and the results were linear to the maximum test voltage (not shown), verifying that the repair was successful and machine was ready to be returned to service.

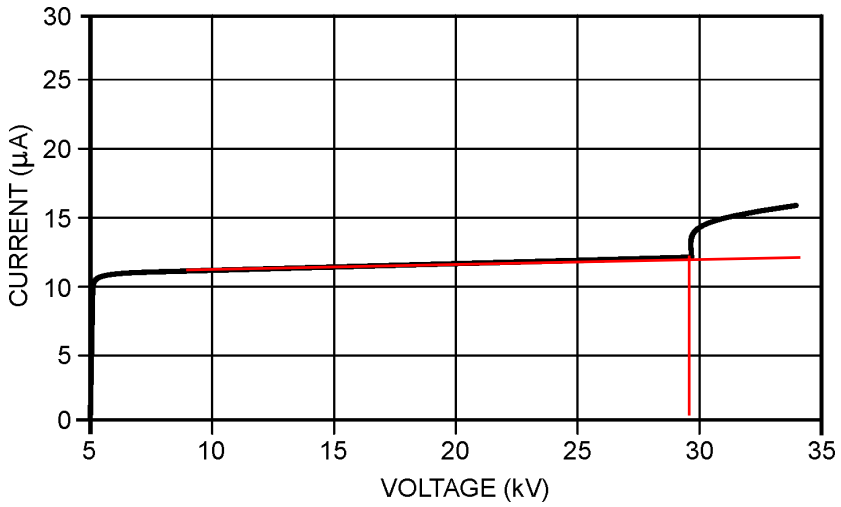

Figure 5.10 Example of a ramped voltage test result for an epoxy-mica winding with an incompletely cured epoxy patch. The conduction current exhibits a sudden abnormal step increase as the electrical stress exceeds a certain value.

Contaminants such as oil, carbon, brake dust, dirt, and insects combined with moisture can cause an undesirable increase in surface conduction during direct high-voltage tests. The conduction may lead to surface tracking or may simply mask more serious developments related to insulation condition. Figure 5.11 represents a severely

contaminated epoxy-mica stator winding tested during the five-year warranty inspection. All three phases were tested individually, each displaying an irregular and slightly increasing current response at the higher test voltages. Benchmark data obtained five years earlier, just after the winding installation was finished, showed no such nonlinearities. Physical inspection of the machine revealed significant contamination on the upper and lower portions of the stator winding and core. A sample of the substance was collected for laboratory analysis and determined to be caused by excessive slip ring brush wear (*i.e.*, carbon contamination). Subsequent cleaning and retesting of the stator winding showed a marked improvement in the linearity of the test response (not shown). In this situation, the ramped voltage test results were useful in identifying a need to make adjustments to the slip ring brush configuration.

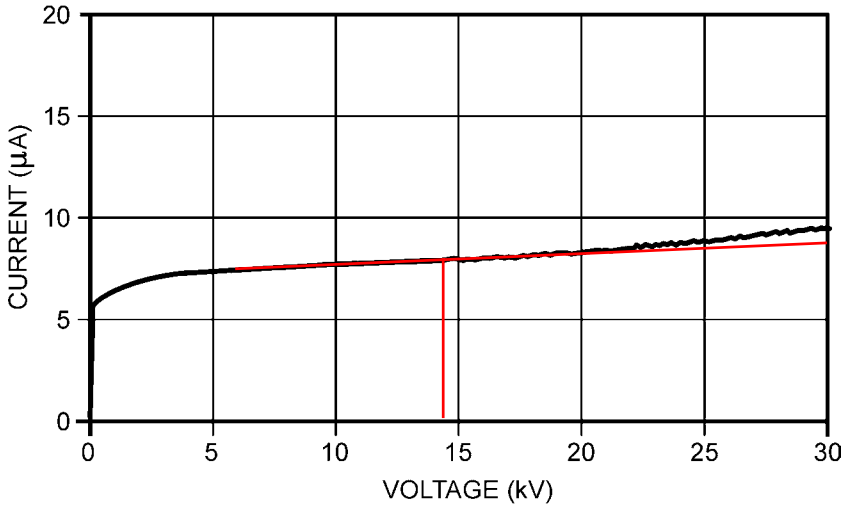

Figure 5.11 Example of a ramped voltage test result for an epoxy-mica winding with contaminated endwindings. Nonlinearities in the current response are due to increased surface conduction.

CHAPTER VI

CONCLUSIONS

The principal goals of this research investigation were to develop a detailed theoretical explanation of the measured current response observed during ramped direct high-voltage testing and to compare the ramped voltage technique to other methods of evaluating stator winding insulation. These objectives were achieved by first identifying the important microscopic phenomena underlying the electrical properties of dielectric materials and insulation systems, *i.e.*, geometric capacitance charging, polarization, conduction, and ionization mechanisms. Using lumped electrical circuit parameters to represent these phenomena, an insulation model was developed to describe the insulation's macroscopic response to an applied voltage, emphasizing how and why the current changes as the insulation ages or is subjected to the types of defects typically seen in service. For instance, improperly cured or incompletely cross-linked insulation has been shown to possess a higher than normal density of conductive and polar molecules and, therefore, exhibits increased conduction and dipole polarization when exposed to an applied voltage. Insufficiently impregnated insulation or insulation that has become delaminated due to loss of bonding between layers may exhibit space charge polarization and/or high intensity partial discharges, with a corresponding increase in losses. Cracked or otherwise faulted insulation may not be able to withstand the required level of electrical stress. As the applied voltage exceeds the withstand capability of the

insulation, breakdown will occur at the site of the defect and an exponential increase in conduction current will be observed.

Comparative Tests

The ability of the ramped voltage test to detect different types of insulation problems was assessed and compared to several other diagnostic methods using a set of epoxy-mica stator winding coils manufactured with specific insulation defects. In addition to two standard production coils, two coils were also made with each of the following deficiencies: incomplete resin cure, reduced density of the groundwall insulation, loosely applied tape layers, internal conductive contamination, and exposure to thermal cycling at excessive temperature. Comparative tests included insulation resistance, polarization index, recovery voltage, dissipation factor, dielectric spectroscopy, partial discharge, and ramped direct high-voltage tests.

Test results obtained during this investigation revealed differences among coil specimens due to variations within the insulation associated with the physical defects. As expected, insulation resistance measurements were most effective at detecting changes in the conduction properties in the insulation. The ramped direct high-voltage tests were found to correlate with the 1- and 10-minute insulation resistance values, particularly in tests involving the severely overheated and incompletely cured coils. Because the ramp test is performed over a higher range of voltage, it was also able to detect the existence of internal contamination that was not evident during the insulation resistance measurements. Polarization index was found to be a fairly insensitive indicator of insulation condition. The polarization index values of all coils significantly exceeded the

minimum value specified by industry standards, and though subtle differences were observed, these were not sufficient to diagnose insulation defects or damage. Recovery voltage measurements were also unsuccessful in providing meaningful differences between specimens. Modification of the test procedure is recommended to allow determination of the polarization spectra, which may lead to more useful results. Partial discharge measurements also failed to reveal consistent differences between the coil specimens, nor absolute discharge values that could be definitively linked to insulation condition. More conclusive results may have been obtained if a specialized laboratory instrument had been available for making the PD measurements.

Dielectric spectroscopy tests were found to be informative, presenting individual displacement and loss components of permittivity, and measuring these properties over a wide range of frequency and test voltage. The greatest difference among the experimental coils was observed at the lowest frequencies, where dipole and space charge polarization effects have more time to react to the changing electric field. In general, the defective coils displayed higher displacement and losses relative to the standard production coils. But because this novel method has rarely been used on rotating machine insulation, no guidelines exist for determining typical versus abnormal deviations. Still, this diagnostic technique shows promise. Dissipation factor measurements made at power frequency (60 Hz) were not as discerning. Only in the case of the contaminated coils was there a marked difference in dissipation factor tip-up; it was several times greater than that of all other specimens.

The ramped voltage test curves were analyzed by quantifying the magnitude of the measured current at 5 kV, the slope of the *I-V* response between 5 and 10 kV, and by noting the voltage at which the trace becomes nonlinear as well as the severity of the nonlinearity. As expected, the standard production coils were linear over the greatest range of voltage and the observed nonlinearities were the least pronounced. The general characteristics of the traces were typical of new epoxy-mica insulation. The *I-V* response for the coils with no final cure exhibited a significant positive offset and larger slope due to a greater density of polar molecules. The traces also became nonlinear at a lower voltage, an indication of additional conductive species. The overheated coils showed a similar, although negative, offset and a lower voltage threshold for becoming nonlinear, possibly indicating ionizations within the thermally-damaged insulation. The contaminated coils exhibited a dramatic spiking behavior as the voltage exceeded the threshold for excessive conduction. The coils with loose tapes and reduced density also became nonlinear at a lower voltage and the overall increase in current over the range of applied voltage was higher as compared to the normal coils. To a greater or lesser extent, all stator coil specimens presented discrepancies related to the type and severity of their insulation defects.

Ramped Direct High-Voltage Test

When relating an *I-V* response to the physical condition of the insulation it is understood that the separate and combined effects of conduction, polarization, and ionization mechanisms can alter the observed current. An abnormal *I-V* characteristic may be an indication of contaminants, either in the insulation or on exposed surfaces;

internal void ionization or surface corona; space charge polarization between layers of delaminated insulation; anomalous dipole polarization due to inadequate resin cure or overheating, as well as numerous other possible deficiencies. In some cases, distinctly different insulation problems appear to affect the measured current in outwardly similar ways. Because the current measuring instrumentation cannot separate charging, polarization, conduction, and ionization components, the *I-V* response must be visually unraveled to assess insulation condition and properly identify problems. Thus, although ramped voltage tests are relatively simple to perform, knowledge of high-voltage insulation and previous diagnostic experience may be required to properly interpret anomalous test results. (This requirement is generally true for other diagnostic tests as well.) In the vast majority of circumstances, however, the ramped voltage test can be performed and the insulation condition established to be in either excellent or good condition by non-specialists working in the field.

Direct high-voltage tests are widely recognized as being able to detect insulation problems such as cracks and fissures, surface contamination, incomplete resin cure, and absorbed moisture—that is, adverse conditions that significantly increase the volume or surface conductivity of the insulation system. The ability of direct-voltage tests to find these types of problems has been supported by decades of experience with insulation resistance, polarization index, and leakage current measurements (via stepped direct-voltage tests). Direct-voltage testing is not, however, generally credited with being able to diagnose poorly impregnated, delaminated, or thermally-aged insulation. These conditions tend to alter the dielectric polarization characteristics (especially dipole and

space charge polarization) and ionization effects more than conductivity. Because dc conductivity often remains extremely low in situations involving these types of defects, insulation resistance measurements obtained using the usual test instruments often indicate a resistance value of "infinite," implying the insulation is normal. Even when a laboratory-quality meter is available to measure very high values of insulation resistance, normal dipole polarization varies with time in response to an applied voltage step, hindering the ability of conventional direct-voltage techniques to detect and discern subtle variations in electrical behavior. Alternating-voltage tests, such as dissipation factor and partial discharge measurements, are understood to be more effective in these circumstances.

The ramped direct high-voltage method is often presumed to encounter the same limitations as other direct-voltage techniques. However, fundamental dielectric principles and test results presented herein have demonstrated that this is not the case. The stator winding model developed in Chapter III shows that when a time-varying voltage is applied to an insulation, the electrical response is comprised of geometric capacitance charging, dielectric polarization, conduction current, and partial discharge effects. When the rate-of-change of voltage is very slow, the capacitance charging current is minimized, enabling small changes in dipole and space charge polarization, conduction, and ionizations to be detected. High-quality insulation will exhibit an *I-V* response that is practically linear over a range of applied voltage. In situations involving defective insulation, however, anomalous behavior on the insulation surface, within the bulk dielectric, and at heterogeneous interfaces can be observed [65-67].

Insulation theory and testing experience obtained during this investigation were applied to a collection of sample test results obtained from in-service machines during the past ten years. These results and analyses provide a practical illustration of the ability of the ramped voltage test method to distinguish between normal insulation and that with problems, and to help identify the cause and extent of the deficiencies. While no single diagnostic method is ideally suited to detect all possible stator winding insulation problems, ramped voltage tests are useful in determining when corrective actions are needed and what the appropriate actions are. When done properly, the test can identify stator windings that are approaching failure without accelerating the deterioration process. The ramped voltage test may also serve as a high-potential proof test, ensuring that the stator winding groundwall insulation has the dielectric strength needed to provide reliable operation in the future.

REFERENCES

[1] Rodenburg, R. L., “Replacements, Units, Service Lives, Factors,” Prepared for U.S. Department of Energy, U.S. Department of the Interior and U.S. Bureau of Reclamation, 1995, PO No. AA-P0-12652-22503.

[2] Stone, G.C., H.G. Sedding, B.A. Lloyd and B.K. Gupta, “The Ability of Diagnostic Tests to Estimate the Remaining Life of Stator Insulation,” *IEEE Transactions on Energy Conversion*, December 1988, Vol. 3, No. 4, pp. 833-840.

[3] Evershed, S., “The Characteristics of Insulation Resistance,” *Journal of the Institution of Electrical Engineers*, London, England, Vol. 52, No. 224, 1913, pp. 51-73.

[4] Sidway, C. L., “A Survey of Generator Insulation Tests,” *Minutes of the Edison Electrical Institute Electrical System and Equipment Committee Meeting*, February 1959, Atlanta, GA.

[5] Hill, G. L., “Testing Electrical Insulation of Rotating Machinery with High-Voltage Direct Current,” *AIEE Transactions (Power Apparatus and Systems)*, Vol. 72, Part III, 1953, pp. 159-174.

[6] Cameron, A.W.W., “Diagnosis of A-C Generator Insulation Condition by Non-Destructive Tests,” *AIEE Transactions (Power Apparatus and Systems)*, Vol. 71, Part III, 1952, pp. 263-269.

[7] Cameron, A.W.W. and A.M. Sinclair, "Experience and Development in Nondestructive D-C Testing for Maintenance of High-Voltage Stators," 1956, *AIEE Transactions (Winter General Meeting)*.

[8] Schleif, F.R., "Corrections for Dielectric Absorption in High Voltage D-C Insulation Tests, "*AIEE Transactions (Power Apparatus and Systems)*, Vol. 75, Part III, 1956, pp. 513-517.

[9] Schleif, F.R. and L.R. Engvall, “Separation of Absorption and Leakage Components in High Voltage D-C Insulation Tests,” *Transactions of the AIEE Winter General Meeting*, 1958, Conference Paper 58-204.

[10] Schleif, F.R. and L.R. Engvall, “Experience in Analysis of D-C Insulation Tests for Maintenance Programming,” *AIEE Transactions*, Part III, *Power Apparatus and Systems*, Vol. 78, 1959, pp. 156-161.

[11] Johnson, J.S. and A.W. Zwiener, “D-C Testing Experience on Rotating Machine Insulation,” *AIEE Transactions (Power Apparatus and Systems)*, Vol. 76, Part III, 1957, pp. 416-420.

[12] IEEE Std. 95-1977, “Recommended Practice for Insulation Testing of Large A-C Rotating Machinery with High Direct Voltage.”

[13] McHenry, B.L., "New Techniques in High Direct Voltage Generator Insulation Tests," *Ontario Hydro Research Quarterly*, Vol. 16, 1964, fourth quarter.

[14] McHenry, B.L., "Generator Insulation Testing by Continuous Time-function Application of Direct Voltage," *IEEE Transactions on Power Apparatus and Systems*, Vol. PAS-86, 1967, pp. 1329-133.
[15] Milano, B. and R.C. Arbour, "A Portable Ramped D-C Test Set Using a USBR Developed High-Voltage D-C Power Supply," September 1983, Report No. GR-83-7. Available from Bureau of Reclamation, Denver, CO, 80225.
[16] McDermid, W. and B.G. Solomon, "Significance of Defects Found During High Direct Voltage Ramp Tests," *Proceedings of the 1999 EIC/EMCW*, 1999, pp. 631-636.
[17] Kurtz, M., "The High Voltage Ramp Test Set," Ontario Hydro Research Division Report, 1975, E75-81-K.
[18] Nilsson, N.E., "Report on the Working Group to Review IEEE Std. 95-1977," *IEEE Panel Session on High Voltage Testing of Rotating Machines*, 1997, 97TP119-0, pp. 18-20.
[19] IEEE Std. 95-2002, "Recommended Practice for Insulation Testing of AC Electric Machinery (2300 V and Above) with High Direct Voltage."
[20] Rux, L. M., "Ramped High-Voltage D-C Testing of Large Rotating Machine Stator Windings," *Minutes of the Sixty-Third Annual International Conference of Doble Clients*, 1996, Sec. 7-8.
[21] Rux, L. M., "Ramped High-Voltage DC Testing: A Refined Method of Evaluating Stator Winding Insulation," *IEEE Panel Session on High Voltage Testing of Rotating Machines*, 1997, 97TP119-0, pp. 21-24.
[22] ASTM D 1711-99, "Standard Terminology Relating to Electrical Insulation," 1999.
[23] Deer, W.A., R.A. Howie and J. Zussman, *An Introduction to the Rock Forming Minerals*, Wiley, New York, 1966, pp. 191-210.
[24] Hepburn, D.M., I.J. Kemp and A.J. Shields, "Mica," *IEEE Electrical Insulation Magazine*, September/October 2000, Vol. 16, No. 6, pp. 1924.
[25] Clark, F.M., *Insulating Materials for Design and Engineering Practice*, Wiley, New York, 1962, pp. 1109-1154.
[26] Culbert, I.M., H. Dhirani and G.C. Stone, *Handbook to Assess the Insulation Condition of Large Rotating Machines*, 1991, EPRI Vol. 16, Wiley.
[27] "Bitumen," 2000, Microsoft® Encarta® Online Encyclopedia, http://encarta.msn.com © 1997-2000 Microsoft Corporation.
[28] Abraham, H., *Asphalts and Allied Substances*, Van Nostrand C., New York, Vol. 1, 1960, pp. 52-78.
[29] Roberts, F.L., P.S. Kandhal, E.R. Brwon, D. Lee and T.W. Kennedy, "Hot Mix Asphalt Materials, Mixture, Design, and Construction," NAPA Education Foundation, Maryland, 1991, pp. 70-84.
[30] Freemantle, M., "Asphalt," Chemical & Engineering News, Vol. 77, No. 77, November 1999, pg. 81.

[31] Allinger, N.L., *Organic Chemistry*, Worth Publishers, New York, NY, 1973, pg. 82.
[32] Sillars, R., *Electrical Insulating Materials and Their Application*, Stevenge, England, Peter Peregrinus for the Institution of Electrical Engineers, 1973, pp. 180-197.
[33] Shugg, W.T., *Handbook of Electrical and Electronic Insulating Materials*, IEEE Press, New York, NY, 1995, pg. 183.
[34] von Hippel, A., *Dielectric Materials and Applications*, Artech House, London, 1954, pg.83.
[35] Bartnikas, R., *Engineering Dielectrics, Vol. IIA, Electrical Properties of Solid Insulating Materials: Molecular Structure and Electrical Behavior*, ASTM Special Technical Publication 783, New Jersey, 1983, pg. 101.
[36] Jackson, W., *The Insulation of Electrical Equipment*, John Wiley & Sons, New York, 1954, pg. 62.
[37] Frohlich, H., *Theory of Dielectrics*, McGraw-Hill, New York, 1973, pg. 391-408.
[38] Barrow, G.M., *Physical Chemistry*, John Wiley & Sons, New York, 1954, pg. 62.
[39] Bartnikas, R., *Engineering Dielectrics, Vol. IIA, Electrical Properties of Solid Insulating Materials: Molecular Structure and Electrical Behavior*, ASTM Special Technical Publication 783, New Jersey, 1983, pp. 168.
[40] IEC 60270-2000, "High-Voltage Test Techniques – Partial Discharge Measurements."
[41] Paoletti, G., "Partial Discharge Theory and Technologies Related to Medium Voltage Electrical Equipment," Sixty-Seventh Annual International Conference of Doble Clients, March 2000, Paper No. 7G.
[42] Dakin, T.W., "The Relation of Capacitance Increase with High Voltages to Internal Electric Discharges and Discharging Void Volume," *AIEE Transactions*, Paper 59-151, October 1959, pp. 790-795.
[43] Boggs, S. A., "Partial Discharge: Overview and Signal Generation," *IEEE Electrical Insulation Magazine,* Vol. 6, No. 4, July/August 1990, pp 33-39.
[44] Kuffel, E. and W.S. Zaengle, *High Voltage Engineering*, Pergamon Press, 1984, pp. 311-320.
[45] Khalifa, M., *High-Voltage Engineering, Theory and Practice*, Marcel Dekker, Inc., New York, 1990, pp. 72-91.
[46] *ibid.* S. A. Boggs, "Partial Discharge: Overview and Signal Generation," *IEEE Electrical Insulation Magazine,* Vol. 6, No. 4, July/August 1990, pp 33-39.
[47] Nattrass, D. A., "Partial Discharge Measurement and Interpretation," *IEEE Electrical Insulation Magazine,* Vol. 4, No. 3, May/June 1988.
[48] Weber, H. J., R.E. Seeberger and G. Stolpe, "Field Measurements of Partial Discharges in Potential Transformers," *IEEE Electrical Insulation Magazine,* Vol. 2, No. 5, September 1986.
[49] "Tutorial on Partial Discharge Measurement in Rotating Machinery," Doble Client Committee Fall Meetings, October 1994, Indianapolis, IN.

[50] Danikas, M. G., "A Novel Diagnostic Technique to Study the Aging of Rotating Machine Insulation," *Proceedings of the International Conference on Electrical Machines*, August 2000, pp. 959-963.

[51] Wilson, A., R.J. Jackson and N. Wang, "Discharge Detection Techniques for Stator Windings," IEE Proceedings, Vo. 132, Pt. B, No. 5, September 1985, pp. 234-244.

[52] Stone, G.C., "Techniques for On-Line Partial Testing of Motors and Generators," CEA/Ontario Hydro Conference on Partial Discharge Testing, April 1994, Toronto, Canada.

[53] Krahn, J. R., "Partial Discharge Diagnosis and Prognosis for an Ozone-Producing Large AC Motor," Fourth International Conference on Generator and Motor Partial Discharge Testing, Houston, Texas, 1996, pp. 295-302.

[54] Anderson, J.C, *Dielectrics*, Reinhold Publishing Corporation, New York, 1963, pg. 2.

[55] IEEE Std. 43-2000, "Recommended Practice for Testing Insulation Resistance of Rotating Machinery."

[56] Csepes, G., I. Hamos, R. Brooks and V. Karius, "Practical Foundations of the RVM (Recovery Voltage Method for Oil/Paper Insulation Diagnostics)," Conference of Electrical Insulation and Dielectric Phenomena, 1998.

[57] Krivda, A., R. Neimanis and S.M. Gubanski, "Assessment of Insulation Condition of 130 kV Oil-Paper Current Transformers Using Return Voltage Measurements and an Expert System," *1997 IEEE Annual Report - Conference on Electrical Insulation and Dielectric Phenomena*, pp. 210-213.

[58] Sedding, H., "Application of Low Frequency Techniques for Stator Insulation Diagnostics," Proceedings of the Iris Rotating Machine Conference, 2002.

[59] Paithankar, A. and C. Pinto, "Transformer Insulation Diagnosis: Recovery Voltage Measurements and DC Absorption Test," *Proceedings of the IEEE Electrical Insulation Conference*, October 2001, pp. 597-600.

[60] Islam, S., P.R.S. Jota and M. Stace, "Detection of Oil-Paper Equilibrium Moisture Content in Power Transformers Using Hybrid Intelligent Interpretation of Polarisation Spectrums from Recovery Voltage Measurements," *Conference Record of the 1998 International Symposium on Electrical Insulation*, pp. 16-19.

[61] Cherukupalli, S., R.A. Huber and G.L. Halldorson, "Application of Some Novel Non-Destructive Diagnostic Tests for Condition Assessment of Stator Coils and Bars Following Voltage Endurance Tests," *Conference Record of the 2002 IEEE International Symposium on Electrical Insulation*, 2002, pp. 565-569.

[62] IEEE Std. 286-2000, "Recommended Practice for the Measurement of Power Factor Tip-Up of Electric Machinery Stator Coil Insulation."

[63] CEI/IEC 250:1969, "Recommended Methods for the Determination of the Permittivity and Dielectric Dissipations Factor of Electrical Insulation Materials at Power, Audio and Radio Frequencies Including Metre Wavelengths."

[64] IEEE Std. 1434-2000, "Trial-Use Guide to the Measurement of Partial Discharges in Rotating Machinery."

[65] Rux, L. M. and S. Grzybowski, "Detecting Delaminated Stator Winding Insulation Using the Ramped High-Voltage D-C Test Method," *Proceedings of the 11th*

International Symposium on High Voltage Engineering, No. 467, Vol. 5, 1999, pp. 331-334.

[66] Rux, L. M. and S. Grzybowski, "Evaluation of Delaminated High Voltage Rotating Machine Stator Winding Groundwall Insulation," *Conference Record of the 2000 IEEE International Symposium on Electrical Insulation*, 2000, pp. 520-523.

[67] McDermid, W. and J. C. Bromley, "Response of Ramp Test to Delamination in Stator Groundwall Insulation," *Proceedings 2001 EIC/EMCW*.

[68] Rux, L. M. and W. McDermid, "Assessing the Condition of Hydrogenerator Stator Winding Insulation Using the Ramped High Direct-Voltage Test Method," *IEEE Electrical Insulation Magazine*, November/December 2001, Vol. 17, No. 6.

[69] Rux, L. M. and D. Bertenshaw, "The Ramped Direct High-Voltage Method of Generator Stator Winding Insulation Testing," *Proceedings of Hydro 2003 Conference*, November 2003, pp. 539-545.

[70] DeHaan, J., E. Eastment, and L. Rux, "Isolating Failed Coils: Glen Canyon Generator Case Study," *Hydro Review Magazine*, November 2003, Vol. XXII, No. 7.

[71] Moore, D.S, *Statistics*, W. H. Freeman and Co., New York, 1985.

[72] Microsoft®Excel 2002.

APPENDIX A

STATISTICAL ANALYSIS

Method of Least Squares Curve Fitting

In curve fitting [70,71] we are given n data points (x_1, y_1), ..., (x_n, y_n) and we want to determine a function such that $f(x_i) \approx y_i$, $i = 1, ..., n$. The type of function (*eg*., linear, exponential, polynomial, etc.) is suggested by the nature of the problem and the underlying physical law. The mathematical procedure for determining the best-fit equation for a given set of data involves minimizing the differences between the y-values predicted by the approximating function and the actual data. Vertical least squares fitting proceeds by finding the sum of the squares of the vertical deviations

$$\prod = \sum [y_i - f(x_i, a_1, a_2, \ldots, a_n)]^2$$

where $a_1, a_2, \ldots, a_n$ are coefficients of the approximating function. The condition for $\prod$ to be minimized is that

$$\frac{\partial \Pi}{\partial a_i} = 0$$

for $i = 1, ..., n$. The best-fitting curve is called the least-squares regression line.

To fit an exponential function $y = ae^{bx}$ to a set of data, take the logarithm of both sides

$$\ln y = \ln a + bx$$

Letting $u = \ln y$ and $c = \ln a$, the equation becomes

$$u = bx + c$$

which is the equation for a straight line. We now proceed with the least squares curve fitting method where

$$b\sum_{i=1}^{n} x_i + cn = \sum_{i=1}^{n} \ln y_i$$

$$b\sum_{i=1}^{n} x_i^{\,2} + c\sum_{i=1}^{n} x_i = \sum_{i=1}^{n} \ln y_i$$

After solving for b and c, the original coefficient a is determined by taking the antilog of c; that is,

$$a = e^c$$

Pearson Correlation Coefficient

The correlation coefficient is a calculated quantity which measures the relative strength of the association between the independent variable x and the dependent variable y. It is used to assess the quality of the fit of the regression line to the original data. There are a number of different correlation coefficients that might be appropriate depending on the kinds of variables being studied. The most common formula used in conjunction with the least squares method of curve fitting is the product-moment coefficient of correlation, also known as the Pearson correlation,

$$\mathrm{R} = \frac{\sum xy - \dfrac{\sum x \sum y}{n}}{\sqrt{\left(\sum x^2 - \dfrac{\left(\sum x\right)^2}{n}\right)\left(\sum y^2 - \dfrac{\left(\sum y\right)^2}{n}\right)}}$$

Correlation coefficients always have a value between –1 and +1. The magnitude of the correlation coefficient indicates how tightly the data points cluster about a straight line. Positive correlations indicate that an increase in the first variable is associated with an increase in the second variable. Negative correlations indicate that as the first variable increases the second variable decreases. A correlation coefficient equal to –1, for

example, means that all data points fall on a perfectly straight line having a negative slope. A correlation coefficient of 0 indicates that the two variables are not associated. A regression analysis is most reliable when the R^2 value is at or near 1.

APPENDIX B

INSULATION RESISTANCE MEASUREMENTS

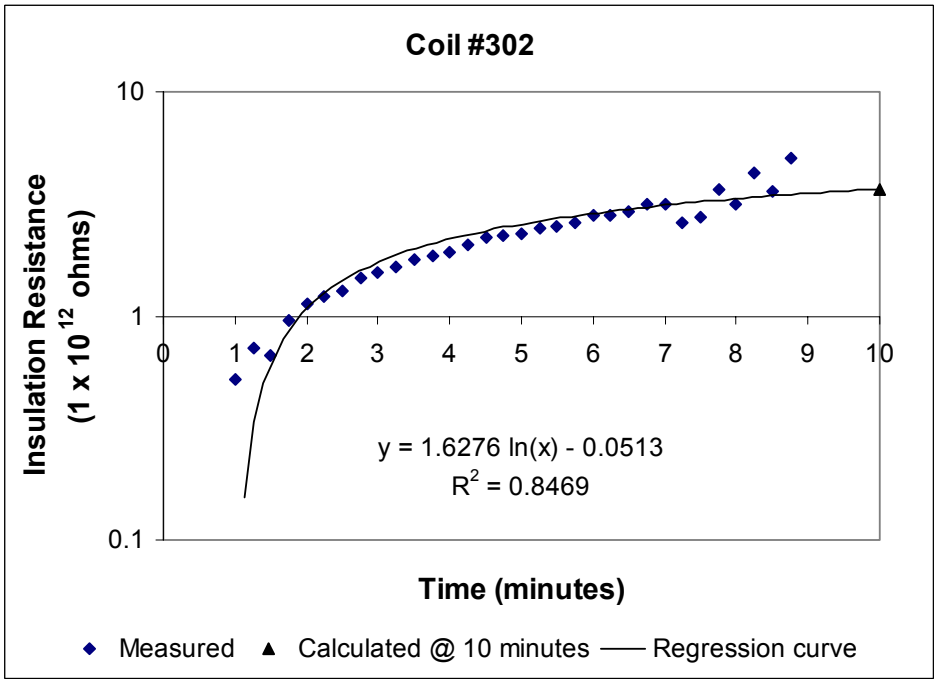

Figure B.1 Insulation resistance measurements for coil 302 (no final cure).

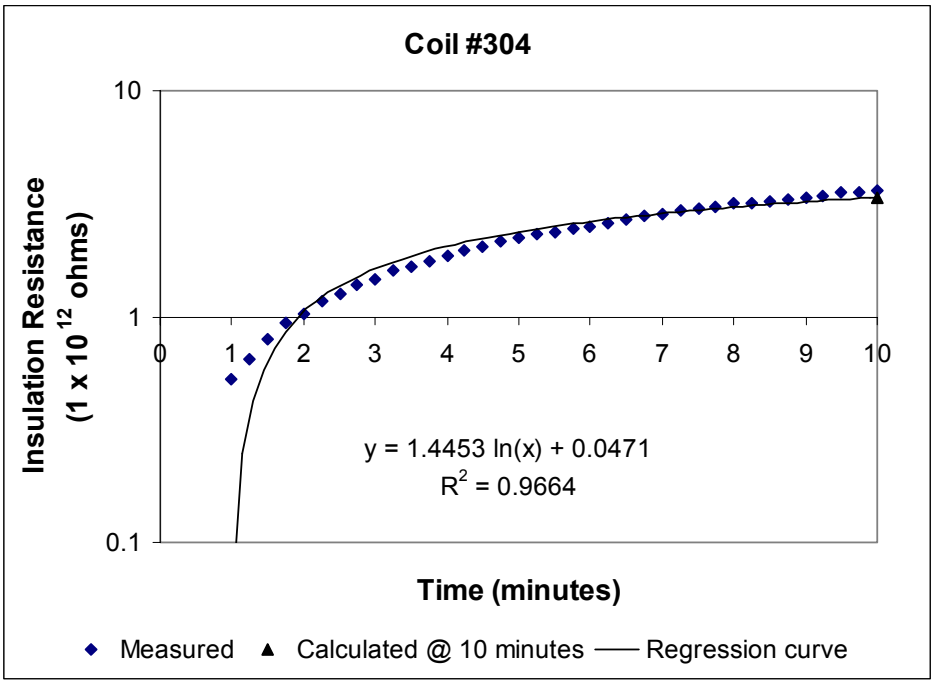

Figure B.2 Insulation resistance measurements for coil 304 (no final cure).

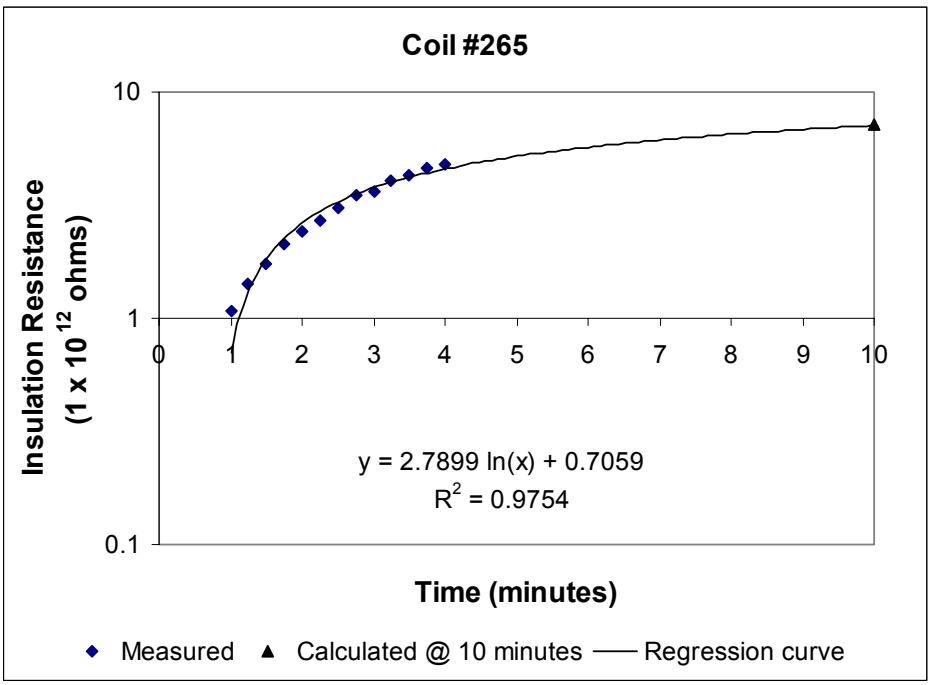

Figure B.3 Insulation resistance measurements for coil 265 (overheated).

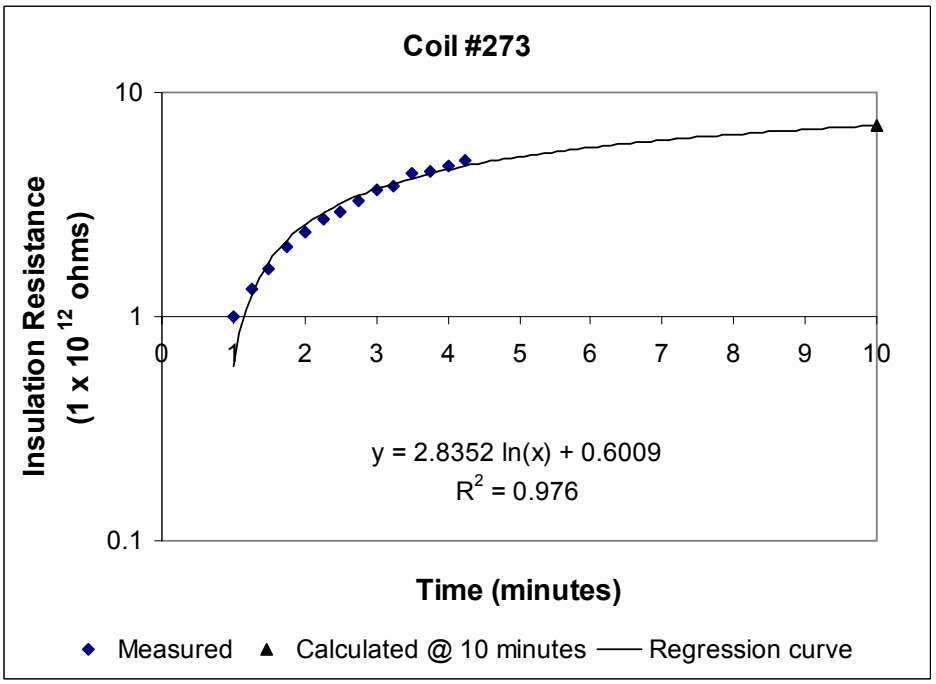

Figure B.4 Insulation resistance measurements for coil 273 (overheated).

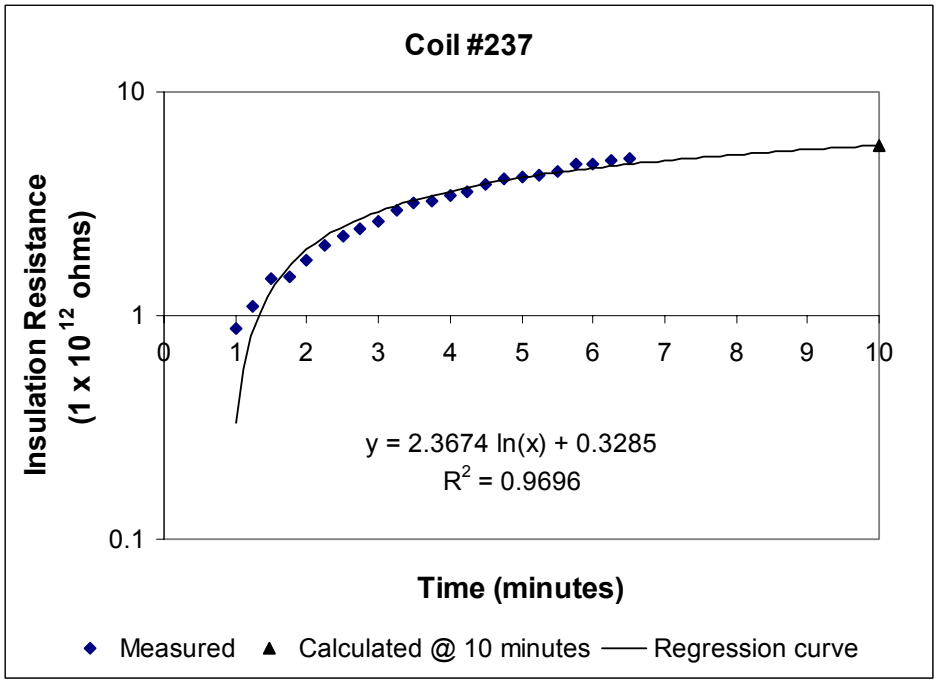

Figure B.5 Insulation resistance measurements for coil 237 (standard production).

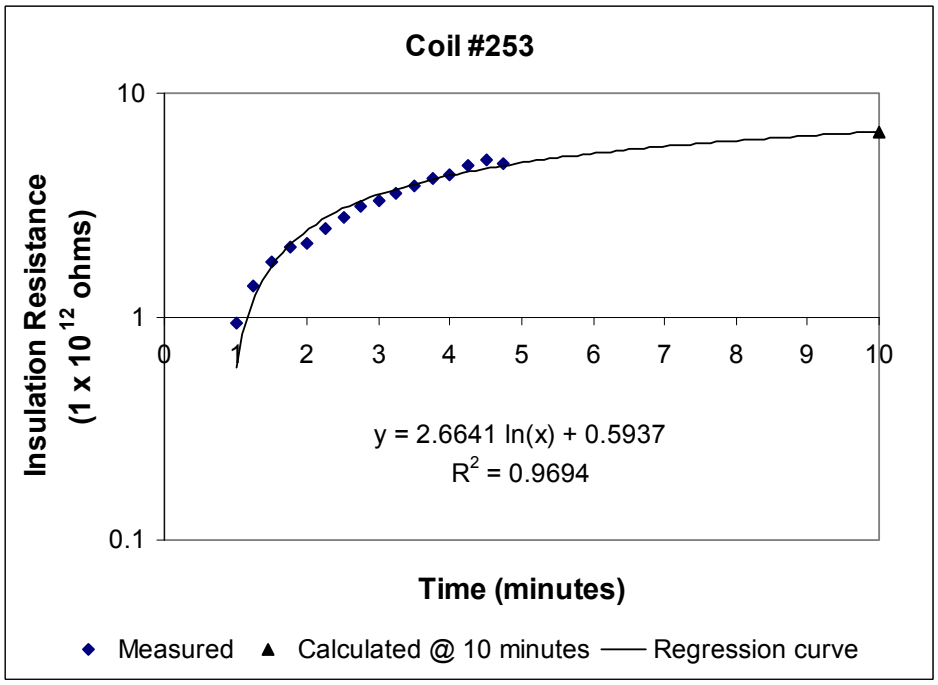

Figure B.6 Insulation resistance measurements for coil 253 (standard production).

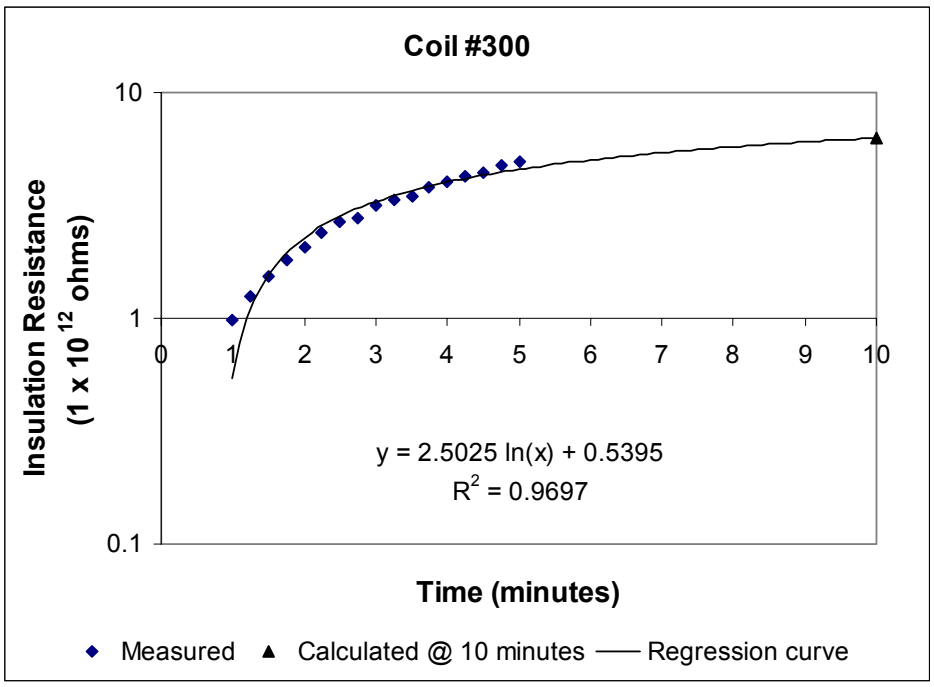

Figure B.7 Insulation resistance measurements for coil 300 (internal contamination).

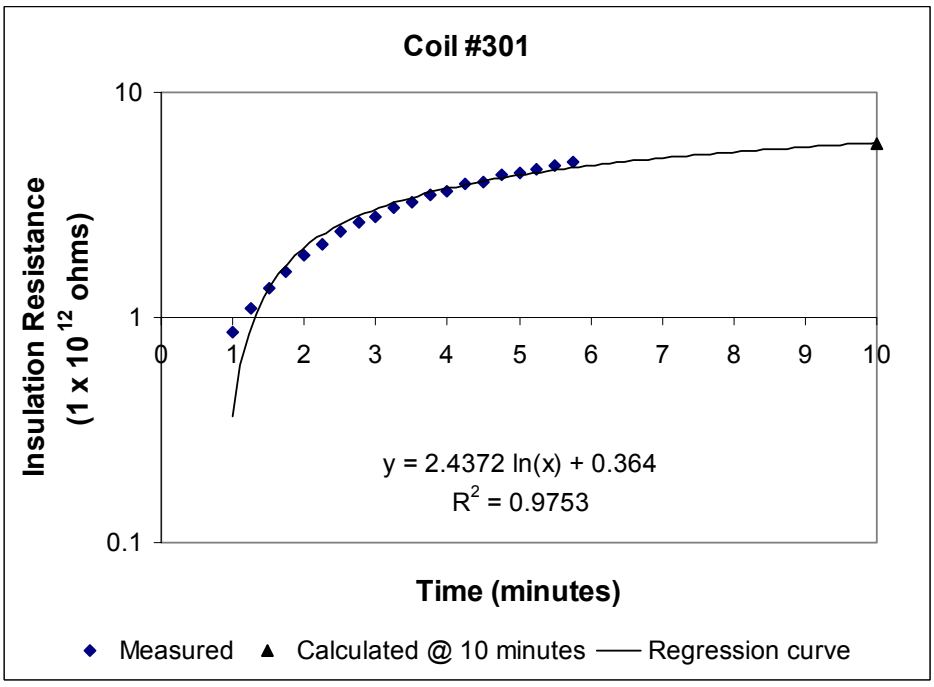

Figure B.8 Insulation resistance measurements for coil 301 (internal contamination).

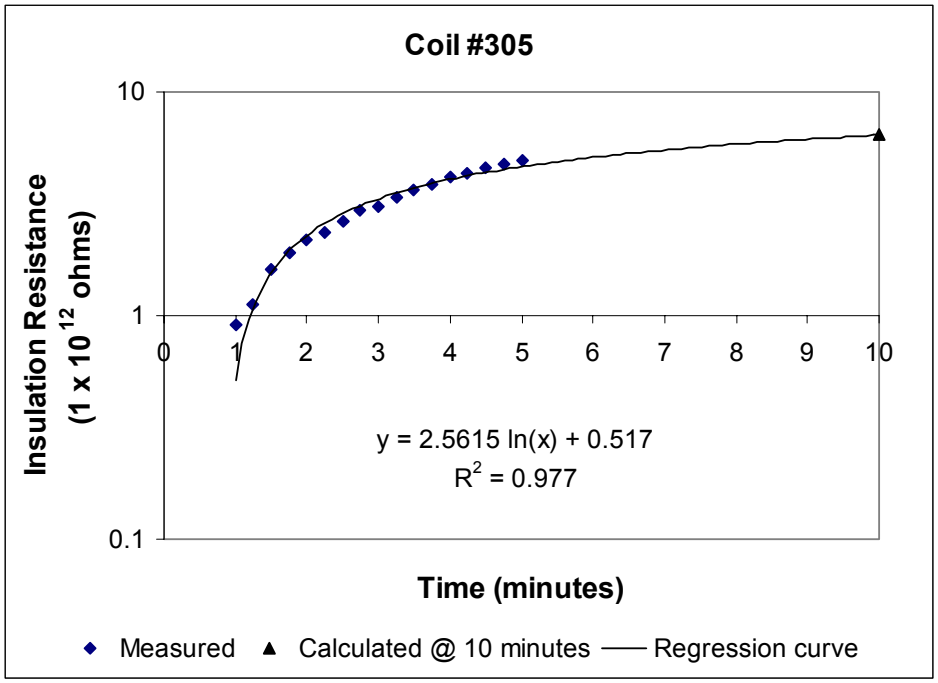

Figure B.9 Insulation resistance measurements for coil 305 (loose tapes).

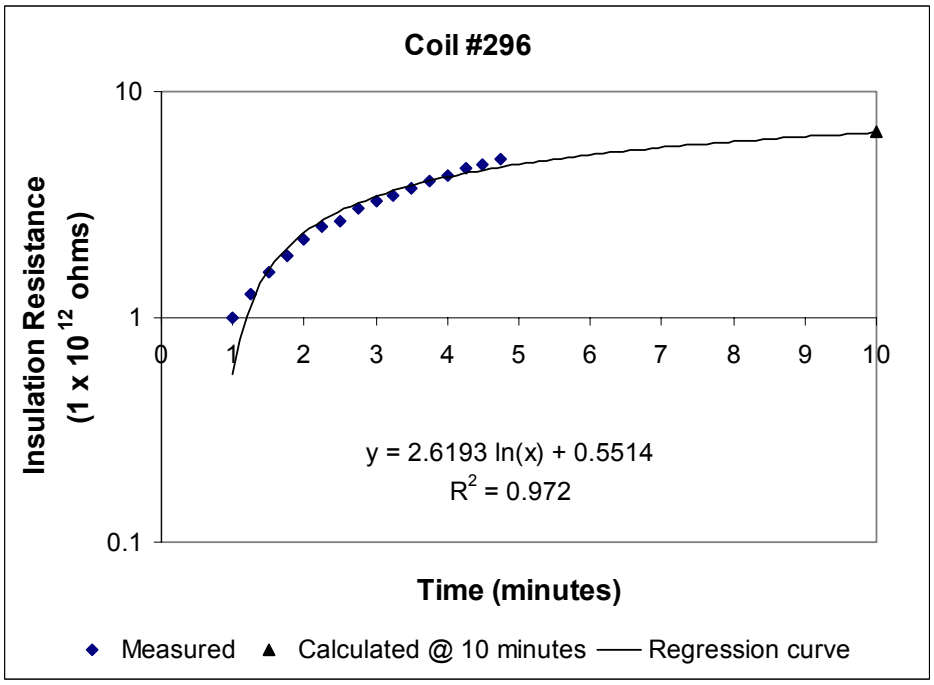

Figure B.10 Insulation resistance measurements for coil 296 (loose tapes).

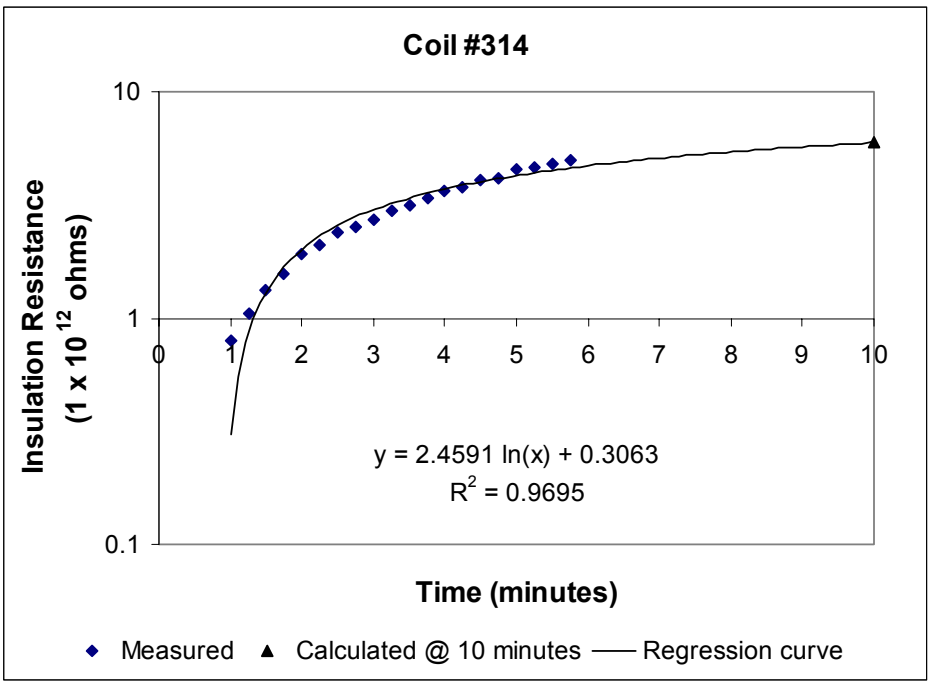

Figure B.11 Insulation resistance measurements for coil 314 (reduced tape layers).

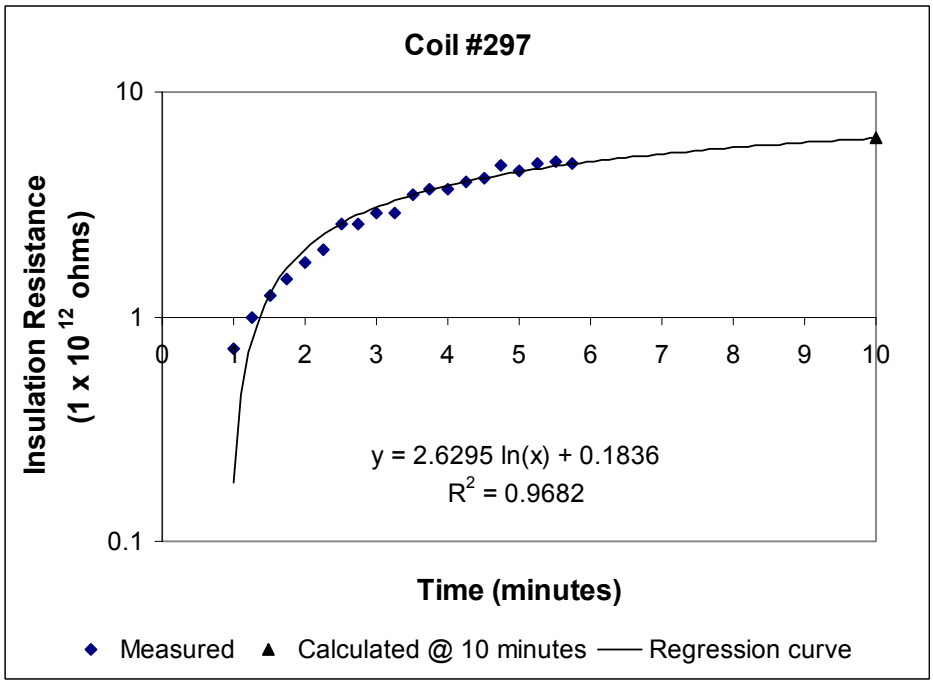

Figure B.12 Insulation resistance measurements for coil 297 (reduced tape layers).

APPENDIX C

DISSIPATION FACTOR MEASUREMENTS

Table C.1

Dissipation Factor and Permittivity Measurements at 60 Hz

Coil 237 Normal
C : 1.9143E-9 F
TanD : 6.845E-3
BalancingFactor : -2.056E-4
Measurement_Data

Amp(kV)	Freq(Hz)	EpsilonPrim	EpsilonBis	DEpsilonPrim	TanD
0.5	60	0.99395	0.00551	-0.00505	0.00554
2.0	60	0.99482	0.00587	-0.00418	0.00590
4.0	60	0.99531	0.00572	-0.00369	0.00575
6.0	60	0.99610	0.00630	-0.00290	0.00632
8.0	60	0.99864	0.00829	-0.00036	0.00830
10.0	60	1.00325	0.01198	0.00425	0.01194

Coil 253 Normal
C : 1.9309E-9 F
TanD : 6.484E-3
BalancingFactor : 1.029E-4
Measurement_Data

Amp(kV)	Freq(Hz)	EpsilonPrim	EpsilonBis	DEpsilonPrim	TanD
0.5	60	0.99389	0.00501	-0.00511	0.00504
2.0	60	0.99427	0.00562	-0.00473	0.00565
4.0	60	0.99484	0.00596	-0.00416	0.00599
6.0	60	0.99551	0.00640	-0.00349	0.00643
8.0	60	0.99674	0.00720	-0.00226	0.00722
10.0	60	0.99872	0.00874	-0.00028	0.00876

Coil 273 Overheated
C : 1.8329E-9 F
TanD : 6.968E-3
Measurement_Data

Amp(kV)	Freq(Hz)	EpsilonPrim	EpsilonBis	DEpsilonPrim	TanD
0.5	60	0.99416	0.00454	-0.00484	0.00457
2.0	60	0.99409	0.00521	-0.00491	0.00524
4.0	60	0.99519	0.00562	-0.00381	0.00565
6.0	60	0.99576	0.00611	-0.00324	0.00613
8.0	60	0.99834	0.00803	-0.00066	0.00805
10.0	60	1.00262	0.01250	0.00362	0.01247

Coil 265 Overheated
C : 1.8304E-9 F
TanD : 6.759E-3
BalancingFactor : 5.921E-5

Amp(kV)	Freq(Hz)	EpsilonPrim	EpsilonBis	DEpsilonPrim	TanD
0.5	60	0.99387	0.00491	-0.00513	0.00494
2.0	60	0.99413	0.00549	-0.00487	0.00552
4.0	60	0.99481	0.00599	-0.00419	0.00602
6.0	60	0.99565	0.00644	-0.00335	0.00647
8.0	60	0.99891	0.00939	-0.00009	0.00940
10.0	60	1.00390	0.01465	0.00490	0.01459

Coil 302 No Cure
C : 2.0036E-9 F
TanD : 1.022E-2
BalancingFactor : -1.286E-4

Amp(kV)	Freq(Hz)	EpsilonPrim	EpsilonBis	DEpsilonPrim	TanD
0.5	60	0.99184	0.00673	-0.00716	0.00678
2.0	60	0.99322	0.00796	-0.00578	0.00802
4.0	60	0.99472	0.00848	-0.00428	0.00852
6.0	60	0.99542	0.00839	-0.00358	0.00843
8.0	60	0.99732	0.00955	-0.00168	0.00958
10.0	60	0.99976	0.01169	0.00076	0.01169

Coil 304 No Cure
C : 1.9988E-9 F
TanD : 9.553E-3
BalancingFactor : -4.209E-5
Measurement_Data

Amp(kV)	Freq(Hz)	EpsilonPrim	EpsilonBis	DEpsilonPrim	TanD
0.5	60	0.99231	0.00616	-0.00669	0.00621
2.0	60	0.99323	0.00734	-0.00577	0.00739
4.0	60	0.99474	0.00812	-0.00426	0.00817
6.0	60	0.99529	0.00762	-0.00371	0.00765
8.0	60	0.99621	0.00796	-0.00279	0.00799
10.0	60	0.99834	0.00980	-0.00066	0.00982

Coil 300 Contamination
C : 1.9531E-9 F
TanD : 6.816E-3
BalancingFactor : 4.571E-5
Measurement_Data

Amp(kV)	Freq(Hz)	EpsilonPrim	EpsilonBis	DEpsilonPrim	TanD
0.5	60	0.99378	0.00505	-0.00522	0.00508
2.0	60	0.99413	0.00542	-0.00487	0.00545
4.0	60	0.99461	0.00560	-0.00439	0.00563
6.0	60	0.99712	0.00773	-0.00189	0.00775
8.0	60	1.00185	0.01057	0.00285	0.01055
10.0	60	1.00709	0.01497	0.00809	0.01487

Coil 301 Contamination
C : 1.9527E-9 F
TanD : 7.088E-3
BalancingFactor : 7.768E-5
Measurement_Data

Amp(kV)	Freq(Hz)	EpsilonPrim	EpsilonBis	DEpsilonPrim	TanD
0.5	60	0.99339	0.00517	-0.00561	0.00521
2.0	60	0.99381	0.00574	-0.00519	0.00578
4.0	60	0.99381	0.00574	-0.00519	0.00622
6.0	60	1.00096	0.01086	0.00196	0.01085
8.0	60	1.00844	0.01478	0.00944	0.01466
10.0	60	1.01566	0.02076	0.01666	0.02044

Coil 297 Reduced Tape Layers
C : 1.9094E-9 F
TanD : 7.888E-3
BalancingFactor : 2.816E-5
Measurement_Data

Amp(V)	Freq(Hz)	EpsilonPrim	EpsilonBis	DEpsilonPrim	TanD
0.5	60	0.99298	0.00546	-0.00602	0.00550
2.0	60	0.99339	0.00609	-0.00561	0.00613
4.0	60	0.99377	0.00614	-0.00523	0.00618
6.0	60	0.99430	0.00635	-0.00470	0.00639
8.0	60	0.99635	0.00793	-0.00265	0.00796
10.0	60	1.00164	0.01269	0.00264	0.01267

Coil 314 Reduced Tape Layers
C : 1.8522E-9 F
TanD : 1.065E-2
BalancingFactor : 1.756E-4
Measurement_Data

Amp(kV)	Freq(Hz)	EpsilonPrim	EpsilonBis	DEpsilonPrim	TanD
0.5	60	0.98915	0.00929	-0.00985	0.00939
2.0	60	0.98802	0.00687	-0.01098	0.00696
4.0	60	0.98701	0.00647	-0.01199	0.00655
6.0	60	0.98690	0.00644	-0.01211	0.00653
8.0	60	0.98895	0.00800	-0.01005	0.00809
10.0	60	0.99368	0.01171	-0.00532	0.01179

Coil 296 Loose Tapes
C : 1.9531E-9 F
TanD : 7.789E-3
BalancingFactor : -1.213E-4
Measurement_Data

Amp(kV)	Freq(Hz)	EpsilonPrim	EpsilonBis	DEpsilonPrim	TanD
0.5	6.02E+01	0.99316	0.00535	-0.00584	0.00538
2.0	6.02E+01	0.99395	0.00628	-0.00505	0.00632
4.0	6.02E+01	0.99551	0.00686	-0.00349	0.00689
6.0	6.02E+01	0.99606	0.00724	-0.00294	0.00727
8.0	6.02E+01	0.99880	0.00877	-0.00020	0.00878
10.0	6.02E+01	1.00255	0.01195	0.00355	0.01192

Coil 305 Loose Tapes
C : 1.9514E-9 F
TanD : 8.081E-3
Measurement_Data

Amp(kV)	Freq(Hz)	EpsilonPrim	EpsilonBis	DEpsilonPrim	TanD
0.5	6.02E+01	0.99372	0.00526	-0.00528	0.00529
2.0	6.02E+01	0.99387	0.00660	-0.00513	0.00664
4.0	6.02E+01	0.99498	0.00702	-0.00402	0.00705
6.0	6.02E+01	0.99542	0.00679	-0.00358	0.00682
8.0	6.02E+01	0.99641	0.00715	-0.00259	0.00718
10.0	6.02E+01	0.99875	0.00903	-0.00025	0.00904

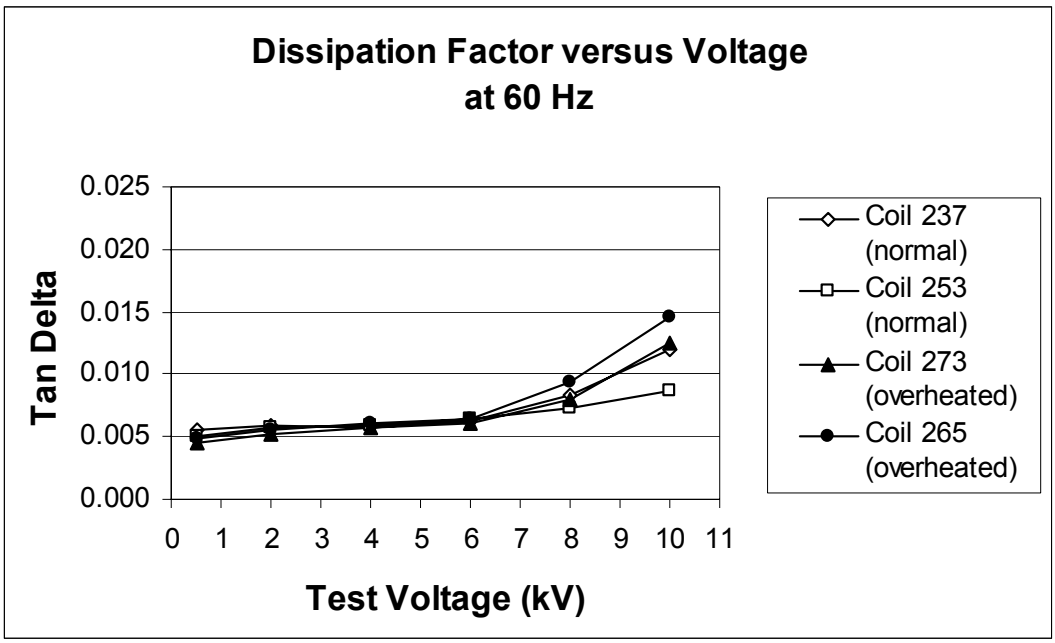

Figure C.1 Comparison of normal and overheated stator coils.

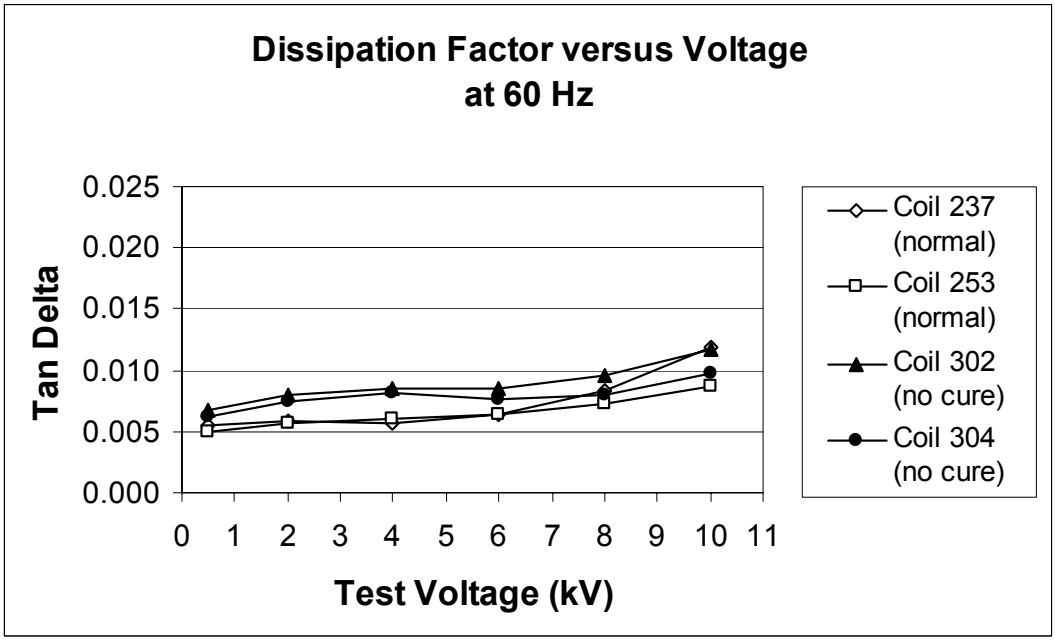

Figure C.2 Comparison of normal stator coils and those with no final cure.

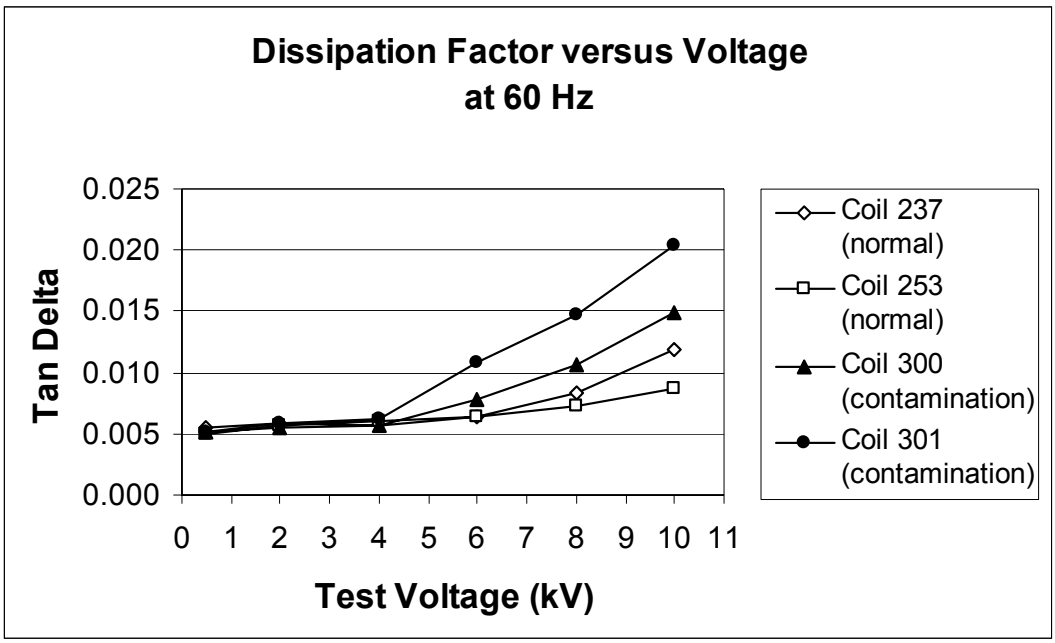

Figure C.3 Comparison of normal and contaminated stator coils.

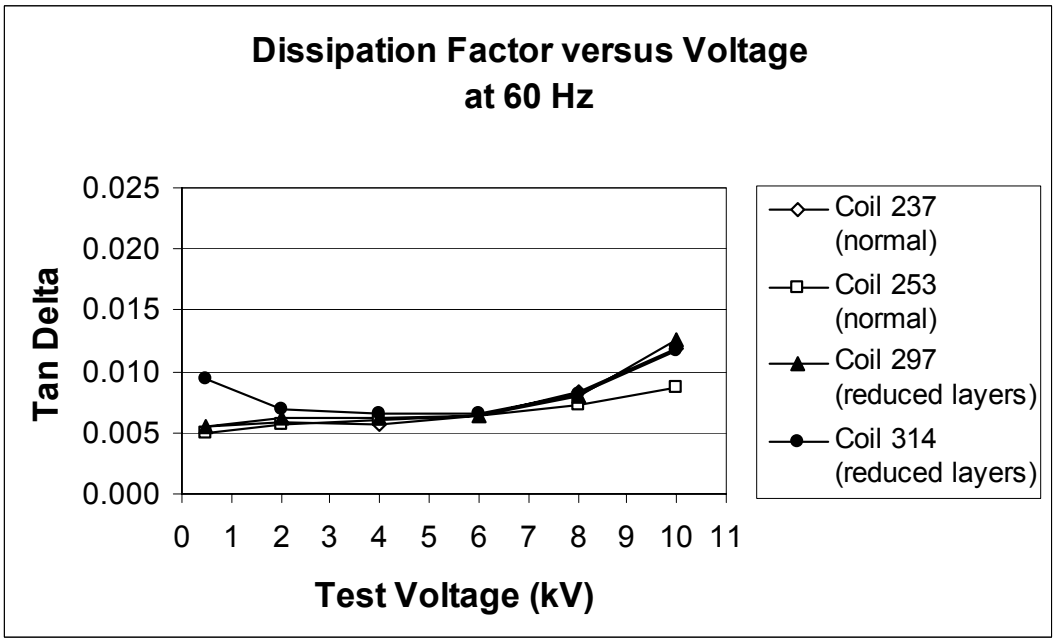

Figure C.4 Comparison of normal stator coils and those with a reduced number of tape layers.

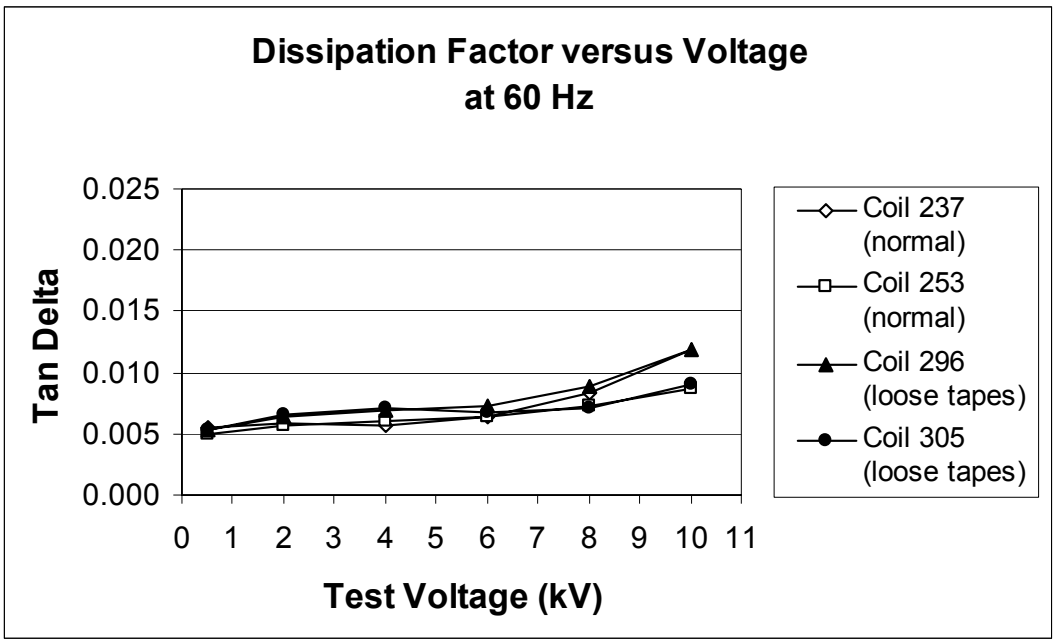

Figure C.5 Comparison of normal stator coils and those with loose tapes.

APPENDIX D

DISPLACEMENT AND LOSS MEASUREMENTS AT 0.01 HZ

Table D.1

Dissipation Factor and Permittivity Measurements at 0.01 Hz

Coil 237 Normal
C : 1.9143E-9 F
TanD : 6.845E-3
BalancingFactor : -2.056E-4
Measurement_Data

Amp(kV)	Freq(Hz)	EpsilonPrim	EpsilonBis	DEpsilonPrim	TanD
0.5	0.01	1.05792	0.01779	0.05892	0.01682
2.0	0.01	1.05827	0.01841	0.05927	0.01739
4.0	0.01	1.05874	0.01901	0.05974	0.01795
6.0	0.01	1.05986	0.02034	0.06086	0.01919
8.0	0.01	1.06294	0.02321	0.06394	0.02184
10.0	0.01	1.06837	0.02720	0.06937	0.02546

Coil 253 Normal
C : 1.9309E-9 F
TanD : 6.484E-3
BalancingFactor : 1.029E-4

Amp(kV)	Freq(Hz)	EpsilonPrim	EpsilonBis	DEpsilonPrim	TanD
0.5	0.01	1.06235	0.02020	0.06335	0.01902
2.0	0.01	1.06319	0.02051	0.06419	0.01929
4.0	0.01	1.06613	0.02068	0.06713	0.01940
6.0	0.01	1.06648	0.02144	0.06748	0.02011
8.0	0.01	1.06838	0.02349	0.06939	0.02198
10.0	0.01	1.07193	0.02663	0.07293	0.02484

Coil 273 Overheated
C : 1.8329E-9 F
TanD : 6.968E-3
Measurement_Data

Amp(kV)	Freq(Hz)	EpsilonPrim	EpsilonBis	DEpsilonPrim	TanD
0.5	0.01	1.09113	0.02106	0.09213	0.01930
2.0	0.01	1.09276	0.02091	0.09376	0.01914
4.0	0.01	1.09443	0.02117	0.09543	0.01934
6.0	0.01	1.09503	0.02225	0.09603	0.02032
8.0	0.01	1.09817	0.02482	0.09917	0.02260
10.0	0.01	1.10348	0.02941	0.10448	0.02665

Coil 265 Overheated
C : 1.8304E-9 F
TanD : 6.759E-3
BalancingFactor : 5.921E-5

Amp(kV)	Freq(Hz)	EpsilonPrim	EpsilonBis	DEpsilonPrim	TanD
0.5	0.01	1.06873	0.02302	0.06973	0.02154
2.0	0.01	1.07185	0.02298	0.07285	0.02144
4.0	0.01	1.07371	0.02323	0.07471	0.02163
6.0	0.01	1.07535	0.02429	0.07635	0.02259
8.0	0.01	1.07890	0.02760	0.07990	0.02558
10.0	0.01	1.08430	0.03232	0.08530	0.02981

Coil 302 No Cure
C : 2.0036E-9 F
TanD : 1.022E-2
BalancingFactor : -1.286E-4

Amp(kV)	Freq(Hz)	EpsilonPrim	EpsilonBis	DEpsilonPrim	TanD
0.5	0.01	1.10915	0.04040	0.11015	0.03642
2.0	0.01	1.11077	0.03627	0.11177	0.03265
4.0	0.01	1.11116	0.03410	0.11216	0.03069
6.0	0.01	1.11257	0.03354	0.11357	0.03015
8.0	0.01	1.11301	0.03402	0.11401	0.03057
10.0	0.01	1.11517	0.03604	0.11617	0.03232

Coil 304 No Cure
C : 1.9988E-9 F
TanD : 9.553E-3
BalancingFactor : -4.209E-5
Measurement_Data

Amp(kV)	Freq(Hz)	EpsilonPrim	EpsilonBis	DEpsilonPrim	TanD
0.5	0.01	1.09228	0.03168	0.09328	0.02901
2.0	0.01	1.09503	0.02987	0.09604	0.02728
4.0	0.01	1.09620	0.02883	0.09720	0.02630
6.0	0.01	1.09735	0.02848	0.09835	0.02595
8.0	0.01	1.09905	0.02918	0.10005	0.02655
10.0	0.01	1.10149	0.03109	0.10249	0.02822

Coil 300 Contamination
C : 1.9531E-9 F
TanD : 6.816E-3
BalancingFactor : 4.571E-5
Measurement_Data

Amp(kV)	Freq(Hz)	EpsilonPrim	EpsilonBis	DEpsilonPrim	TanD
0.5	0.01	1.06835	0.02132	0.06935	0.01996
2.0	0.01	1.06856	0.02157	0.06956	0.02019
4.0	0.01	1.06790	0.02176	0.06890	0.02038
6.0	0.01	1.06911	0.02428	0.07011	0.02271
8.0	0.01	1.07548	0.02837	0.07648	0.02638
10.0	0.01	1.08165	0.03202	0.08265	0.02960

Coil 301 Contamination
C : 1.9527E-9 F
TanD : 7.088E-3
BalancingFactor : 7.768E-5
Measurement_Data

Amp(kV)	Freq(Hz)	EpsilonPrim	EpsilonBis	DEpsilonPrim	TanD
0.5	0.01	1.07413	0.02499	0.07513	0.02327
2.0	0.01	1.07677	0.02460	0.07777	0.02285
4.0	0.01	1.07891	0.02459	0.07991	0.02280
6.0	0.01	1.07906	0.02703	0.08006	0.02505
8.0	0.01	1.09290	0.03415	0.09390	0.03125
10.0	0.01	1.10336	0.03850	0.10436	0.03489

Coil 297 Reduced Tape Layers
C : 1.9094E-9 F
TanD : 7.888E-3
BalancingFactor : 2.816E-5
Measurement_Data

Amp(kV)	Freq(Hz)	EpsilonPrim	EpsilonBis	DEpsilonPrim	TanD
0.5	0.01	1.08131	0.02705	0.08231	0.02502
2.0	0.01	1.08070	0.02644	0.08170	0.02446
4.0	0.01	1.08184	0.02664	0.08284	0.02463
6.0	0.01	1.08260	0.02746	0.08360	0.02537
8.0	0.01	1.08663	0.03078	0.08763	0.02833
10.0	0.01	1.09298	0.03579	0.09398	0.03275

Coil 314 Reduced Tape Layers
C : 1.8522E-9 F
TanD : 1.065E-2
BalancingFactor : 1.756E-4
Measurement_Data

Amp(kV)	Freq(Hz)	EpsilonPrim	EpsilonBis	DEpsilonPrim	TanD
0.5	0.01	1.05801	0.02184	0.05901	0.02064
2.0	0.01	1.06210	0.02323	0.06310	0.02187
4.0	0.01	1.06528	0.02418	0.06628	0.02269
6.0	0.01	1.06568	0.02561	0.06668	0.02403
8.0	0.01	1.07224	0.02927	0.07324	0.02730
10.0	0.01	1.07818	0.03474	0.07918	0.03222

Coil 296 Loose Tapes
C : 1.9531E-9 F
TanD : 7.789E-3
BalancingFactor : -1.213E-4
Measurement_Data

Amp(kV)	Freq(Hz)	EpsilonPrim	EpsilonBis	DEpsilonPrim	TanD
0.5	0.01	1.09078	0.03040	0.09178	0.02787
2.0	0.01	1.09268	0.02934	0.09368	0.02685
4.0	0.01	1.09350	0.02883	0.09450	0.02636
6.0	0.01	1.09319	0.02904	0.09419	0.02656
8.0	0.01	1.09724	0.03169	0.09824	0.02888
10.0	0.01	1.10190	0.03493	0.10290	0.03170

Coil 305 Loose Tapes
C : 1.9514E-9 F
TanD : 8.081E-3
Measurement_Data

Amp(kV)	Freq(Hz)	EpsilonPrim	EpsilonBis	DEpsilonPrim	TanD
0.5	0.01	1.09181	0.04206	0.09281	0.03852
2.0	0.01	1.09348	0.02446	0.09448	0.02237
4.0	0.01	1.09629	0.02586	0.09729	0.02359
6.0	0.01	1.09537	0.02495	0.09637	0.02278
8.0	0.01	1.09781	0.02604	0.09881	0.02372
10.0	0.01	1.10155	0.02927	0.10255	0.02657

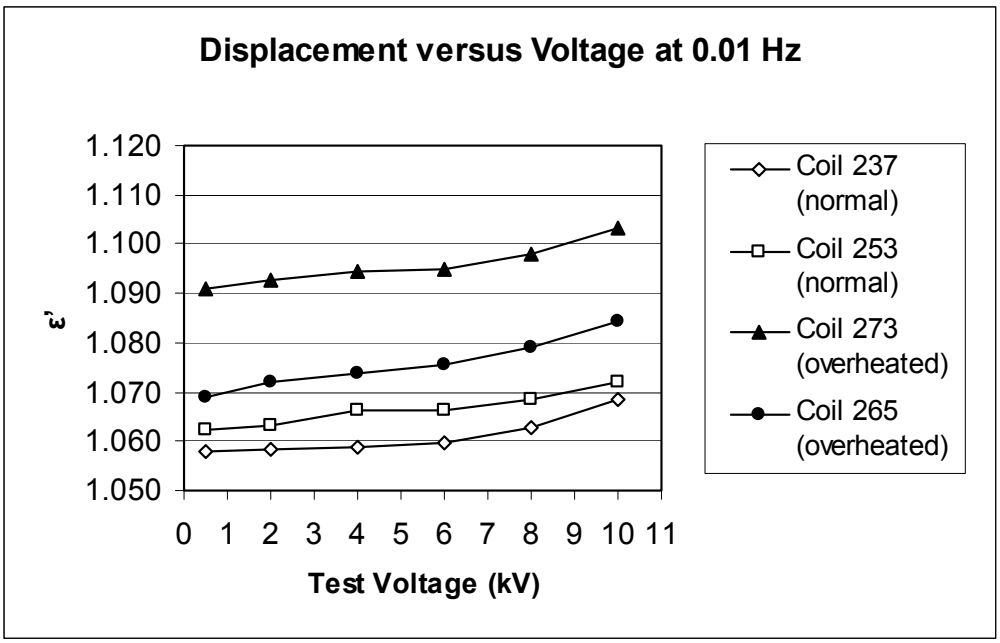

Figure D.1 Comparison of normal and overheated stator coils.

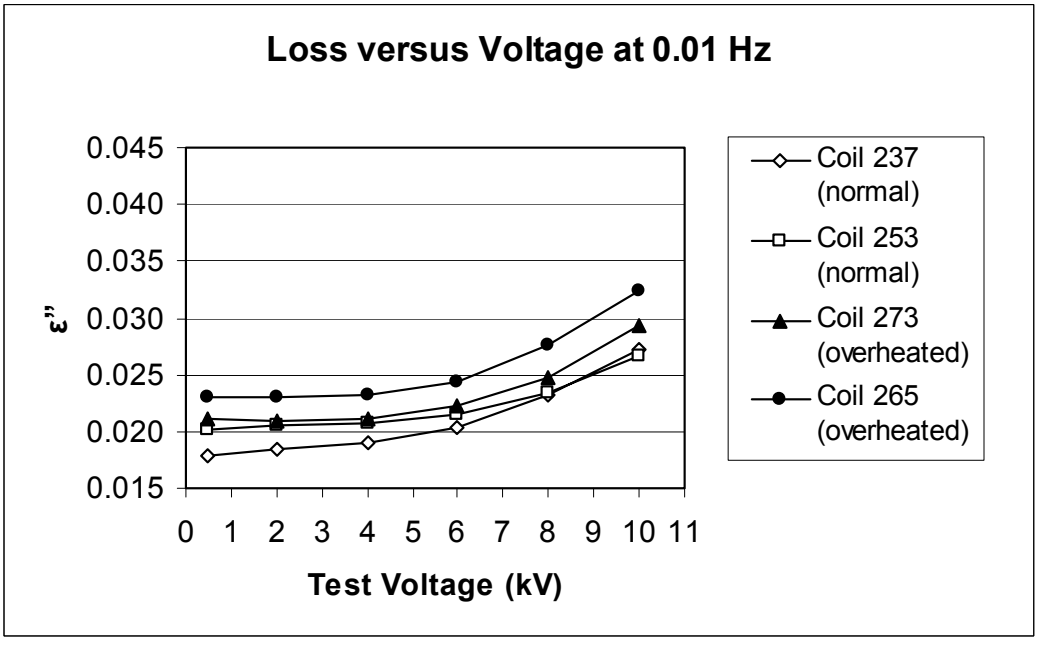

Figure D.2 Comparison of normal and overheated stator coils.

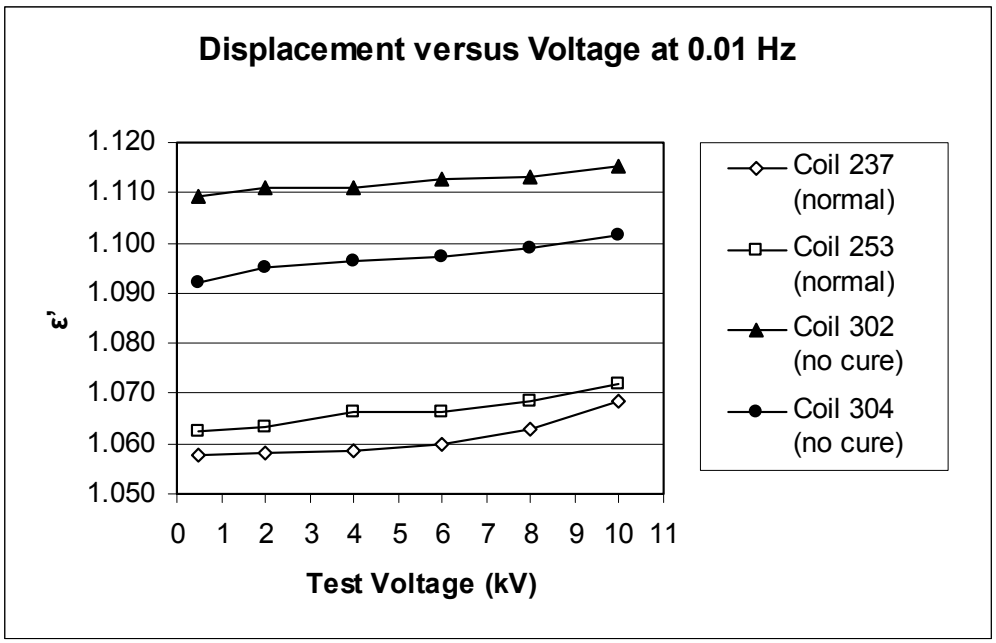

Figure D.3 Comparison of normal and incompletely cured stator coils.

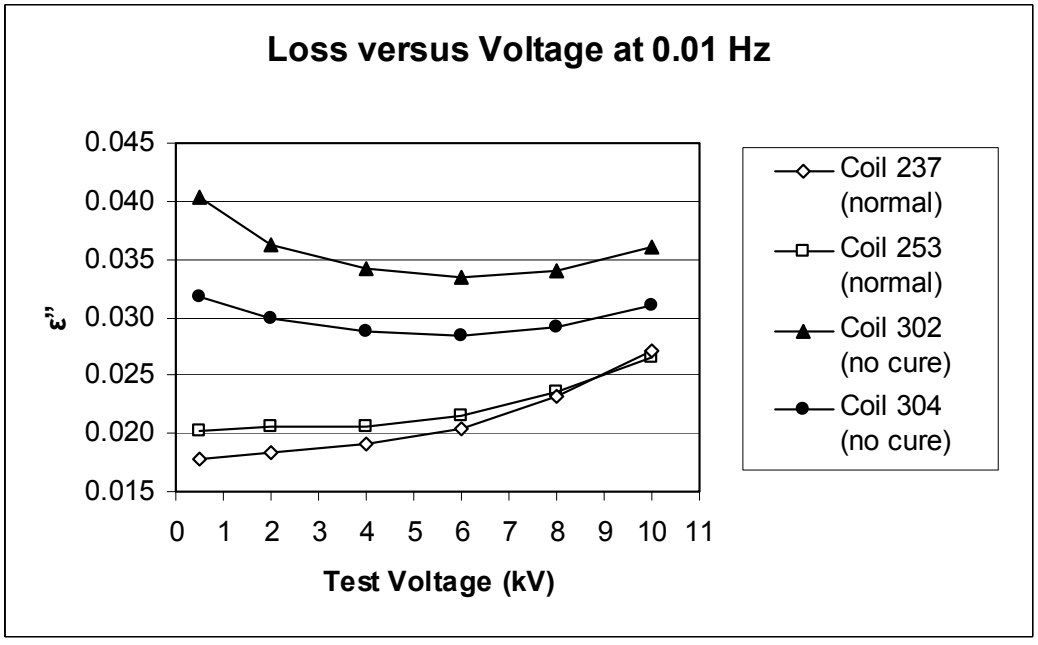

Figure D.4 Comparison of normal and incompletely cured stator coils.

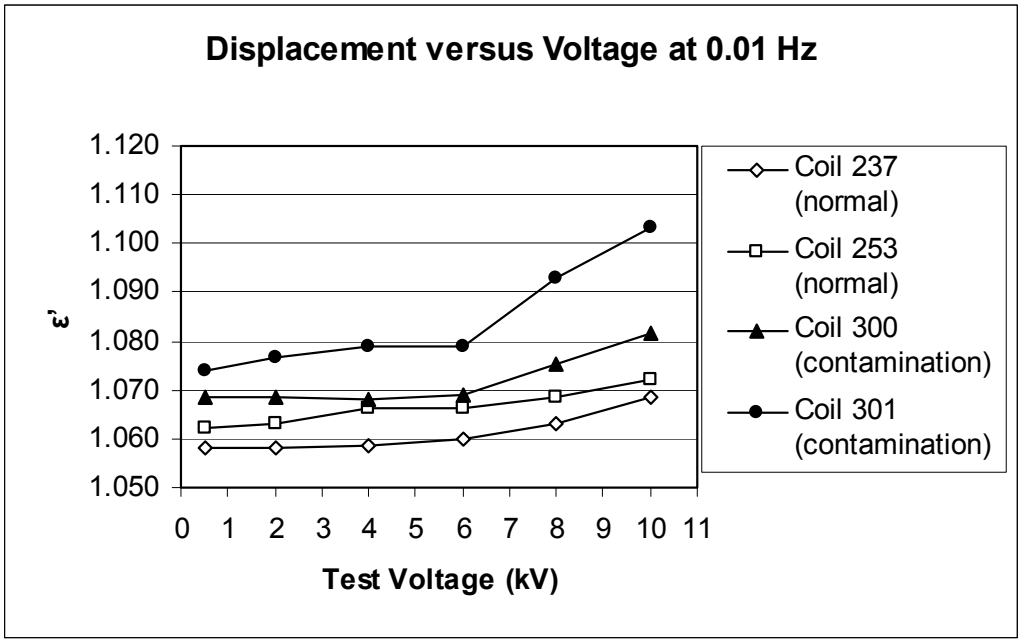

Figure D.5 Comparison of normal and contaminated stator coils.

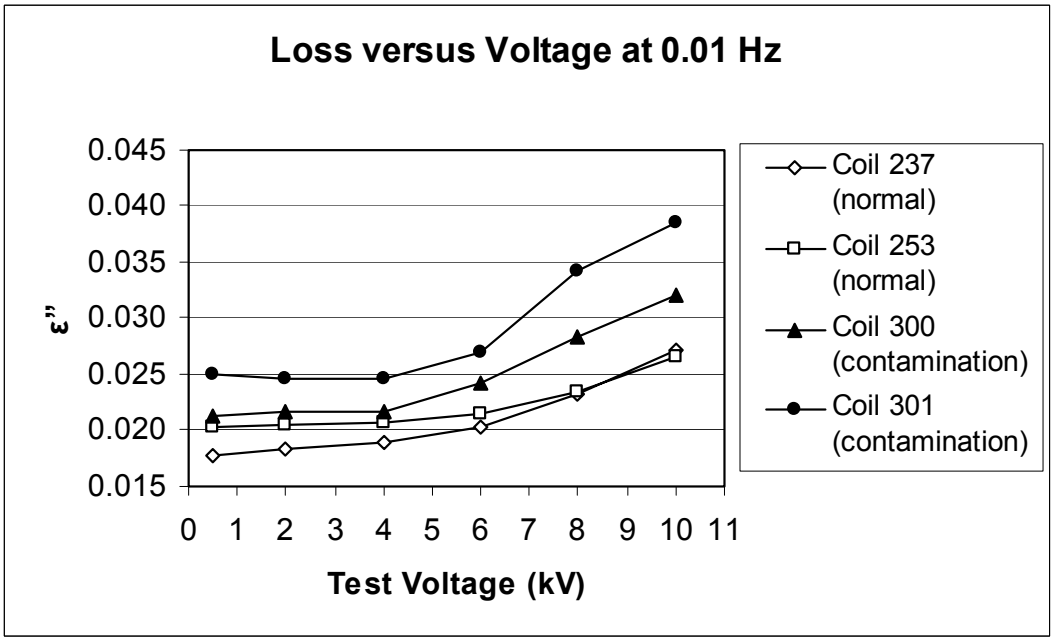

Figure D.6 Comparison of normal and contaminated stator coils.

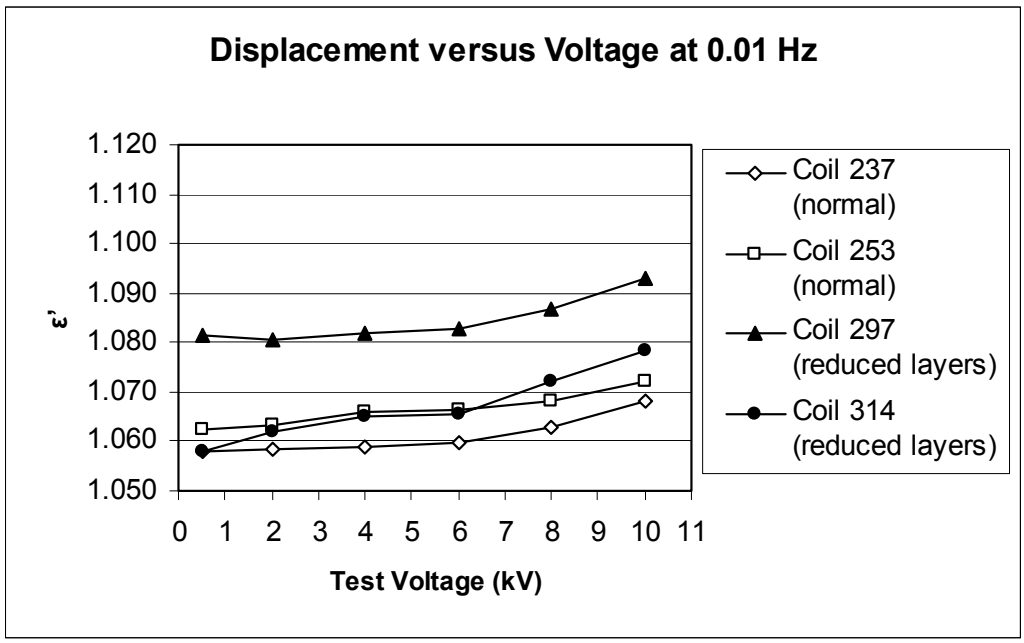

Figure D.7 Comparison of normal stator coils and those with reduced tape layers.

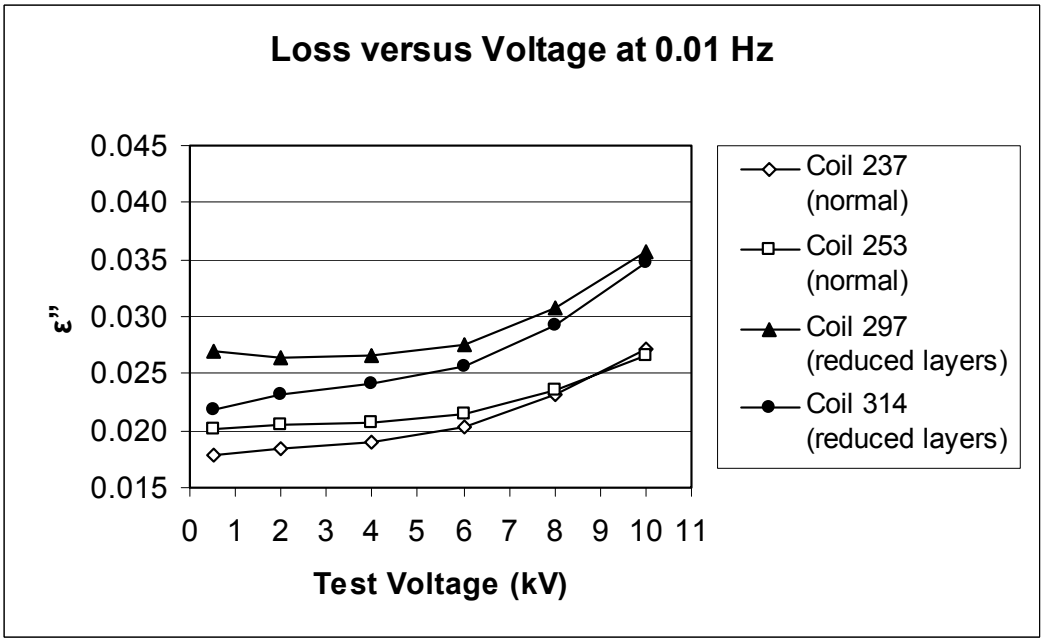

Figure D.8 Comparison of normal stator coils and those with reduced tape layers.

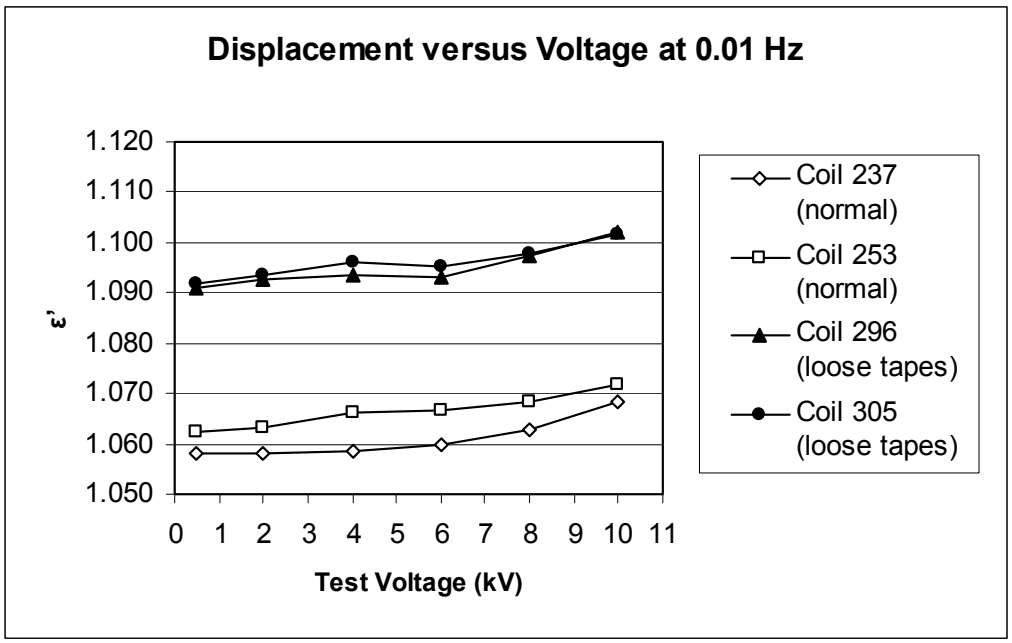

Figure D.9 Comparison of normal stator coils and those with loose or wrinkled tapes.

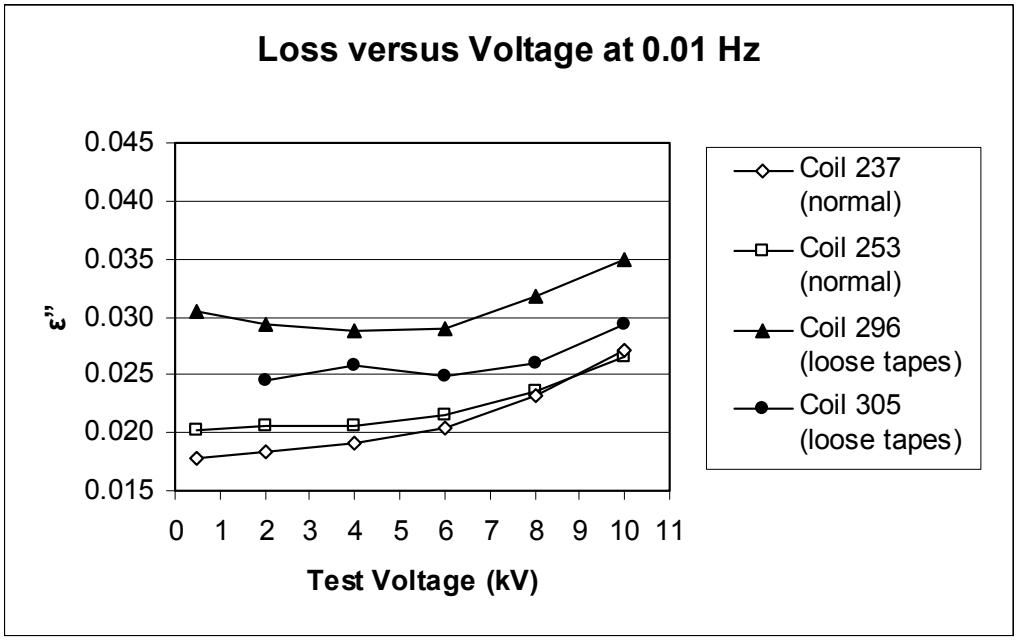

Figure D.10 Comparison of normal stator coils and those with loose or wrinkled tapes. (The data recorded at 0.5 kV for coil 305 appeared aberrant and was not plotted.)

APPENDIX E

PARTIAL DISCHARGE MEASUREMENTS

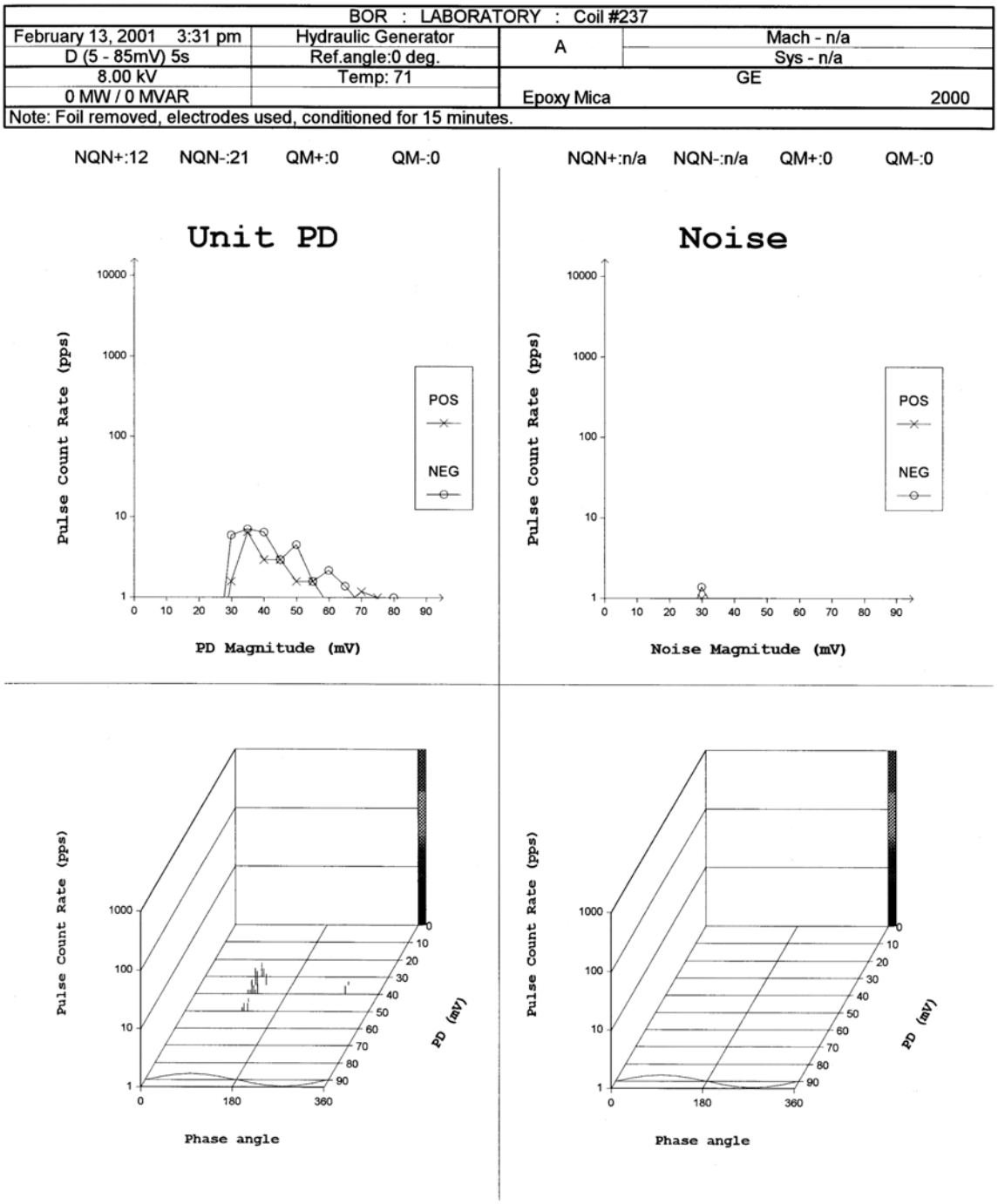

Figure E.1 Partial discharge measurements of Coil #237 (standard production). Tests results show no pulse polarity predominance.

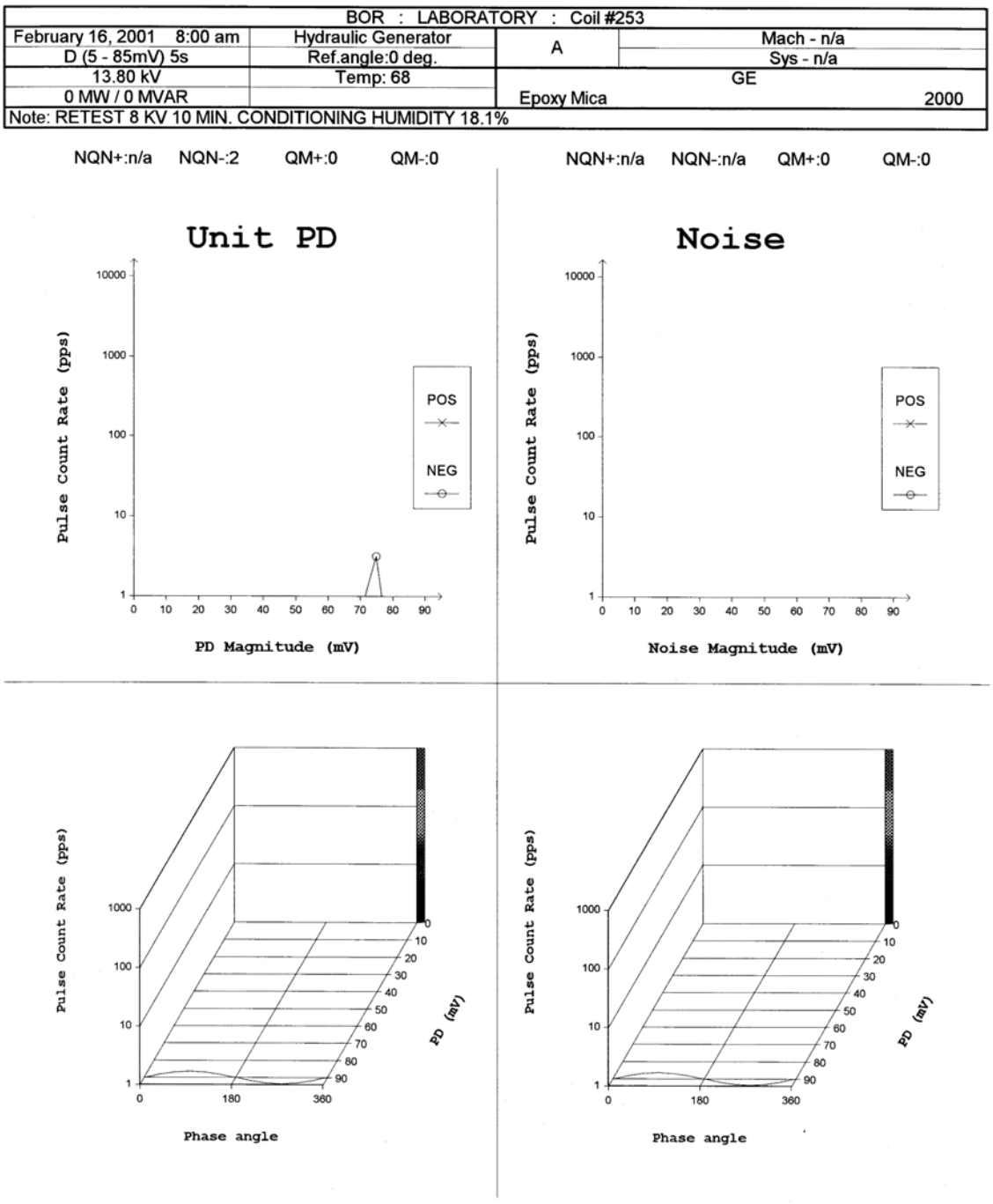

Figure E.2 Partial discharge measurements of Coil #253 (standard production). Tests results show negligible PD.

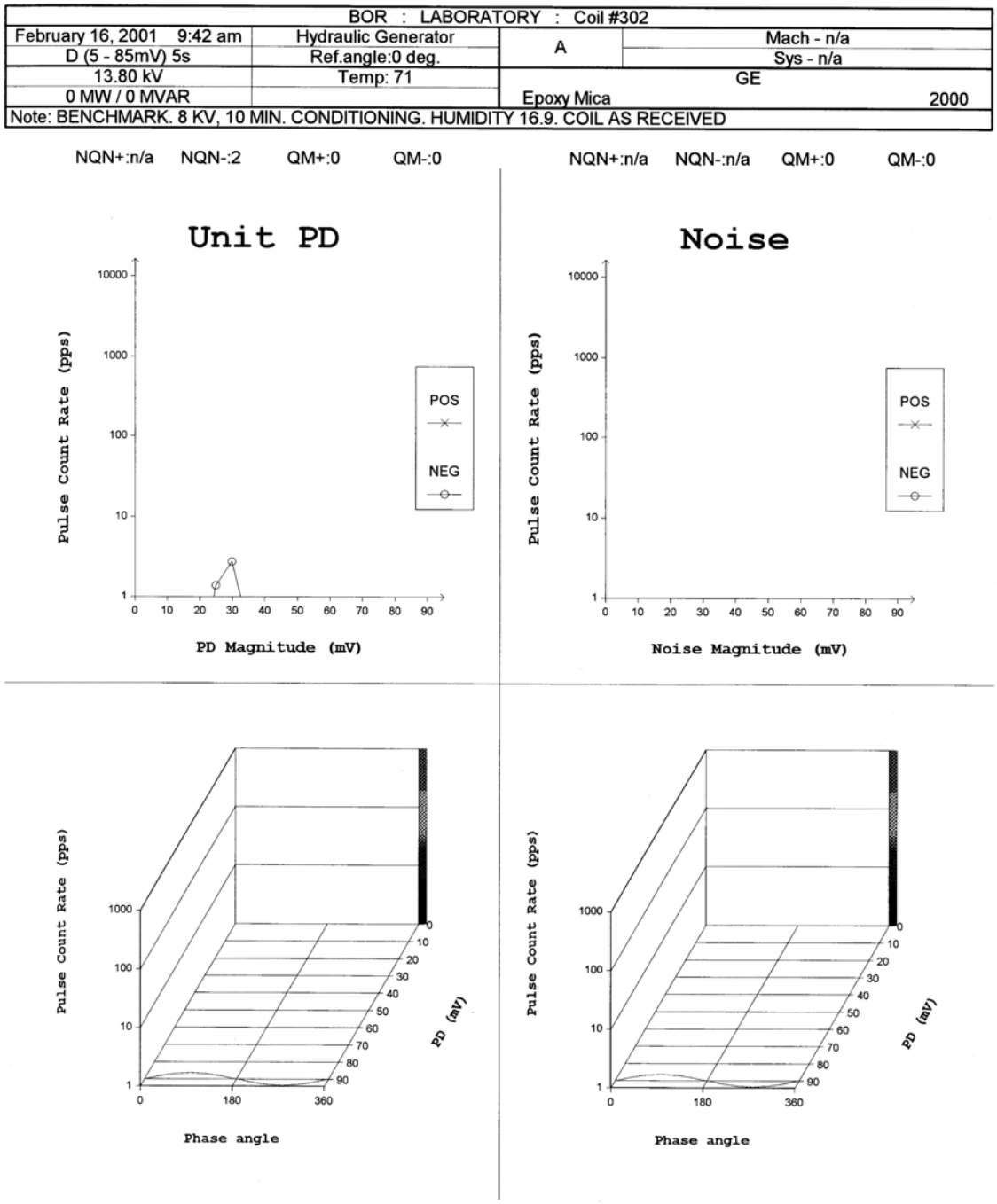

Figure E.3 Partial discharge measurements of Coil #302 (no final cure). Tests results show negligible PD.

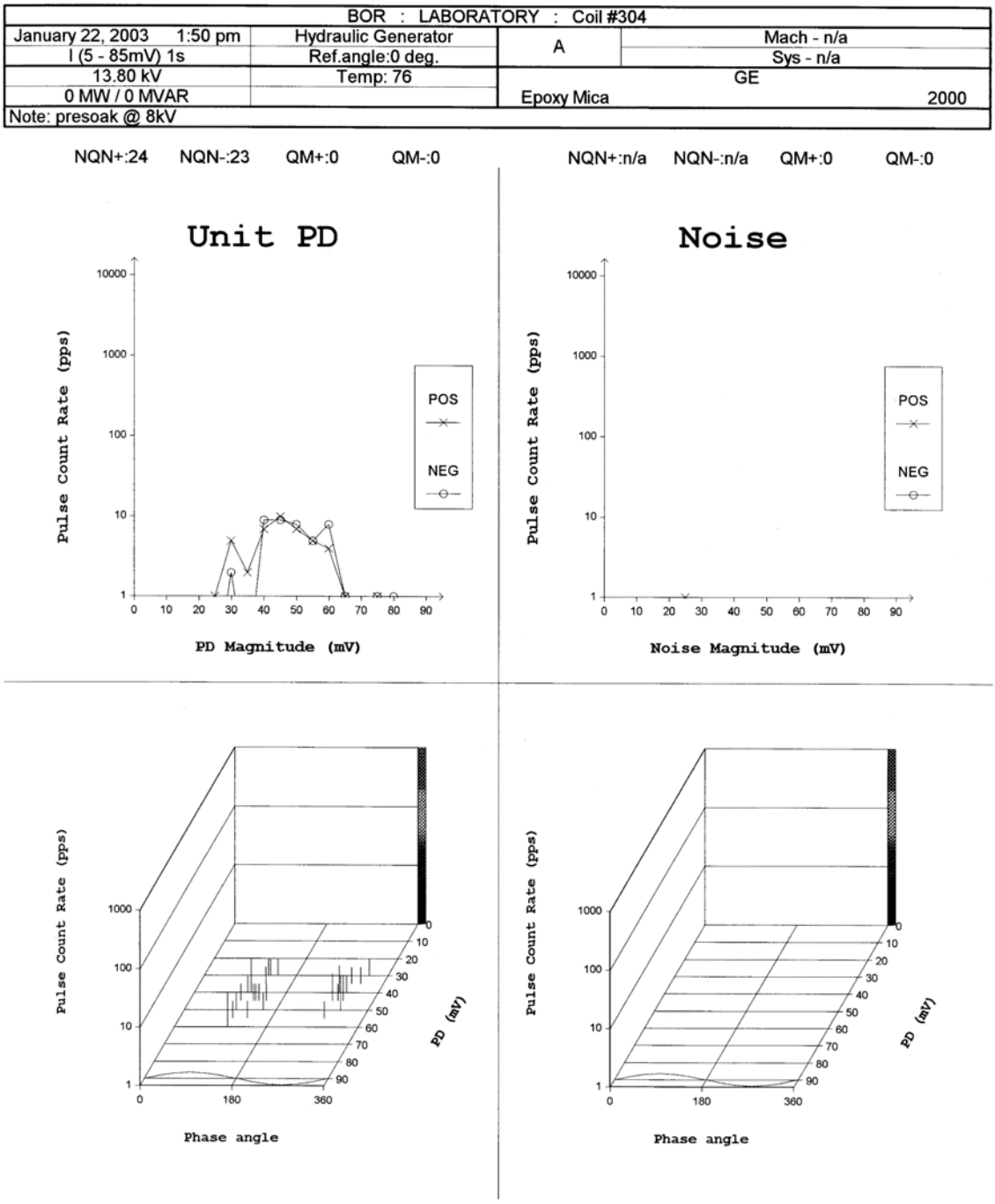

Figure E.4 Partial discharge measurements of Coil #304 (no final cure). Tests results show no pulse polarity predominance.

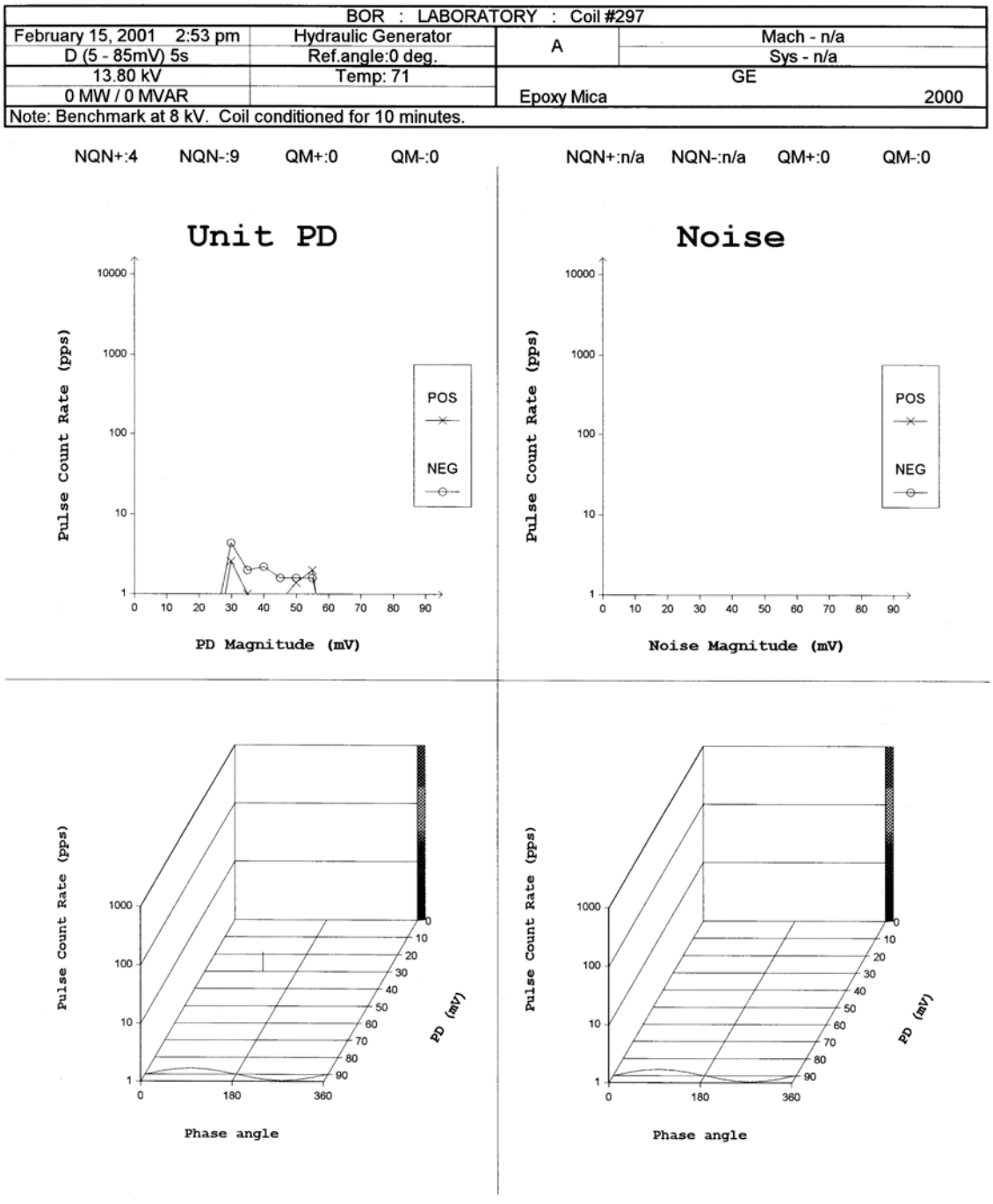

Figure E.5 Partial discharge measurements of Coil #297 (reduced layers). Tests results show negligible PD.

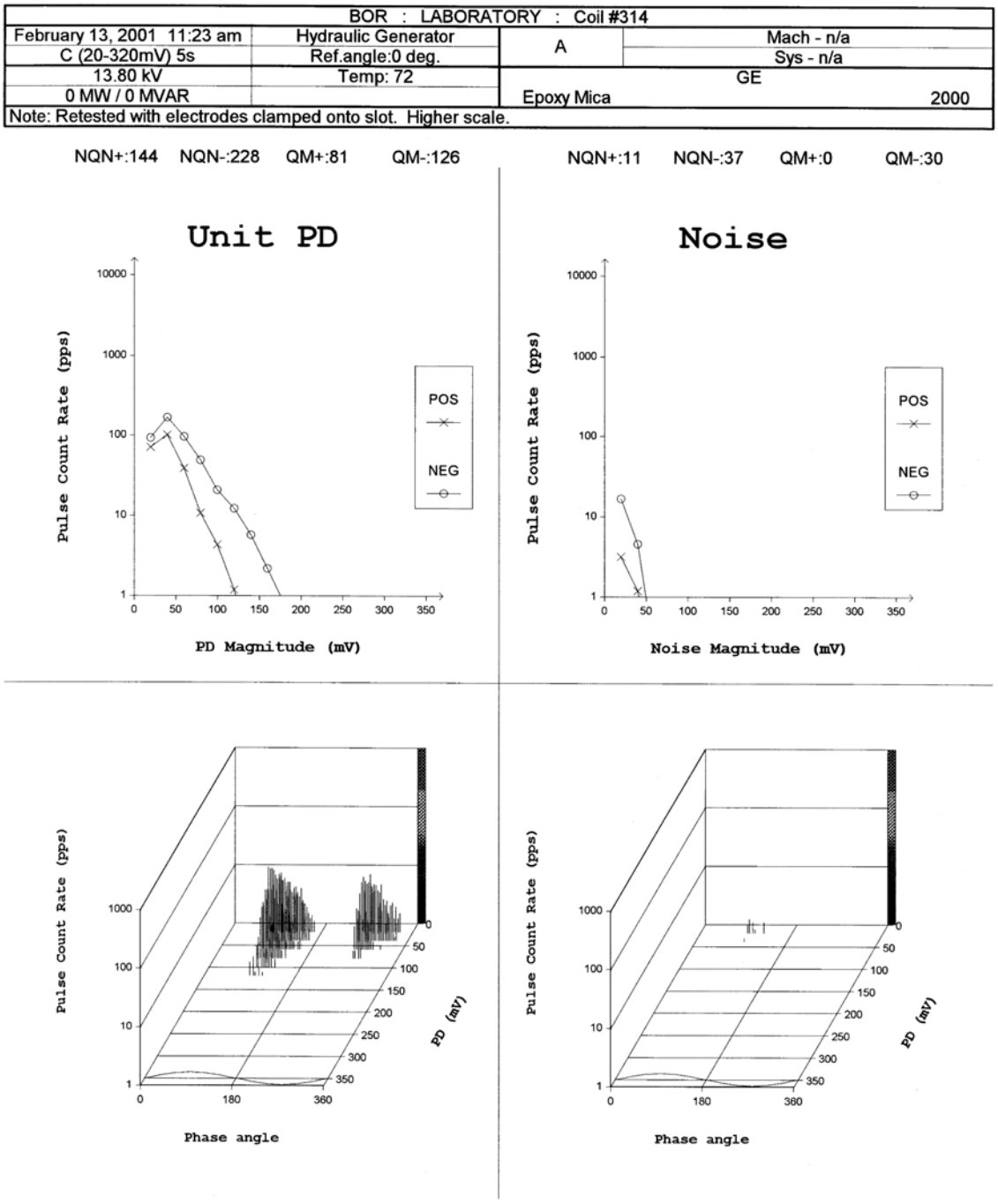

Figure E.6 Partial discharge measurements of Coil 314 (reduced layers). Tests results show a slight negative pulse polarity predominance.

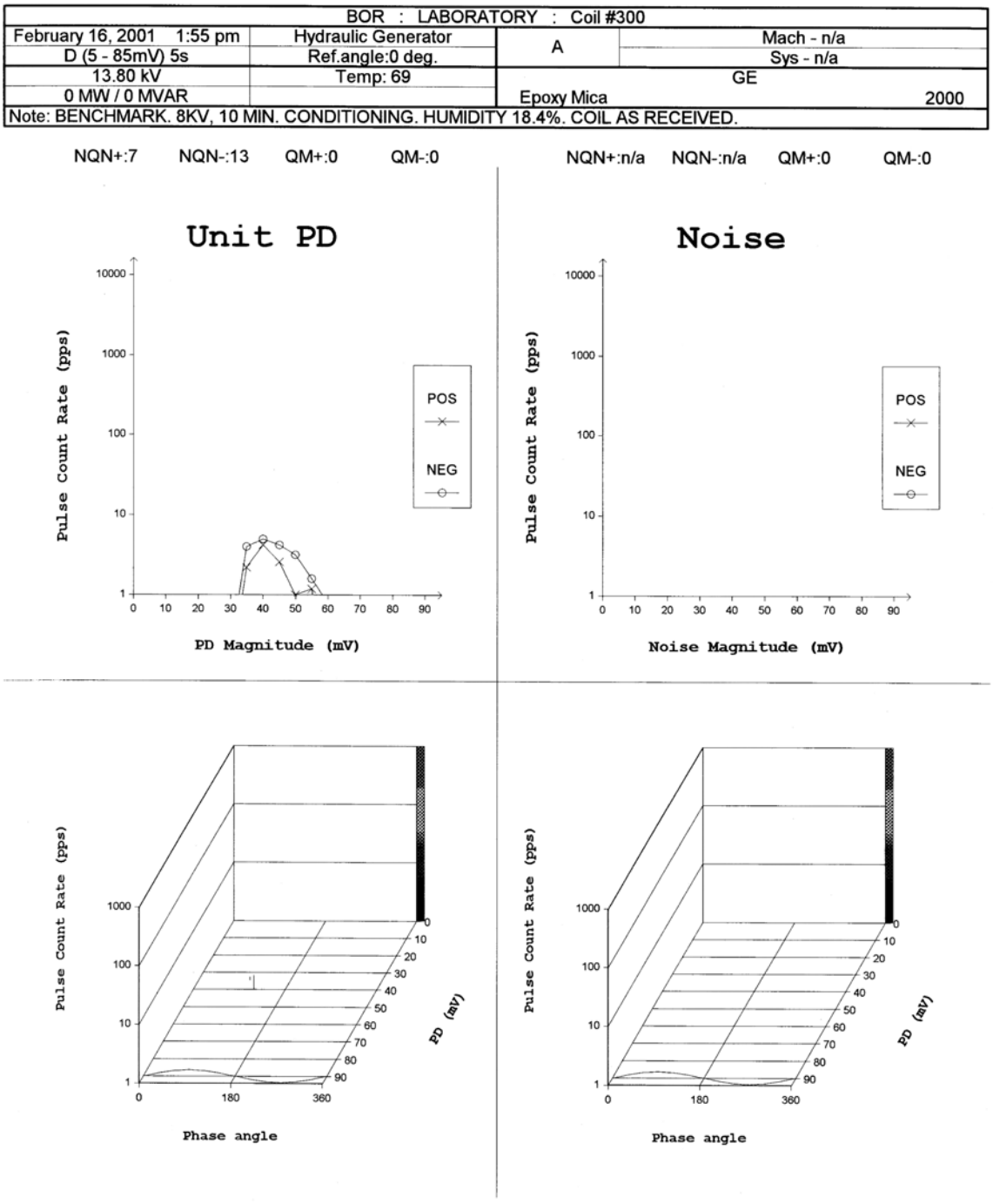

Figure E.7 Partial discharge measurements of Coil #300 (contamination). Tests results show no pulse polarity predominance.

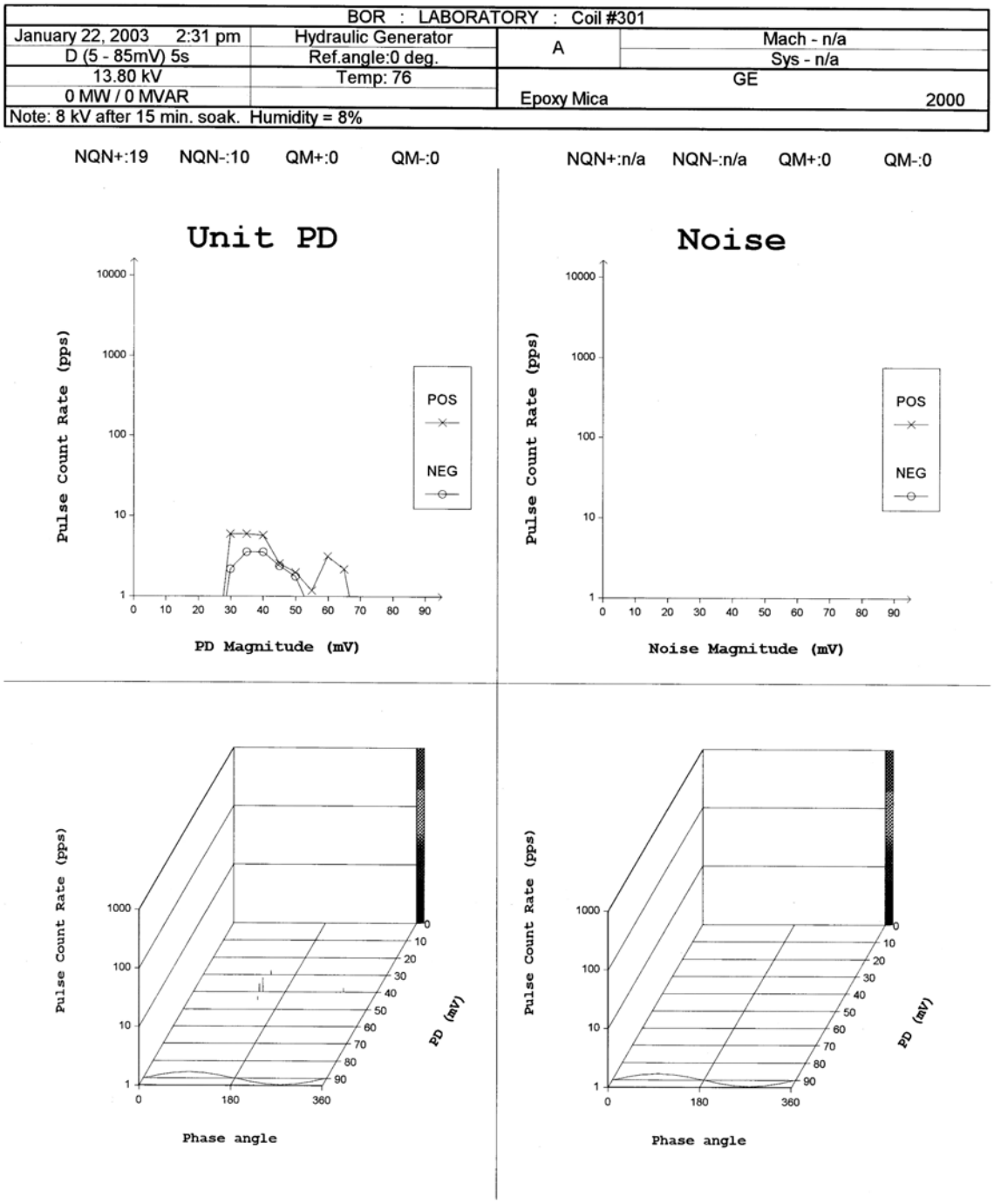

Figure E.8 Partial discharge measurements of Coil #301 (contamination). Tests results show no pulse polarity predominance.

BOR : LABORATORY : Coil #296			
February 16, 2001 1:35 pm	Hydraulic Generator	A	Mach - n/a
C (20-320mV) 5s	Ref.angle:0 deg.		Sys - n/a
13.80 kV	Temp: 69	GE	
0 MW / 0 MVAR		Epoxy Mica	2000
Note: BENCHMARK. 8 KV, 17 MIN. CONDITIONING. HUMIDITY 18.8. COIL AS RECEIVED.			

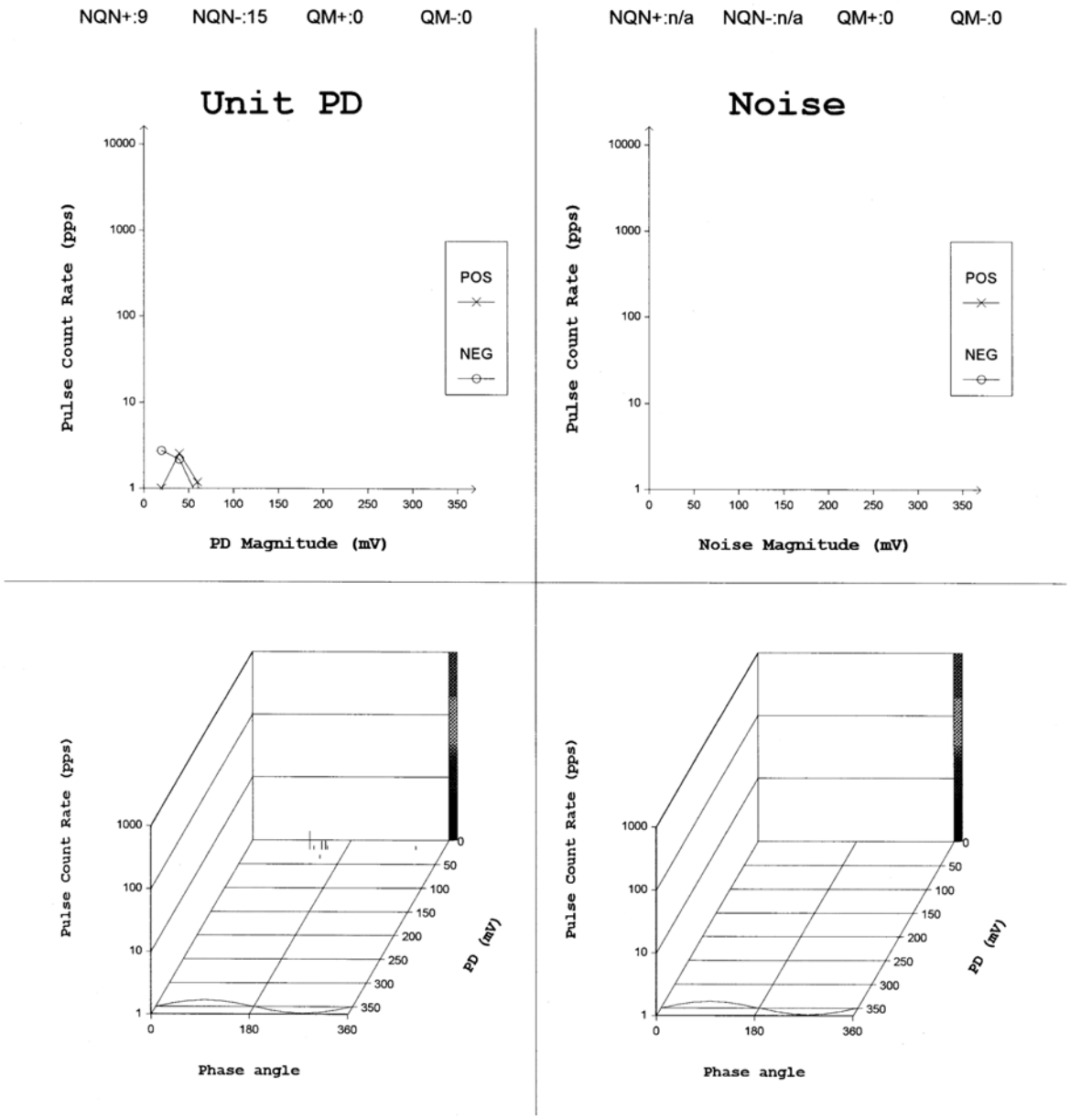

Figure E.9 Partial discharge measurements of Coil #296 (loose tapes). Tests results show negligible PD and no pulse polarity predominance.

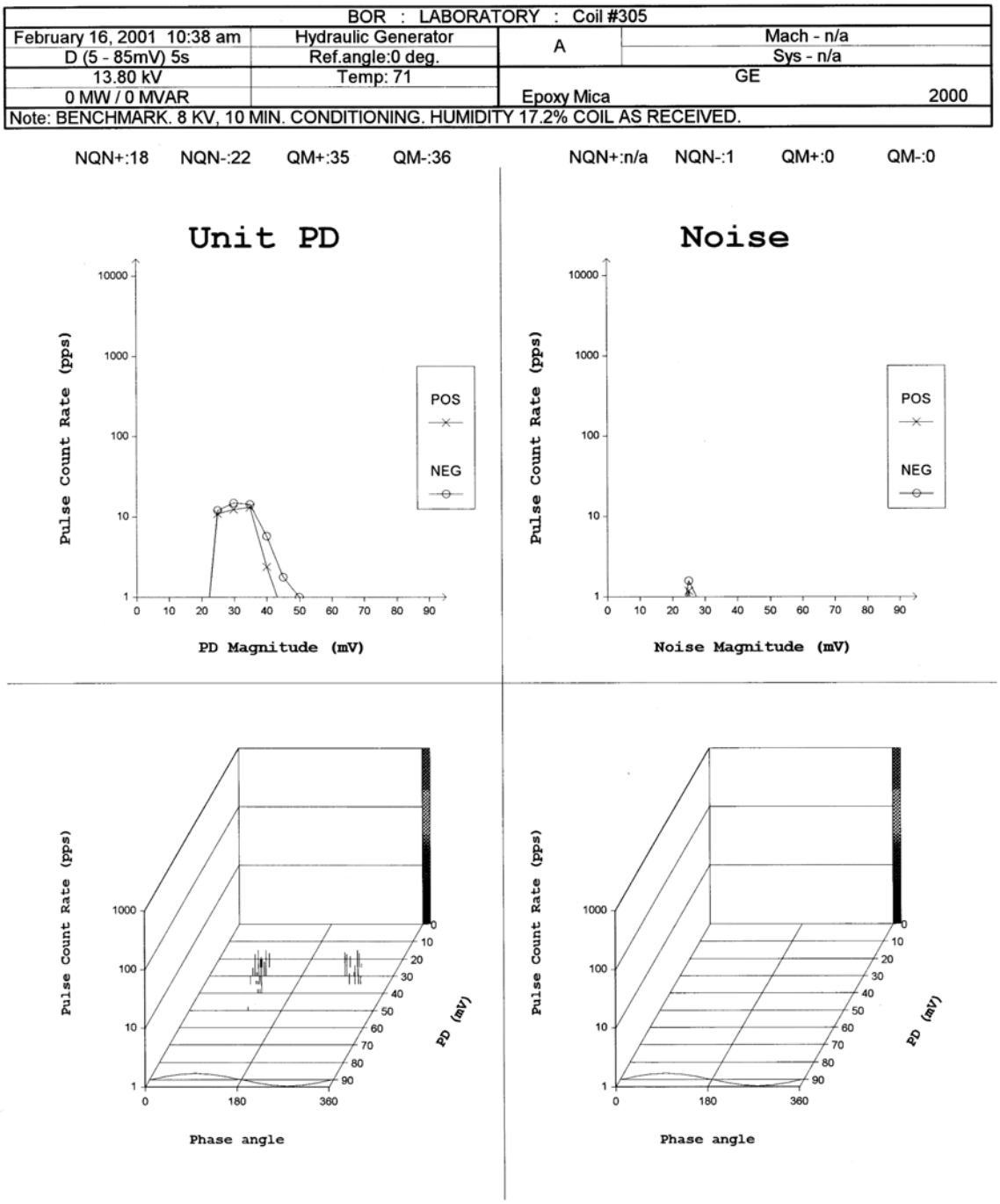

Figure E.10 Partial discharge measurements of Coil #305 (loose tapes). Tests results show no pulse polarity predominance.

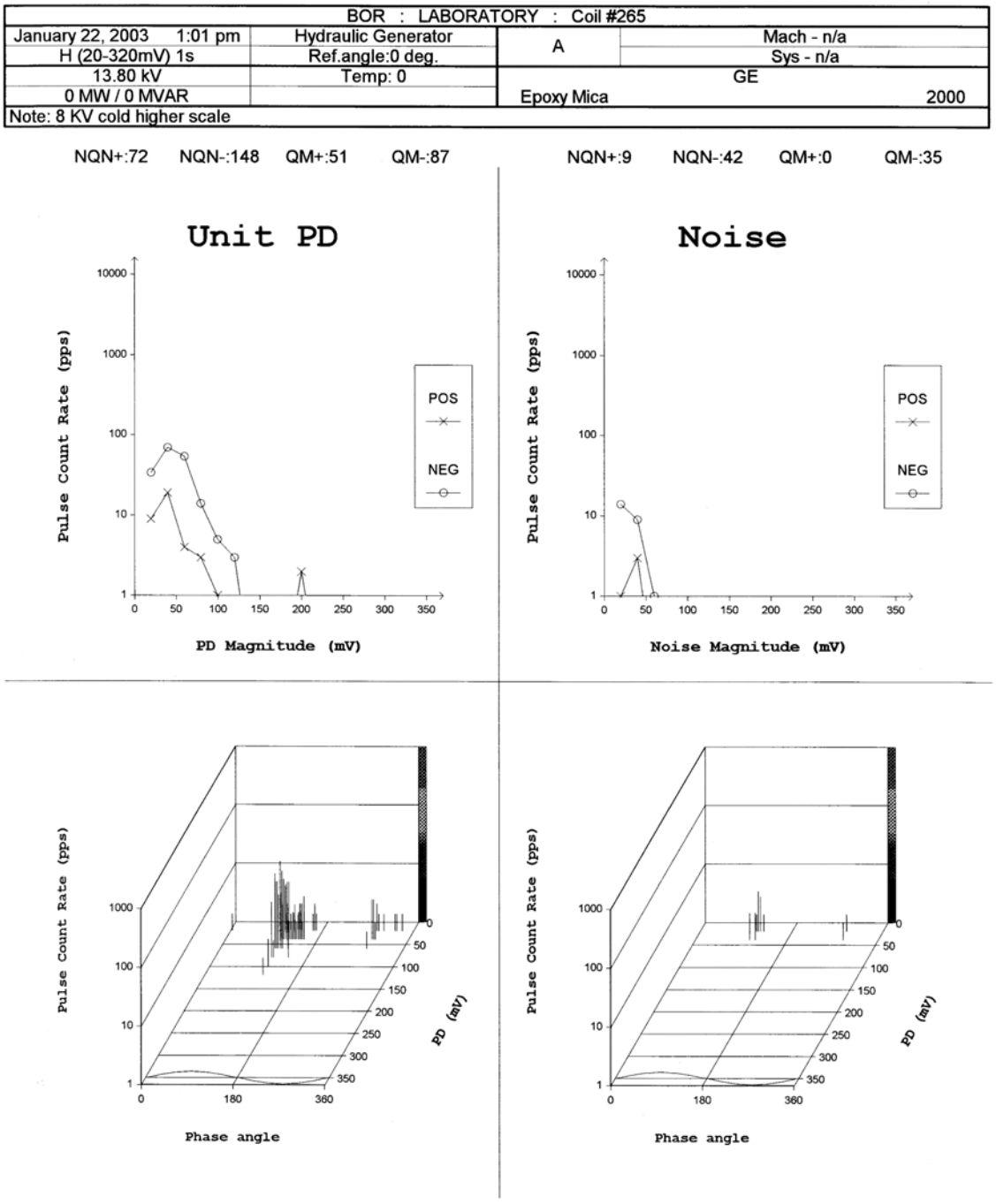

Figure E.11 Partial discharge measurements of Coil #265 (overheated). Tests results show slightly negative pulse predominance.

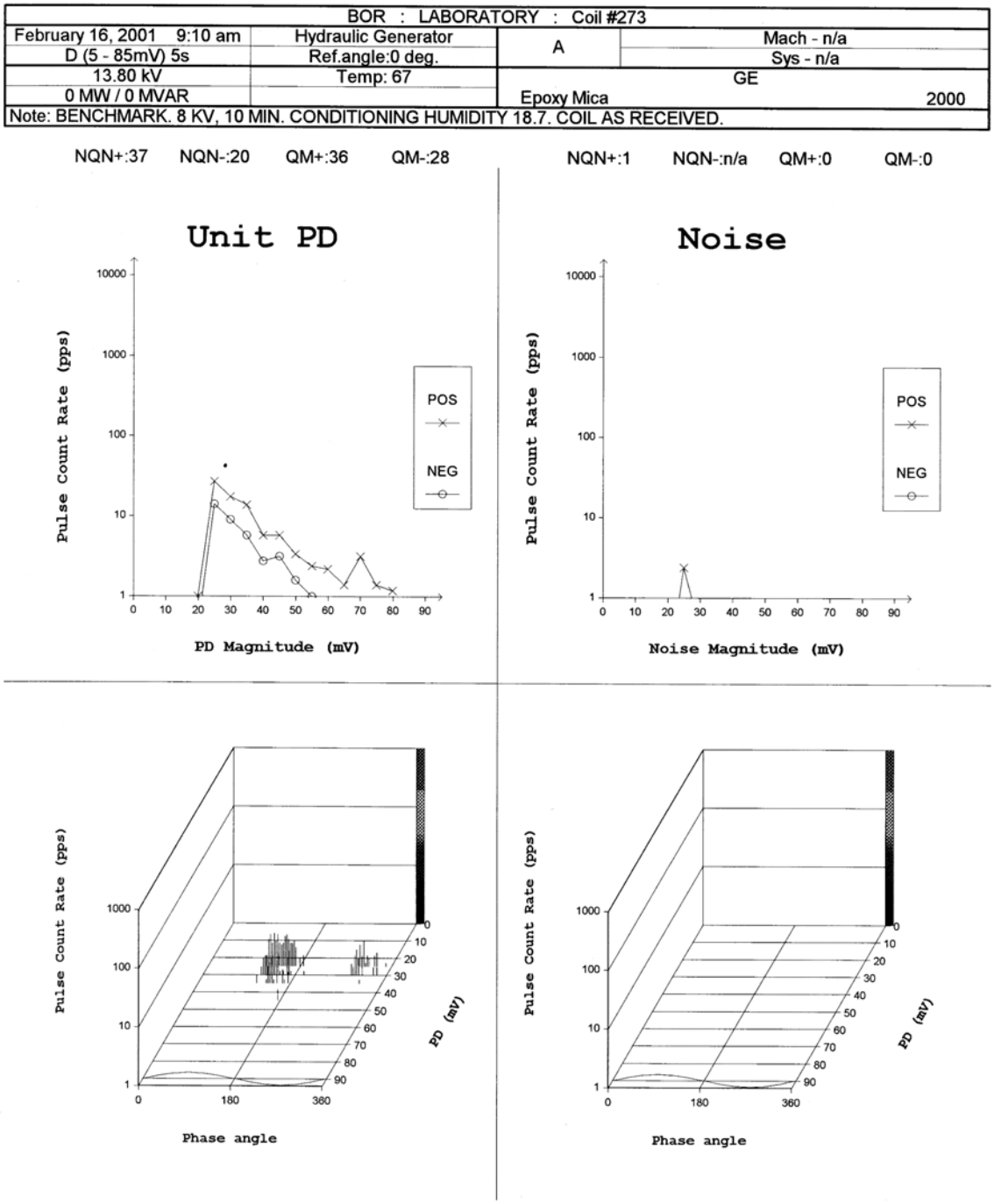

Figure E.12 Partial discharge measurements of Coil #273 (overheated). Tests results show negligible PD.

APPENDIX F

RAMPED VOLTAGE TEST RESULTS

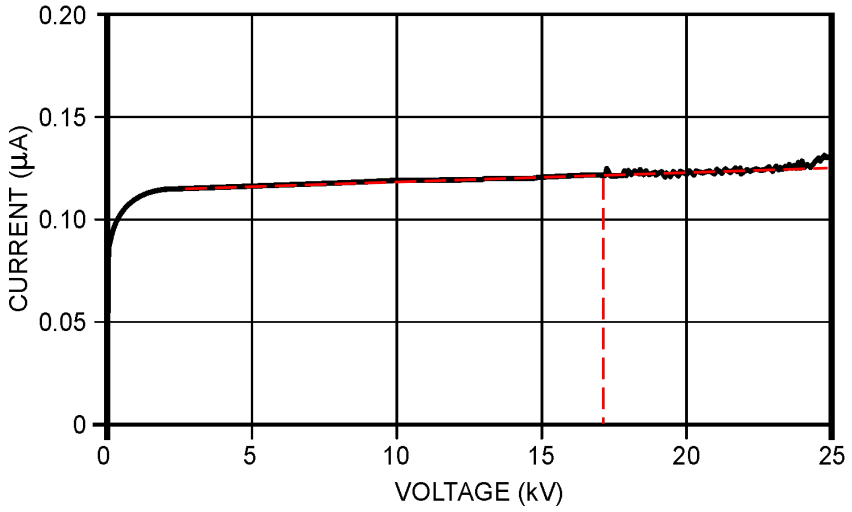

Figure F.1 Ramped voltage test result for coil 237 (standard production).

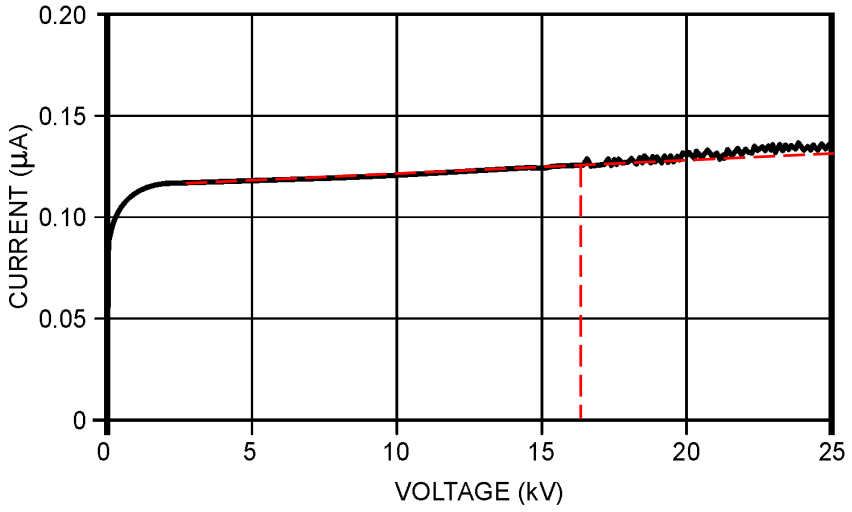

Figure F.2 Ramped voltage test result for coil 253 (standard production).

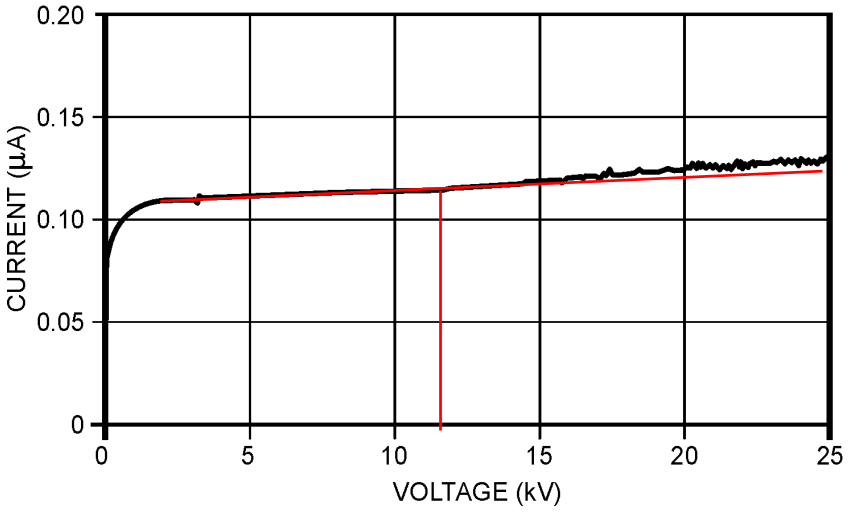

Figure F.3 Ramped voltage test result for coil 265 (overheated).

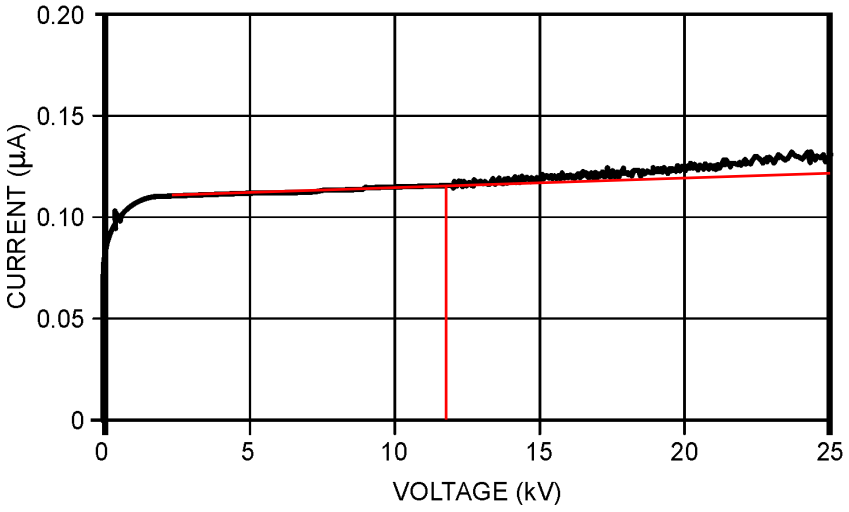

Figure F.4 Ramped voltage test result for coil 273 (overheated).

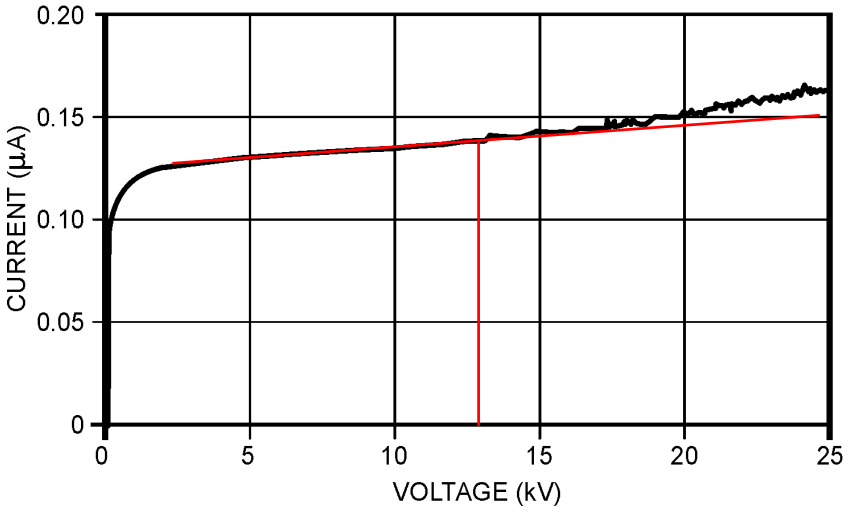

Figure F.5 Ramped voltage test result for coil 302 (no final cure).

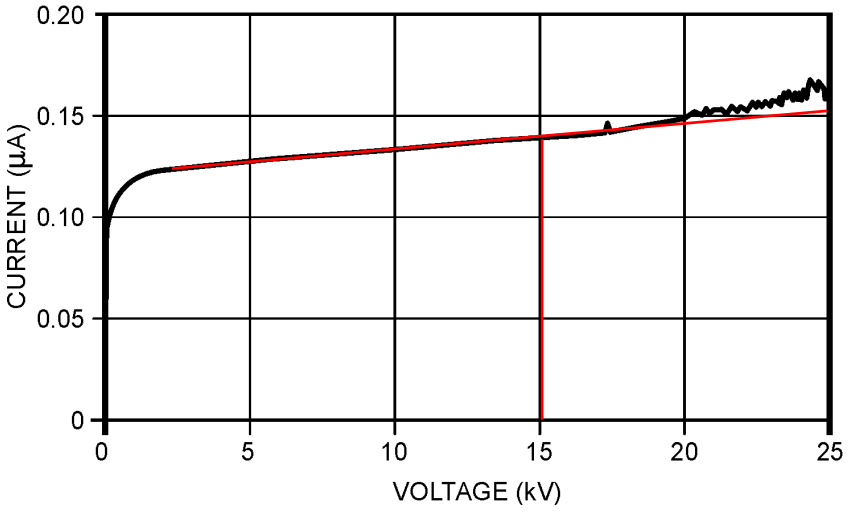

Figure F.6 Ramped voltage test result for coil 304 (no final cure).

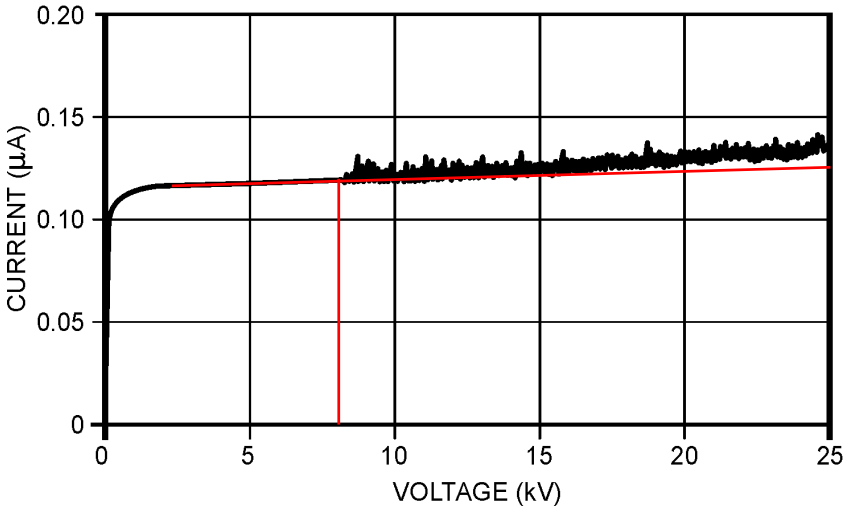

Figure F.7 Ramped voltage test result for coil 300 (conductive contamination).

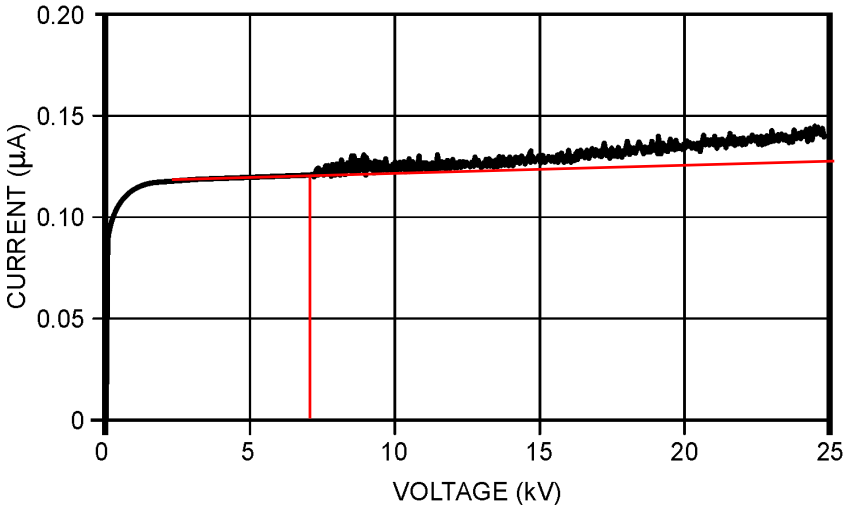

Figure F.8 Ramped voltage test result for coil 301 (conductive contamination).

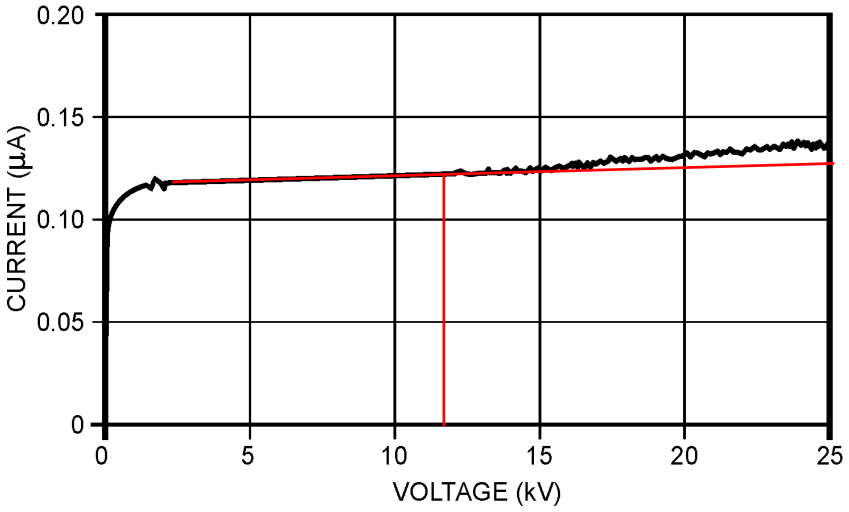

Figure F.9 Ramped voltage test result for coil 296 (loose tapes).

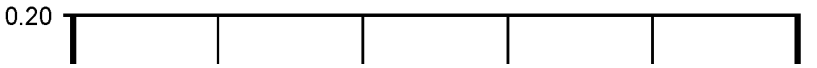

Figure F.10 Ramped voltage test result for Coil 305 (loose tapes).

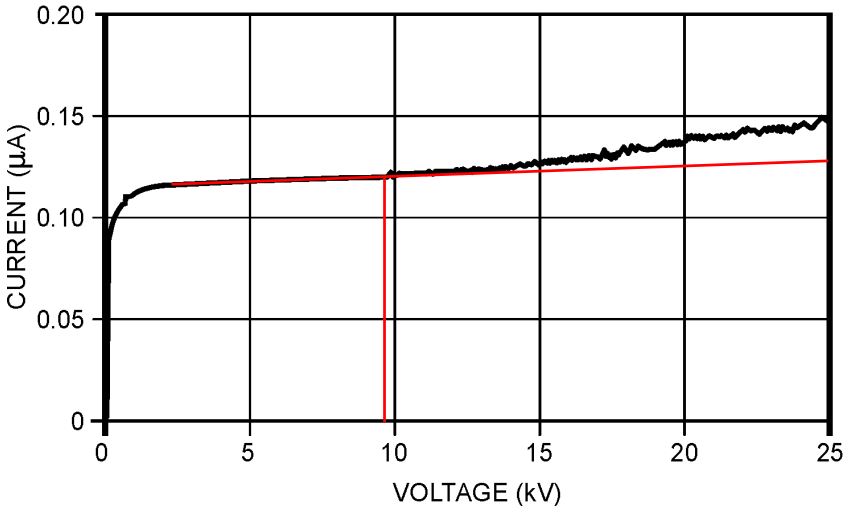

Figure F.11 Ramped voltage test result for Coil 297 (reduced layers).

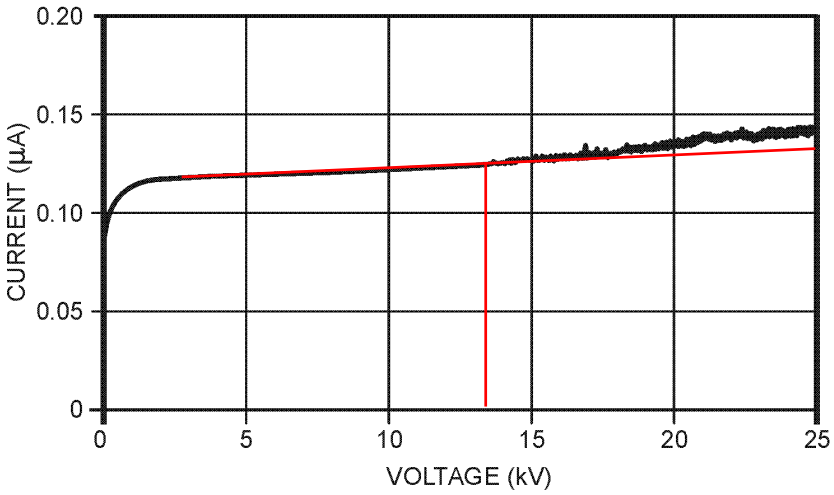

Figure F.12 Ramped voltage test result for Coil 314 (reduced layers).